

The A Dependence of Open Charm and Bottom Production

R. Vogt^{a,b*}

^aNuclear Science Division, MS 70-319
Lawrence Berkeley Laboratory,
University of California, Berkeley, California 94720

^bPhysics Department,
University of California, Davis, California, 95616

Abstract

We study inclusive heavy quark and exclusive heavy quark pair production in pp , pA and AA interactions. Intrinsic transverse momentum is introduced in pp interactions. Nuclear effects, limited to k_T broadening and nuclear shadowing, are introduced in pA and AA interactions. The nuclear dependence is studied over a range of energies, both in fixed target and collider setups.

Introduction

Previously, we calculated the heavy quark production cross section in pp interactions. In that work, we focussed on the scale dependence and fixed the quark mass and scale parameters by comparison to the total cross section data [1]. In this extension to pA and AA interactions, we study the effects of shadowing and k_T broadening on the spectra of heavy quark production.

* This work was supported in part by the Director, Office of Energy Research, Division of Nuclear Physics of the Office of High Energy and Nuclear Physics of the U. S. Department of Energy under Contract Number DE-AC03-76SF00098.

We first briefly update the calculation of the total cross section with new parton distribution functions and then go on to discuss the relevant differential distributions.

Total cross section

Recall that at leading order (LO) heavy quarks are produced by gg fusion and $q\bar{q}$ annihilation while at next-to-leading order (NLO), $qg + \bar{q}g$ scattering is also included. At any order, the partonic cross section may be expressed in terms of dimensionless scaling functions $f_{ij}^{(k,l)}$ that depend only on the variable η [2]

$$\hat{\sigma}_{ij}(\hat{s}, m_Q^2, \mu^2) = \frac{\alpha_s^2(\mu)}{m^2} \sum_{k=0}^{\infty} (4\pi\alpha_s(\mu))^k \sum_{l=0}^k f_{ij}^{(k,l)}(\eta) \ln^l \left(\frac{\mu^2}{m_Q^2} \right), \quad (1)$$

where \hat{s} is the partonic center of mass, m_Q is the heavy quark mass, μ is the scale, and $\eta = \hat{s}/4m_Q^2 - 1$. The cross section is calculated as an expansion in powers of α_s with $k = 0$ corresponding to the Born cross section at order $\mathcal{O}(\alpha_s^2)$. The first correction, $k = 1$, corresponds to the NLO cross section at $\mathcal{O}(\alpha_s^3)$. It is only at this order and above that the renormalization scale dependence enters the calculation since when $k = 1$ and $l = 1$, the logarithm $\ln(\mu^2/m_Q^2)$ appears. The dependence on the factorization scale, the argument of α_s , appears already at LO. We assume that the renormalization and factorization scales are the same. The next-to-next-to-leading order (NNLO) corrections to next-to-next-to-leading logarithm have been calculated near threshold [2] but the complete calculation only exists to NLO.

The total partonic cross section can also be written as

$$\hat{\sigma}_{ij}(\hat{s}, m_Q^2, \mu^2) = \int d\hat{t} d\hat{u} \hat{s}^2 \frac{d^2 \hat{\sigma}_{ij}(\hat{s}, \hat{t}, \hat{u})}{d\hat{t} d\hat{u}} \quad (2)$$

where the double differential partonic cross section at leading order is proportional to the Born cross section,

$$\hat{s}^2 \frac{d^2 \hat{\sigma}_{ij}^{(0)}(\hat{s}, \hat{t}, \hat{u})}{d\hat{t} d\hat{u}} = \delta(\hat{s} - \hat{t} - \hat{u} - 2m_Q^2) \hat{\sigma}_{ij}^B(\hat{s}, \hat{t}, \hat{u}). \quad (3)$$

The expressions for the Born cross section can be found in *e.g.* Ref. [3]. The NLO and NNLO cross sections in the $q\bar{q}$ channel are also proportional to $\hat{\sigma}_{q\bar{q}}^B$, albeit with more complicated scaling functions. In the gg channel, the higher order cross sections are again proportional to the Born cross section to leading logarithm and as are the highest powers of the factorization scale dependent logarithms [2]. However, beyond leading logarithm, the scaling functions also depend on the color state in which the $Q\bar{Q}$ pair was produced. The expressions for the Born cross section in both channels may be found in Ref. [2] along with the NLO and NNLO expressions near threshold.

The cross sections may be calculated in either one-particle inclusive kinematics or pair invariant mass kinematics, depending on whether one or both heavy quarks are detected. Single heavy quark hadroproduction in pp interactions is defined by

$$p(P_1) + p(P_2) \longrightarrow Q(p_1) + X(p_X), \quad (4)$$

where X denotes any hadronic final state containing the heavy antiquark and $Q(p_1)$ is the identified heavy quark. The reaction in Eq. (4) is dominated by the partonic reactions

$$q(k_1) + \bar{q}(k_2) \longrightarrow Q(p_1) + X[\bar{Q}](p_2), \quad (5)$$

$$g(k_1) + g(k_2) \longrightarrow Q(p_1) + X[\bar{Q}](p_2). \quad (6)$$

At LO or if $X[\bar{Q}](p_2) \equiv \bar{Q}(p'_2)$, the reaction is at partonic threshold with \bar{Q} momentum p'_2 . At threshold the heavy quarks do not have to be produced at rest but are instead produced with equal and opposite momentum, leading to trivial values of the pair transverse momentum ($\vec{p}_{T_1} + \vec{p}'_{T_2} = 0$) and azimuthal angle ($\phi = \pi$). The Mandelstam invariants on the hadronic level are

$$s = (P_1 + P_2)^2, \quad t = (P_1 - p_1)^2, \quad u = (P_2 - p_1)^2, \quad (7)$$

with the corresponding partonic invariants

$$\hat{s} = (k_1 + k_2)^2, \quad \hat{t} = (k_2 - p_1)^2, \quad \hat{u} = (k_1 - p_1)^2. \quad (8)$$

The pair invariant mass kinematics are somewhat different. Now the pair is treated as a single unit and we have

$$p(P_1) + p(P_2) \longrightarrow Q\bar{Q}(P') + X(P_X). \quad (9)$$

On the parton level, Eqs. (5) and (6) are now

$$q(k_1) + \bar{q}(k_2) \longrightarrow Q\bar{Q}(p') + X(p_X), \quad (10)$$

$$g(k_1) + g(k_2) \longrightarrow Q\bar{Q}(p') + X(p_X). \quad (11)$$

The square of the heavy quark pair mass is $p'^2 = M^2$. In the case when $p_X \neq 0$, more invariants than the three typical Mandelstam invariants can be defined [4]. At partonic threshold, $p_X = 0$, only the three Mandelstam invariants remain with $\hat{s} = M^2$ and

$$\hat{t} - m_Q^2 = -\frac{M^2}{2}(1 - \beta_M \cos \theta), \quad (12)$$

$$\hat{u} - m_Q^2 = -\frac{M^2}{2}(1 + \beta_M \cos \theta), \quad (13)$$

where $\beta_M = \sqrt{1 - 4m_Q^2/M^2}$, and θ is the scattering angle in the parton center of mass frame.

The total hadronic cross section is obtained by convoluting the total partonic cross section with the parton distribution functions of the initial hadrons,

$$\sigma_{pp}(s, m_Q^2) = \sum_{i,j=q,\bar{q},g} \int_{4m_Q^2/s}^1 \frac{d\tau}{\tau} \delta(x_1 x_2 - \tau) F_i^p(x_1, \mu^2) F_j^p(x_2, \mu^2) \hat{\sigma}_{ij}(\tau, m_Q^2, \mu^2), \quad (14)$$

where the sum i is over all massless partons and x_1 and x_2 are the hadron momentum fractions carried by the interacting partons. The parton distribution functions,

denoted by F_i^p , are evaluated at the factorization scale, assumed to be equal to the renormalization scale in all our calculations.

In our previous work on pp interactions [1], we obtained our results with two sets of parton distribution functions that had successfully predicted the general behavior of the low x deep-inelastic scattering data [5], MRS D-’ [6] and GRV HO [7]. Much more low x data has become available since then which shows that these parton densities are too high at low x and new fits to the most recent data [8] are now available [9]. (The low x region is particularly relevant for $Q\bar{Q}$ production at the LHC.) Our latest calculations employ the most recent NLO parton distribution functions from the MRS group, MRST HO (central gluon) [10]. This group has also made a leading order set available [11]. We compare the MRS D-’, MRST HO, and MRST LO results in Fig. 1 and in Tables 1 and 2, all updated from our earlier work [1]. Table 1 has also been expanded to include the fixed target energies at which we compare the pp and pA calculations. As before, all our numerical results are obtained using the NLO code by Mangano, Nason and Ridolfi (MNR) [4].

All the cross sections are calculated at LO and NLO with the same mass and scale parameters obtained from the pp study— $m_c = 1.2$ GeV, $\mu_c = 2m_c$, $m_b = 4.75$ GeV, and $\mu_b = m_b$. The agreement with the total charm cross section data is at least as good with the MRST sets as with the MRS D-’ set. In fact, the somewhat larger NLO cross section at fixed target energies with MRST HO tends to agree better with the data than the older set, in part because some of the gluon density at low x has been redistributed to higher x . However, at the pp and AA collider energies shown in Tables 1 and 2, the growth of the cross sections is considerably slower with the new distribution functions than with the MRS D-’ set.

The MRST LO results are for comparative purposes only. A LO set is not consistent with a NLO calculation just as a NLO set is inconsistent with a strictly LO calculation. We note however that the tabulated results are all calculated with α_s at two loops, regardless of whether the LO or NLO result is given, because in the MNR code α_s is calculated to two loops regardless of the order of the chosen parton density. Since the QCD scale, Λ , is tuned to fit all available data in global analyses of parton distributions, whether at LO or NLO, the number of loops in the evaluation is important. We remark however, that it is rather standard procedure to evaluate all orders of the hadronic cross section with the same NLO parton density and a two loop calculation of α_s . This is done so that one can study the variation of the partonic cross section alone while keeping the nonperturbative results fixed. Also, beyond NLO, no standard NNLO or resummed evaluations of the parton densities exist, generally because the partonic matrix elements are limited to near threshold beyond NLO. In addition, the data used in the global analyses of the parton densities are typically far from threshold and of only limited use in such an evaluation. Therefore the uncertainties in such an analysis would be large.

We note that when a fully LO calculation of the charm cross section is done with a one loop evaluation of α_s in the global analyses of the parton densities, as with the MRST LO set, the LO cross sections in Table 1 increase by $\sim 60\%$. This change is almost solely due to the difference between the one and two loop evaluations of α_s . The MRST LO Λ is 0.204 GeV when $n_f = 3$, leading to $\alpha_s^{1\text{-loop}} = 0.287$ and

$\alpha_s^{2\text{-loops}} = 0.220$ for $\mu = 2m_c$. The Λ associated with the MRST HO set is larger, $\Lambda = 0.353$ GeV when $n_f = 3$, corresponding to $\alpha_s^{1\text{-loop}} = 0.364$ and $\alpha_s^{2\text{-loops}} = 0.263$ at the same scale. Thus a fully LO calculation with MRST LO partons would be in better agreement with the tabulated LO results for MRST HO partons. These results show that one must use caution when using a LO set with a NLO calculation or a NLO set for a LO calculation.

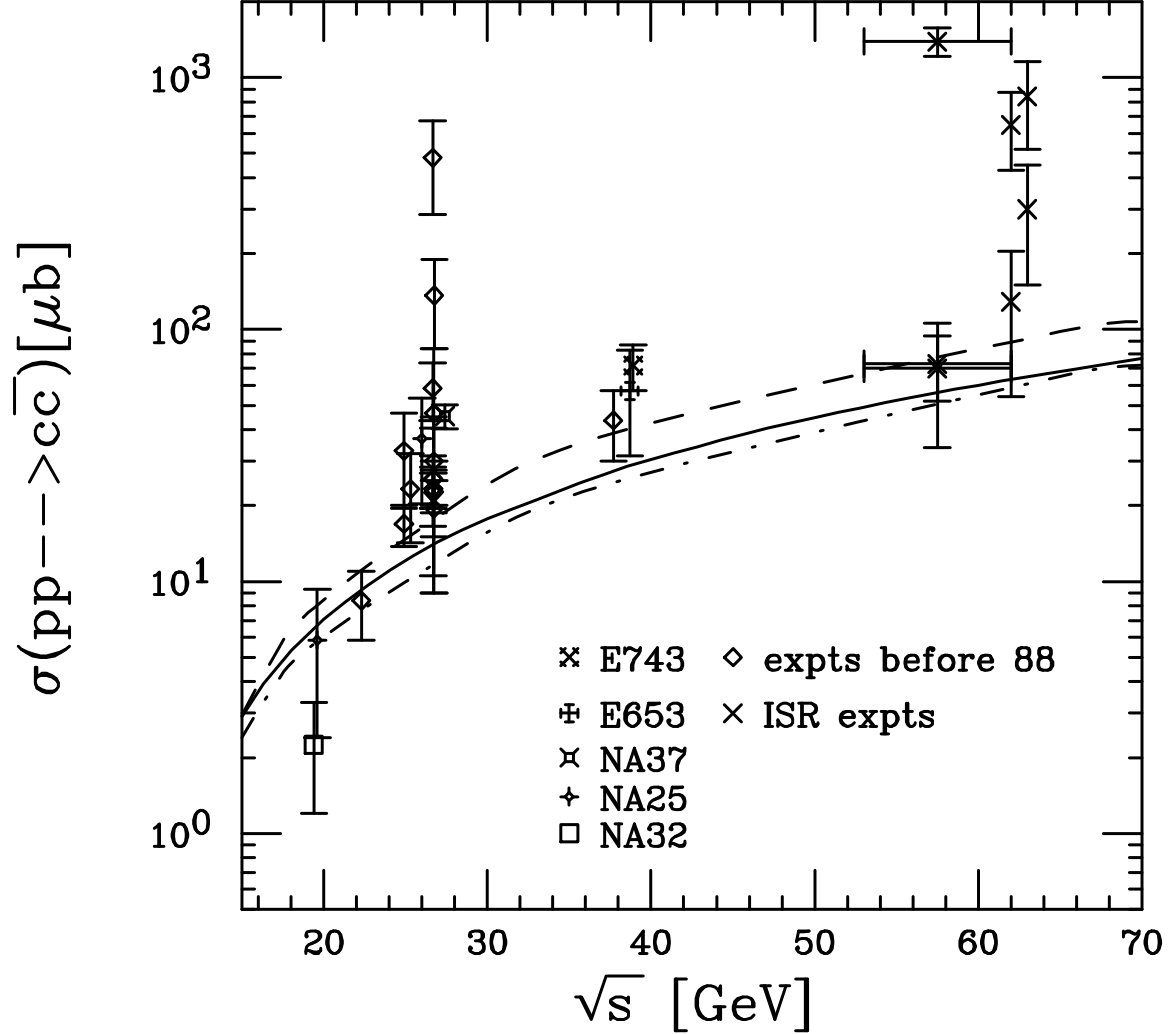


Figure 1: Total charm production cross sections from pp and pA measurements [12, 13, 14, 15, 16] compared to calculations with $m_c = 1.2$ GeV and $\mu = 2m_c$. The parton distributions used are MRS D-' (solid); MRST HO (dashed) and MRST LO (dot-dashed). Updated from Ref. [1].

Differential cross sections

$\sqrt{s}(\text{GeV})$	MRST LO		MRST HO		MRS D-'	
	$\sigma_{c\bar{c}}^{\text{LO}} (\mu\text{b})$	$\sigma_{c\bar{c}}^{\text{NLO}} (\mu\text{b})$	$\sigma_{c\bar{c}}^{\text{LO}} (\mu\text{b})$	$\sigma_{c\bar{c}}^{\text{NLO}} (\mu\text{b})$	$\sigma_{c\bar{c}}^{\text{LO}} (\mu\text{b})$	$\sigma_{c\bar{c}}^{\text{NLO}} (\mu\text{b})$
17.3	1.56	4.16	1.85	5.54	1.67	4.62
19.4	2.16	5.65	2.67	7.87	2.36	6.38
29.1	5.84	14.52	8.04	22.36	6.42	16.24
38.8	10.60	25.85	15.10	40.57	11.47	28.20
63	25.37	60.74	35.79	91.88	26.88	64.97
200	132.6	314.1	152.8	381.7	139.3	343.7
500	374.9	897.0	356.8	922.8	449.4	1138
5500	3040	7733	2002	5833	7013	17680
14000	5668	14920	3332	10240	16450	41770

Table 1: Total $c\bar{c}$ production cross sections at fixed-target and collider energies.

$\sqrt{s}(\text{GeV})$	MRST LO		MRST HO		MRS D-'	
	$\sigma_{b\bar{b}}^{\text{LO}} (\mu\text{b})$	$\sigma_{b\bar{b}}^{\text{NLO}} (\mu\text{b})$	$\sigma_{b\bar{b}}^{\text{LO}} (\mu\text{b})$	$\sigma_{b\bar{b}}^{\text{NLO}} (\mu\text{b})$	$\sigma_{b\bar{b}}^{\text{LO}} (\mu\text{b})$	$\sigma_{b\bar{b}}^{\text{NLO}} (\mu\text{b})$
63	0.0374	0.0688	0.0394	0.0763	0.0397	0.0746
200	0.744	1.371	0.987	1.903	0.796	1.47
500	3.825	7.422	4.809	9.799	3.847	7.597
5500	82.71	186.3	72.85	186.3	98.8	224
14000	211.0	502.2	164.5	454.1	296.8	687.5

Table 2: Total $b\bar{b}$ production cross sections at collider energies.

While the total cross section predicts the yield of heavy quark production over all phase space, it cannot provide much useful information on nuclear effects such as p_T -broadening and shadowing. It is also independent of the choice of kinematic schemes. Any k_T broadening will not affect the total cross section but will have a strong influence on the p_T distributions. Shadowing may reduce or enhance the nuclear cross section relative to that of the proton but the effect may be more apparent in some regions of phase space than others. To obtain more information on nuclear effects, it is thus necessary to turn to distributions. In addition, a real detector does not cover all phase space. The differential distributions can be tuned to a detector acceptance.

The double differential hadronic cross sections are written in the factorized form

$$s^2 \frac{d^2\sigma_{pp}(s, t, u)}{dt du} = \sum_{i,j=q,\bar{q},g} \int_{x_1^-}^1 \frac{dx_1}{x_1} \int_{x_2^-}^1 \frac{dx_2}{x_2} f_i^p(x_1, \mu^2) f_j^p(x_2, \mu^2) \mathcal{J}_K(\hat{s}, \hat{t}, \hat{u}) \hat{s}^2 \frac{d^2\hat{\sigma}_{ij}(\hat{s}, \hat{t}, \hat{u})}{d\hat{t} d\hat{u}} \quad (15)$$

where f_i^p is the parton density, $f_i^p(x, \mu^2) = F_i^p(x, \mu^2)/x$, and \mathcal{J}_K is a kinematics-dependent Jacobian. These results are difficult to calculate analytically and expressions only exist for $\hat{s}^2 d^2\hat{\sigma}_{ij}(\hat{s}, \hat{t}, \hat{u})/d\hat{t} d\hat{u}$, see *e.g.* [2]. However, the MNR code calculates single and double differential distributions as well as total cross sections. In our first paper [1], we neglected any fragmentation effects on the produced heavy quark and intrinsic transverse momentum of the initial partons because the inclusive D meson p_T distributions agreed with the bare charm quark distributions, showing

no need for such effects. However, as pointed out in Ref. [17], the pair distributions, particularly the pair p_T and the azimuthal angle distributions at fixed target energies are broader than can be accounted for by the bare quark distributions. The general behavior of the pair data was reproduced in Ref. [17] by including a Peterson-type fragmentation function [18] along with an intrinsic k_T of the initial partons. Indeed, the combination of fragmentation with an intrinsic average k_T^2 of 1 GeV² leads to single D meson p_T distributions in good agreement with the bare charm distribution. These effects can be added by modifying Eq. (15) to include the additional integrals

$$\int dz_3 dz_4 d^2 k_{T1} d^2 k_{T2} \frac{D_{H/Q}(z_3, \mu^2)}{z_3} \frac{D_{\bar{H}/\bar{Q}}(z_4, \mu^2)}{z_4} g_p(k_{T1}) g_p(k_{T2}) . \quad (16)$$

The fragmentation functions $D_{H/Q}(z)$ describe the hadronization of the heavy quark Q into hadron H . The final-state hadron H carries a fraction z of the heavy quark momentum and is assumed to be collinear to the parent heavy quark. The Peterson fragmentation function [18], fit to D production data in e^+e^- collisions,

$$D_{H/Q}(z) = \frac{N}{z(1 - 1/z - \epsilon_Q/(1 - z))^2} , \quad (17)$$

is used in the code. The parameter ϵ_Q is 0.06 for charm and 0.006 for bottom [19]. The normalization N is defined by $\sum_H \int D_{H/Q}(z) dz = 1$.

The Peterson function results in a nearly 30% decrease in the average charm quark momentum during hadronization. This decrease must be compensated for in inclusive production because the decreased momentum of the D meson would no longer agree with the single D p_T distributions. The intrinsic k_T of the initial partons is such a compensation mechanism which has been used successfully to describe the p_T distributions of other processes such as Drell-Yan [20] and hard photon production [21]. Some of the low p_T Drell-Yan data has subsequently been described by resummation to all orders but the inclusion of higher orders has not eliminated the need for this intrinsic k_T . It was found that assuming $\langle k_T^2 \rangle = 1$ GeV² in pp and πp interactions produces agreement with the inclusive data on the level of that found with the bare quarks alone and does a better job of reconciling the exclusive $D\bar{D}$ data with the calculated distributions [17].

The implementation of intrinsic k_T in the MNR code is not the same as in other processes due to the nature of their calculation. The cancellation of divergences is handled numerically in the code. Since adding additional numerical integrations would slow this process, the k_T kick is added in the final, rather than the initial state. In Eq. (16), the Gaussian function $g_p(k_T)$,

$$g_p(k_T) = \frac{1}{\pi \langle k_T^2 \rangle_p} \exp(-k_T^2 / \langle k_T^2 \rangle_p) , \quad (18)$$

with $\langle k_T^2 \rangle_p = 1$ GeV² [17], multiplies the parton distribution functions, assuming the x and k_T dependencies completely factorize. If this is true, it does not matter whether the k_T dependence appears in the initial or final state modulo the caveat described

below. In the code, the $Q\bar{Q}$ system is boosted to rest from its longitudinal center of mass frame. Intrinsic transverse momenta of the incoming partons, \vec{k}_{T1} and \vec{k}_{T2} , are chosen at random with k_{T1}^2 and k_{T2}^2 distributed according to Eq. (18). A second transverse boost out of the pair rest frame changes the initial transverse momentum of the $Q\bar{Q}$ pair, \vec{p}'_T in Eqs. (10) and (11), to $\vec{p}'_T + \vec{k}_{T1} + \vec{k}_{T2}$. The initial k_T of the partons could have alternatively been given to the entire final-state system, as is essentially done if applied in the initial state, instead of to the $Q\bar{Q}$ pair. There is no difference if the calculation is to LO only but at NLO an additional light parton also appears in the final state. In Ref. [22], it is claimed that the difference in the two methods is rather small if $k_T^2 \leq 2 \text{ GeV}^2$. The effect of the intrinsic k_T decreases as the center of mass energy increases.

k_T broadening in nuclei

The average intrinsic k_T is expected to increase in pA interactions. This broadening is observed in Drell-Yan [23], J/ψ [24], and Υ [23] production and has been used to explain high p_T pion production in nuclear interactions [25]. Since k_T broadening has not been explicitly measured in charm production, we follow the formulation of Ref. [25], similar to Ref. [26] for J/ψ and Drell-Yan production where the k_T broadening arises from multiple scattering of the projectile partons in the target,

$$\langle k_T^2 \rangle_A = \langle k_T^2 \rangle_p + (\langle \nu \rangle - 1) \Delta^2(\mu) . \quad (19)$$

We define the number of collisions in a proton-nucleus interaction, averaged over impact parameter, as

$$\langle \nu \rangle = \sigma_{NN} \frac{\int d^2b T_A^2(b)}{\int d^2b T_A(b)} = \frac{3}{2} \sigma_{NN} \rho_0 R_A , \quad (20)$$

where $T_A(b) = \int dz \rho_A(b, z)$ is the nuclear profile function, and use this to calculate the average broadening. In the definition of $\langle \nu \rangle$, σ_{NN} is the inelastic nucleon-nucleon scattering cross section, ρ_0 is the central nuclear density, and R_A is the nuclear radius. Our calculations are done with $A = 200$, $R_A = 1.2A^{1/3}$, and $\rho_0 = 0.16/\text{fm}^3$.

The strength of the nuclear broadening, Δ^2 , depends on μ , the scale of the interaction [25]

$$\Delta^2(\mu) = 0.225 \frac{\ln^2(\mu/\text{GeV})}{1 + \ln(\mu/\text{GeV})} \text{GeV}^2 . \quad (21)$$

Thus Δ^2 is larger for $b\bar{b}$ production than $c\bar{c}$ production. This empirically reflects the larger k_T broadening of the Υ [23] relative to the J/ψ [24]. We evaluate $\Delta^2(\mu)$ at $\mu = 2m_Q$ for both charm and bottom production. We find $(\langle \nu \rangle - 1)\Delta^2(\mu) = 0.35 \text{ GeV}^2$ for charm and 1.57 GeV^2 for bottom in pA collisions at $b = 0$ and $A = 200$. We can change the centrality by changing $\langle \nu \rangle - 1$. Reducing $\langle \nu \rangle - 1$ by two corresponds to a more peripheral pA collision while multiplying $\langle \nu \rangle - 1$ by two corresponds to

central AA collisions. We will use the central values given above in our pA results and the larger values, 0.70 GeV^2 for charm and 3.14 GeV^2 for bottom, in our AA results. Note that the total $\langle k_T^2 \rangle_A$ in both cases is obtained by adding $\langle k_T^2 \rangle_p = 1 \text{ GeV}^2$ to the above nuclear broadening.

The effects of k_T broadening alone on several pair and single inclusive quantities are shown for a fixed target beam energy of 158 GeV in Figs. 2 and 3. The changes in the shape of the pair quantities in Fig. 2 are rather striking. The bare charm pair distributions alone are compared to results with $\langle k_T^2 \rangle = 1, 1.175, 1.35, \text{ and } 1.7 \text{ GeV}^2$. The differences in the pair p_T and ϕ distributions are quite apparent. The change in the pair p_T distribution is due entirely to k_T broadening since fragmentation effects would steepen the solid curve. The broadening is still important at large pair p_T , causing more than an order of magnitude difference in the cross section between $\langle k_T^2 \rangle = 1 \text{ GeV}^2$ and 1.7 GeV^2 at $p_T = 4 \text{ GeV}$. Likewise, introducing intrinsic k_T changes the ϕ distribution from sharply peaked at $\phi = \pi$ for the bare charm quarks to nearly flat when $\langle k_T^2 \rangle = 1 \text{ GeV}^2$ to a peak at $\phi = 0$ when $\langle k_T^2 \rangle = 1.7 \text{ GeV}^2$. On the contrary, the pair rapidity shows no effect of k_T broadening.

The broadening effect on the single charm distributions shown in Fig. 3 is not as strong. Note that all the distributions, including the charm rapidity distribution, are affected by broadening and fragmentation. The charm p_T distributions for the bare quark and including fragmentation with $\langle k_T^2 \rangle = 1 \text{ GeV}^2$ are almost identical, in accord with the observation that no intrinsic k_T was needed to describe the D meson p_T distributions. The difference between the bare quark and $\langle k_T^2 \rangle = 1.7 \text{ GeV}^2$ is less than a factor of five for $p_T = 3.5 \text{ GeV}$. Fragmentation is the most important effect on the x_F and rapidity distributions since there is little change in the distributions as $\langle k_T^2 \rangle$ is increased. Any type of fragmentation, even that of a delta function, will cause the rapidity and x_F distributions to be modified. This is because fragmentation enhances these distributions in the central region [27]. If $D_{H/Q}(z)$ is a delta function, the momentum does not change, $p_H = p_Q$, but $E_H^2 = E_Q^2 - m_Q^2 + m_H^2$, resulting in a rapidity shift [27] with

$$dn \propto dy_Q = \frac{dp_{zQ}}{E_Q} = \frac{dp_{zH}}{E_Q} = \frac{m_{T,H} \cosh y_H dy_H}{\sqrt{m_{T,H}^2 \cosh^2 y_H - m_H^2 + m_Q^2}} \approx \frac{\cosh y_H dy_H}{\sqrt{\cosh^2 y_H - \alpha^2}} \quad (22)$$

where

$$\alpha^2 = \frac{m_H^2 - m_Q^2}{m_{T,H}^2}. \quad (23)$$

For $m_c = 1.2 \text{ GeV}$, $m_D = 1.87 \text{ GeV}$ and $m_{T,D} \approx \sqrt{2}m_D$, $\alpha^2 = 0.25$, increasing the D cross section at $y_D = 0$ by $\approx 15\%$. The total cross section is unchanged. When $m_b = 4.75 \text{ GeV}$, $m_B = 5.27 \text{ GeV}$ and $m_{T,B} = \sqrt{2}m_B$, $\alpha^2 = 0.09$, increasing the B cross section by $\approx 5\%$ at $y_B = 0$. The range of the enhancement is $|y_H| < 2.5$, independent of energy. If the Peterson function is used instead, α^2 increases to

$$\alpha^2 = \frac{m_H^2 - z^2 m_Q^2}{m_{T,H}^2}, \quad (24)$$

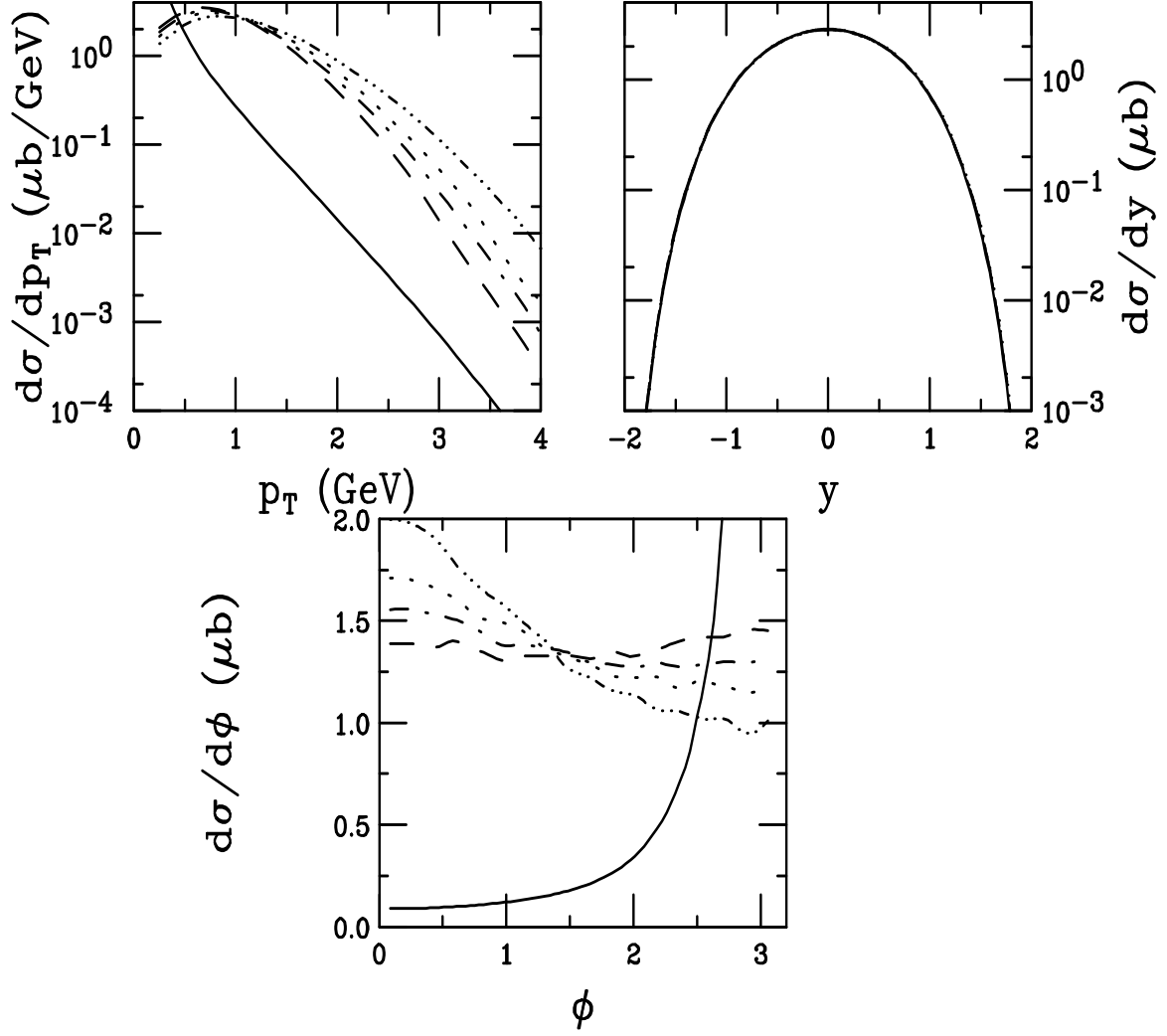


Figure 2: Effects of k_T broadening alone on exclusive NLO $c\bar{c}$ pair production in pA interactions at 158 GeV as a function of p_T , y , and ϕ . The per nucleon cross section is given. The curves are the bare quark distributions alone ($\langle k_T^2 \rangle_A = 0$ and no fragmentation) (solid) and, including fragmentation, $\langle k_T^2 \rangle = 1$ (dashed), 1.175 (dot-dashed), 1.35 (dotted) and 1.7 (dot-dot-dot-dashed) GeV^2 .

increasing the D cross section at $y_D = 0$ by $\approx 30\%$ for $\langle z \rangle \approx 0.7$ and the B cross section by $\approx 15\%$ at $y_B = 0$ for $\langle z \rangle \approx 0.85$. These $\langle z \rangle$ values are typical for the Peterson function with the ϵ_Q values given above. The x_F distribution is also affected because $x_F = 2m_T \sinh y / \sqrt{s}$.

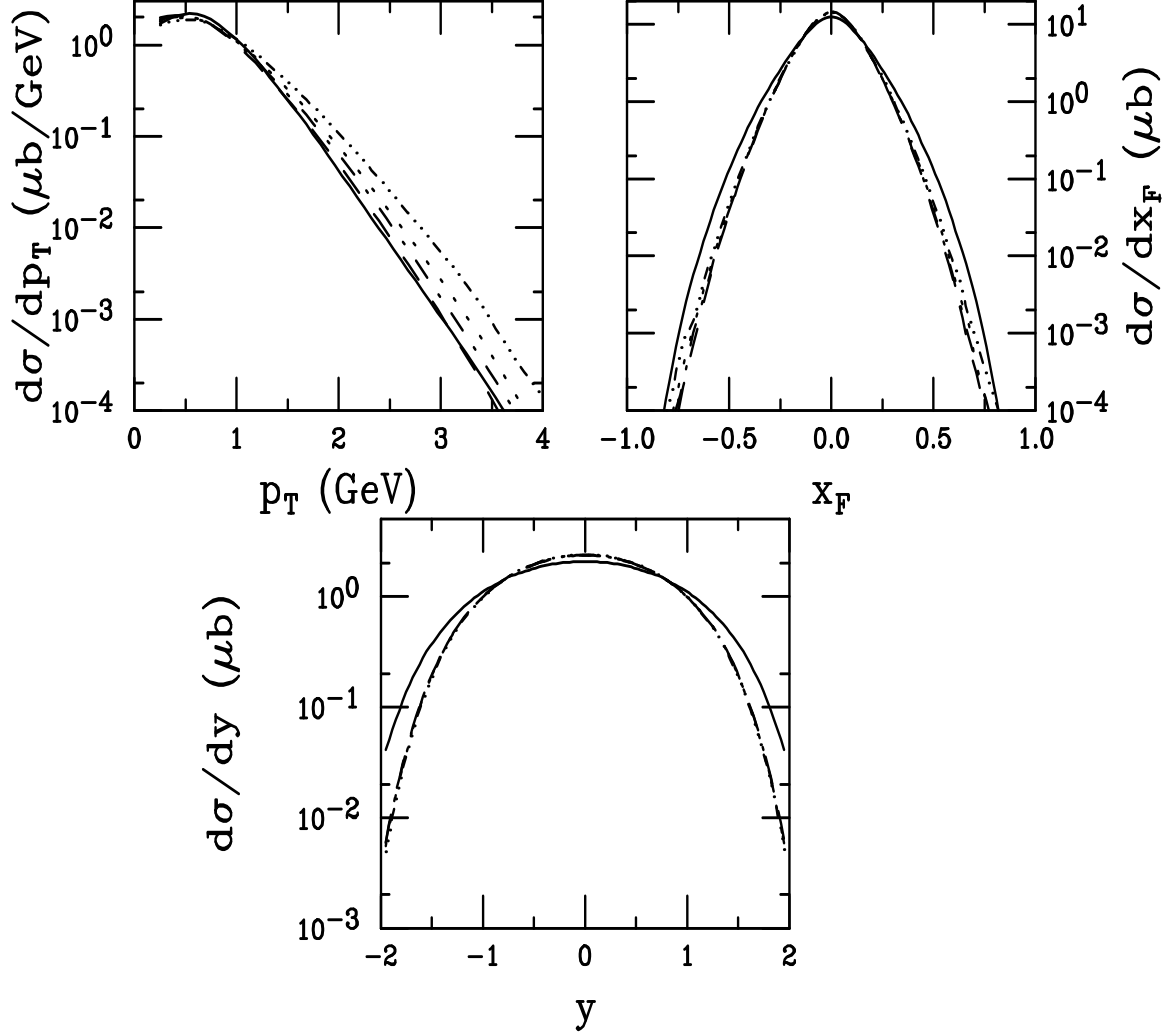


Figure 3: Effects of k_T broadening alone on inclusive NLO c quark production in pA interactions at 158 GeV as a function of p_T , x_F , and y . The per nucleon cross section is given. The curves are the bare quark distributions alone ($\langle k_T^2 \rangle_A = 0$ and no fragmentation) (solid) and, including fragmentation, $\langle k_T^2 \rangle = 1$ (dashed), 1.175 (dot-dashed), 1.35 (dotted) and 1.7 (dot-dot-dot-dashed) GeV^2 .

Nuclear shadowing

Experiments [28] have shown that the proton and neutron structure functions are modified in a nuclear environment. For momentum fractions $x < 0.1$ and $0.3 <$

$x < 0.7$, a depletion is observed in the nuclear parton distributions. The low x , or shadowing, region and the larger x , or EMC region, is bridged by an enhancement known as antishadowing for $0.1 < x < 0.3$. For simplicity, the entire characteristic modification as a function of x has been referred to as shadowing.

Shadowing is an area of intense study with numerous models available in the literature [28]. However, none of the models can satisfactorily explain the behavior of the nuclear parton distributions over the entire x and μ^2 range. Therefore, we choose to use parameterizations of shadowing based on nuclear DIS data. As in DIS with protons, the nuclear gluon distribution is not directly measured and can only be inferred from conservation rules. We use the recent EKS98 parameterization based on the GRV LO [7] parton densities in the proton. (See the contribution to this volume by K.J. Eskola *et al.* for further details.) Each parton type is evolved separately above $\mu_0 = 1.5$ GeV [29, 30]. The initial gluon distribution shows significant antishadowing for $0.1 < x < 0.3$ while the sea quark distributions are shadowed. Figure 4 compares shows the shadowing ratios at $\mu = \mu_0$ and $\mu = 10$ GeV. The valence ratio changes little with scale but the evolution of the gluon and sea ratios with scale is more significant. The gluon ratio changes somewhat more rapidly with scale than the sea ratio but the difference is not large. Less shadowing is seen in the antishadowing region at larger scales for the sea quark ratio while the gluon ratio decreases with scale in the same region. The effects of shadowing alone on the $D\bar{D}$ and $B\bar{B}$ decay contributions to the dilepton continuum have been studied in Ref. [31].

Shadowing should depend on the spatial location of the parton in the nucleus. Unfortunately, there is little data on this topic. One relevant experiment, Fermilab E745, studied the spatial distribution of nuclear parton densities with νN interactions in emulsion. The presence of one or more dark tracks from slow protons is used to infer a more central interaction [32]. For events with no dark tracks, no shadowing is observed while for events with dark tracks, shadowing is enhanced over other experimental measurements insensitive to the spatial location.

The spatial dependence of nuclear shadowing has been studied in charm and bottom production [33, 34]. While the effect can be important in peripheral collisions since nucleons near the nuclear surface are expected to behave as free particles, in central collisions where modifications are larger than average, this increase is $\sim 1\%$ over the average, negligible for our purposes.

Rates

All the results presented here are in units of cross section per nucleon pair. The total rates in pA and AA interactions are obtained by extrapolation. To calculate the rate of charm and bottom production in these interactions as a function of impact parameter, the per nucleon $Q\bar{Q}$ cross sections for pA interactions given in this paper should be multiplied by the nuclear profile function $T_A(b)$,

$$N_A^{Q\bar{Q}}(b) = \sigma_{pA}^{Q\bar{Q}} T_A(b) . \quad (25)$$

Likewise, the AA rates are found by multiplying the AA per nucleon cross section by

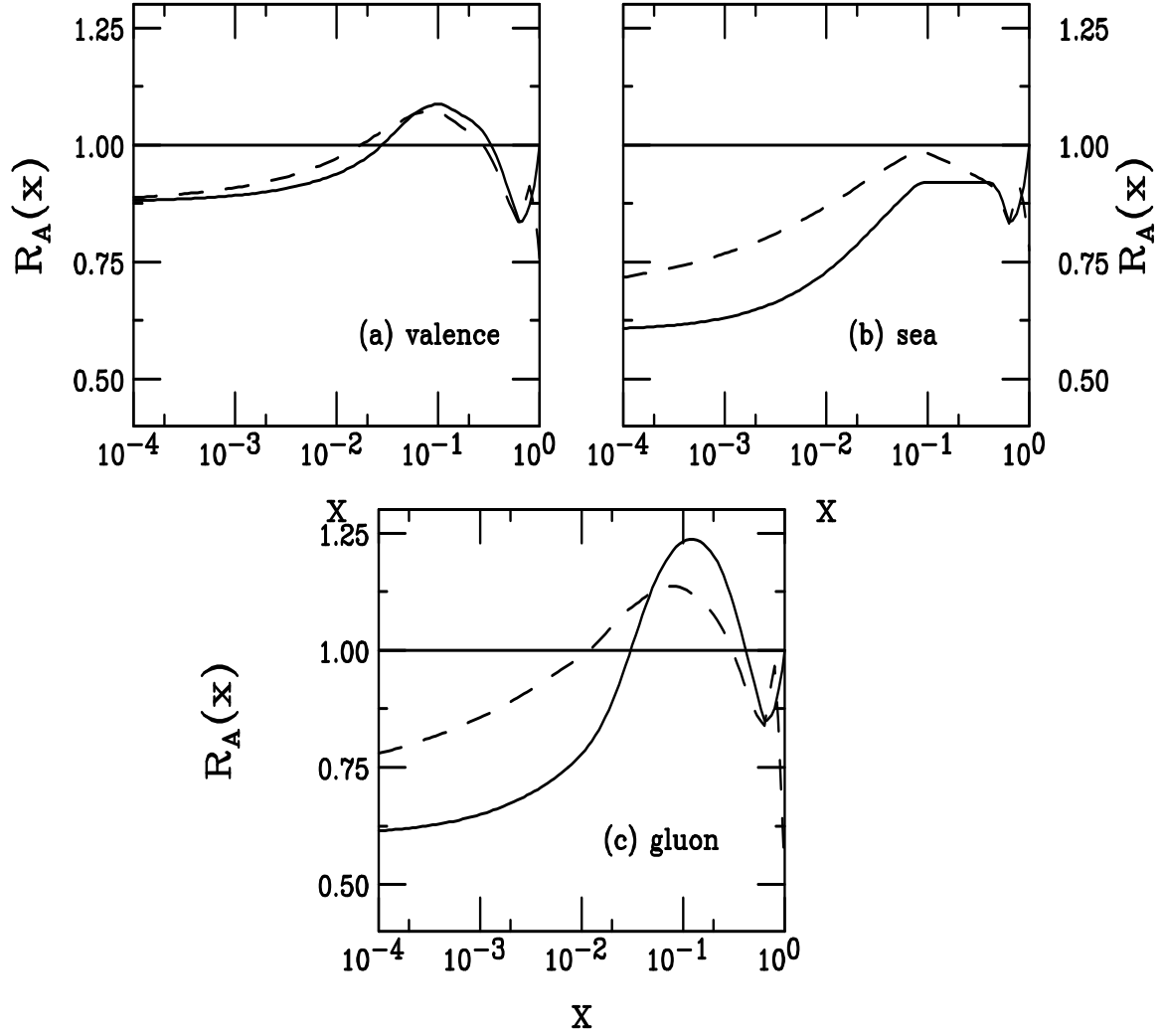


Figure 4: The shadowing parameterizations for $A = 200$ for (a) u_V valence quarks, (b) \bar{u} sea quarks, and (c) gluons. The solid curves show the ratios at $\mu = \mu_0$ while the dashed curves are at $\mu = 10$ GeV.

the nuclear overlap function, $T_{AA}(b) = \int d^2s T_A(s) T_A(|\vec{b} - \vec{s}|)$,

$$N_{AA}^{Q\bar{Q}}(b) = \sigma_{AA}^{Q\bar{Q}} T_{AA}(b) . \quad (26)$$

Thus, integrating over all impact parameters, the pA cross section should scale as A times the pp cross section and the AA cross section by A^2 times the pp cross section without any nuclear effects. Since the only nuclear effect discussed here that can change the total cross section is shadowing, total charm and bottom production should have a nearly linear A dependence. The exact A dependence is energy dependent because higher energies correspond to lower x and larger shadowing effects. One can maximize the A dependence by *e.g.* studying the rapidity distribution of low p_T $Q\bar{Q}$ pairs.

We note that in the case of pA interactions, the impact parameter dependence of charm and bottom production is the same as that of the geometric cross section. This similarity arises because the average number of collisions and the average number of participants is the same in pA interactions. In nucleus-nucleus collisions, hard production is biased toward central collisions, see Ref. [35] for more details.

Results

We will show inclusive charm and bottom and exclusive $c\bar{c}$ and $b\bar{b}$ distributions at several different energies. First we show fixed target charm production at 158, 450, and 800 GeV. These energies are chosen because Pb+Pb interactions are studied at the CERN SPS at 158 GeV/nucleon and it would be useful to examine charm production in pp and pPb interactions at the same energy. However, since this would require a secondary beam, we also show the results at the SPS primary proton beam energy of 450 GeV. The Fermilab fixed target program uses an 800 GeV proton beam which could also be employed in studies of the charm A dependence. Indeed, a great many experiments have studied charm production, both at CERN and at Fermilab, but unfortunately the statistics for proton beams have generally been poor and the newer results have not been used to determine the A dependence except in very limited regions of phase space. Better statistics are available for π beams but the data is typically averaged over all targets to enhance statistics rather than to study the A dependence. Since the RHIC and LHC heavy ion programs will include pA studies, we also show results at the complementary ion-ion energy, $\sqrt{s} = 200$ GeV/nucleon and 5.5 TeV/nucleon, respectively. Our AA results are only shown for RHIC and LHC energies.

All the pp calculations are shown with $\langle k_T^2 \rangle = 1 \text{ GeV}^2$ and all the pA calculations are presented with $\langle k_T^2 \rangle = 1.35 \text{ GeV}^2$ for charm and 2.57 GeV^2 for bottom. The AA results are calculated with $\langle k_T^2 \rangle = 1.7 \text{ GeV}^2$ for charm and 4.16 GeV^2 for bottom. We note that the $\langle k_T^2 \rangle$ values used for bottom are somewhat larger than may be suitable for the implementation in the MNR code. The pA and AA calculations are modified by spatially homogeneous shadowing with the EKS98 parameterization [29, 30] at $A = 200$.

We first show that the theoretical K factor, K_{th} , the ratio of the NLO to LO cross sections, both calculated with MRST HO in the MNR code is constant in pp and pA interactions at 158 GeV in Fig. 5. There is some variation near the edges of phase space where the statistics become poor. However, we have checked that neither shadowing nor k_T broadening leads to significant changes in K_{th} . The bare quark K_{th} has also been calculated at collider energies in Ref. [36] with the MRS D-’ distributions and was shown to be constant with quark p_T and x_F as well as pair mass and rapidity. The exact value of K_{th} depends on the set of parton distributions chosen and the interaction energy.

The exclusive and inclusive cross sections are shown for all energies considered in Figs. 6-19. The exclusive results are given for the pair p_T , rapidity, and ϕ distributions while the inclusive results are given as a function of quark p_T , x_F , and rapidity. Note that at collider energies, we do not show the x_F results since the distributions are very narrow at high energies and the rapidity distributions are thus more useful. The pair p_T and ϕ distributions and the quark p_T distribution all show the effect of k_T broadening in pA and AA over pp interactions. The broadening is most apparent at fixed target energies and at low p_T for the collider energies. The effect is always stronger on the pair quantities. On the other hand, information on nuclear shadowing is more likely to be obtained from the rapidity distributions. The most useful variable for studying shadowing effects is the pair rapidity distribution since Fig. 2 showed that neither k_T broadening nor fragmentation affects the pair rapidity. While the quark rapidity distribution in Fig. 3 did show a difference between the bare quark rapidity distribution and the distributions with k_T broadening included, the change is due to fragmentation rather than the k_T effect. Since shadowing is not symmetric around $y = 0$, we present results over all rapidity and x_F . Tables of the pair and single quark p_T and pair and single quark rapidity for the pp , pA and AA results are also given.

As the center of mass energy is increased, the effect of k_T broadening on the $c\bar{c}$ pair p_T and ϕ distributions is seen to diminish in Figs. 6, 8, 10, 12, and 16. At the same time, the pA pair rapidity distributions exhibit a depletion at forward x_F relative to the pp distribution. This effect, most obvious on the linear scale of Fig. 16, is due to shadowing and is biased toward forward rapidities where the smallest target x values are probed, $x_2 \sim 3 \times 10^{-6}$ for pairs with $p_T \sim 0$ and $y = 5$. The $b\bar{b}$ pair results in Figs. 14 and 18 exhibit the same basic trends. Note however that the $b\bar{b}$ pairs tend to have much larger p_T than the charm quarks. In AA collisions, the rapidity distributions are again symmetric about $y = 0$ because now negative rapidity corresponds to low x_1 and the shadowing results are thus essentially the product of the target shadowing (x_2) and the projectile shadowing (x_1).

The pair p_T is generally higher than for single quarks at any given energy. At NLO, large p_T $Q\bar{Q}$ pairs come from *e.g.* $gg \rightarrow gg$ jets where one final state gluon splits into $Q\bar{Q}$, $g \rightarrow Q\bar{Q}$. In this way, the pair gets the entire p_T of the gluon while the single quark gets only a fraction of the gluon p_T . Conversely the single quark rapidity is generally greater than that of the pair. That is because $y_{Q\bar{Q}} = 1/2 \ln((E_Q + E_{\bar{Q}} + p_{zQ} + p_{z\bar{Q}})/(E_Q + E_{\bar{Q}} - p_{zQ} - p_{z\bar{Q}}))$ so that if p_{zQ} is large and

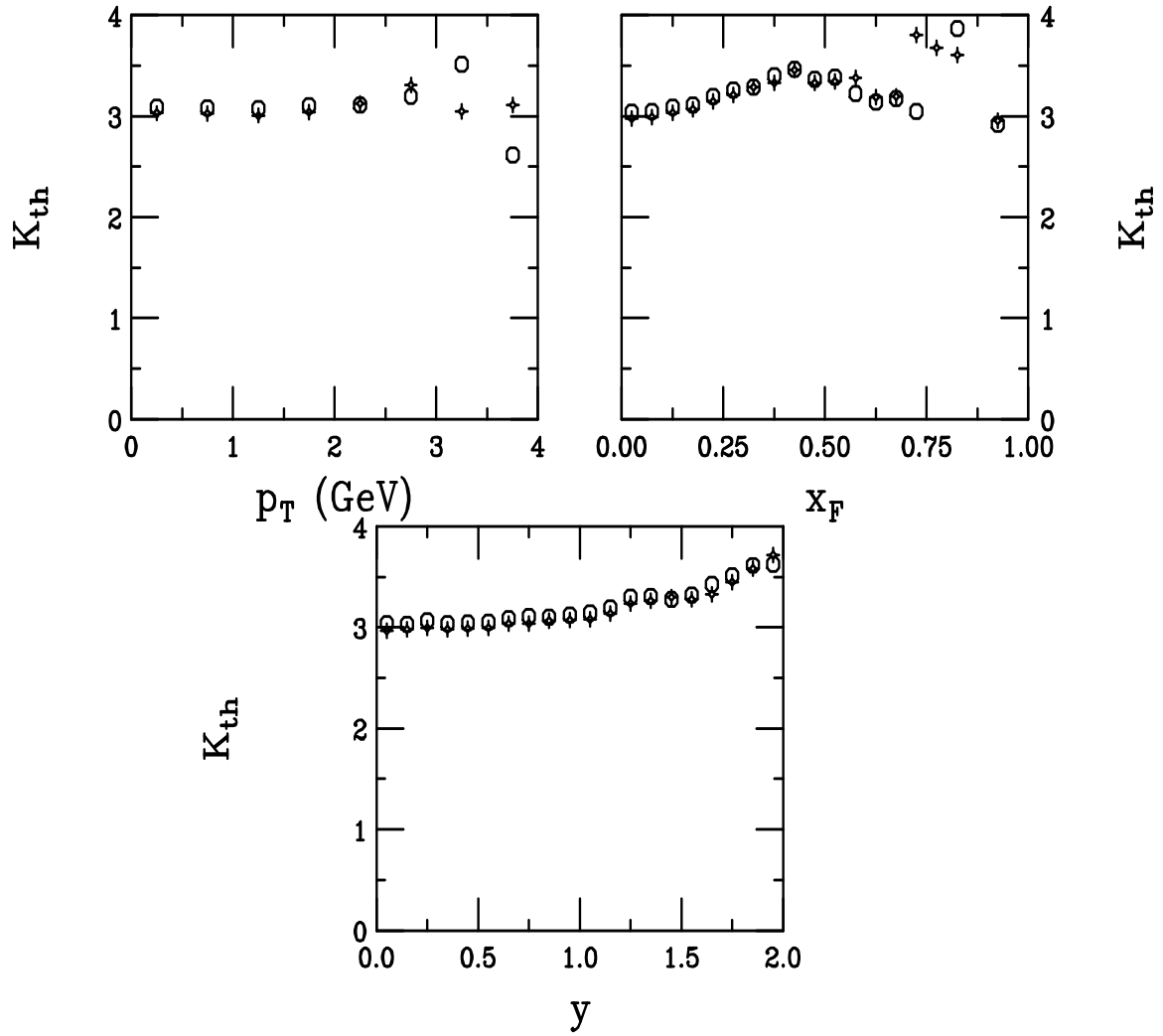


Figure 5: Ratio of NLO to LO c quark production in pp and pA interactions at 158 GeV as a function of p_T , x_F , and y . The crosses are the pp results while the circles are the pA results.

positive, it may be balanced by a large negative $p_{z\bar{Q}}$. The single quark nuclear effects show the same trends as those of the pair. Note that the single quark p_T distributions are all for $x_F > 0$ only.

Figure 20 shows the effect of shadowing alone on the pA/pp ratios of the bare charm quark distributions at 158 GeV. Without k_T broadening, the ratio decreases with p_T since $x_2 \sim 0.5$ at $y = 0$, well into the EMC region where the shadowing ratio decreases with x . The effect at low p_T can be observed in the x_F and y ratios where the ratios tend to be greater than unity since x_2 is in the antishadowing region, $x_2 \sim 0.14$ at $y = 0$ and ~ 0.05 at $y = 1$, still in the antishadowing region for gluons with low μ^2 . The LO and NLO ratios, both calculated with MRST HO, are quite similar so that the order of the calculation is not strongly influenced by shadowing.

Since the differences between the distributions are not always obvious in Figs. 6-19, we have also calculated the pA to pp ratios in Figs. 21-30 and 35-38 and the AA to pp ratios at the same energies in Figs. 31-34 and 39-42. The pair and single quark p_T ratios reflect the effects of the k_T broadening, as do the x_F distributions for $|x_F| > 0.5$. The k_T broadening follows the energy dependent trend predicted in Ref. [37]. The pA/pp ratio increases with p_T at low energies and, as the energy increases, begins to turn over at pair $p_T \sim 3.5 - 4$ GeV for charm, decreasing to unity at large pair p_T . This turnover is at ~ 5 GeV for bottom. As the energy increases, shadowing becomes more important at low p_T , decreasing the ratio below unity in this region. The magnitude of this decrease is a good indication of the strength of gluon shadowing, particularly for the pair. While the single quark ratios follow the trends of the pair ratios at low p_T , the lower statistics of the Monte Carlo at high p_T lead to large fluctuations. We have checked that taking the single p_T ratio for all x_F rather than $x_F > 0$, as is shown in the figures, neither strongly influences the final results nor significantly reduces the fluctuations. These fluctuations are particularly strong in $c\bar{c}$ production at $\sqrt{s} = 5.5$ TeV where both the pair and single charm p_T distributions decrease 4-5 orders of magnitude over the p_T interval shown. The ϕ ratios decrease as ϕ goes from 0 to π because the larger k_T kick in pA flattens this distribution relative to pp so that $pA/pp > 1$ at $\phi \sim 0$ and less than unity at $\phi \sim \pi$, compare Fig. 6 to Fig. 21. The general trend is similar for all energies because variables more sensitive to shadowing are integrated over. The AA/pp ratios exhibit the same trends except that the depletion at low p_T is stronger and the enhancement is larger before the turnover than in the pA/pp ratios. The position of the maximum enhancement is not significantly changed. The stronger depletion at low p_T is, in part, due to nuclear shadowing while the change in the relative enhancement between pA/pp and AA/pp is due to the larger $\langle k_T^2 \rangle$ in AA collisions.

On the other hand, the pA/pp rapidity ratios follow the gluon ratios shown in Fig. 4. The peak at $x \rightarrow 1$ from Fermi motion appears at large negative rapidity, followed by the dip in the EMC region, a broad peak tracing out the antishadowing region, and finally decreasing again as the shadowing region is reached at large, positive rapidity. The shape is inverted from that in Fig. 4 because large x corresponds to large negative rapidity and low x to large positive rapidity. The strength of the shadowing effect increases as energy increases while the antishadowing peak, broad at 158 GeV, narrows with increasing energy. At collider energies, the full rapidity

distribution is not shown in the plots so that the x distribution of Fig. 4 is somewhat truncated. Both the single and pair rapidity distributions follow the shape of the gluon shadowing ratio, suggesting that either can help elucidate gluon modifications in the nucleus without significant distortion from k_T broadening which affects the x_F ratios. The AA/pp rapidity ratios show the shadowing in both the target and projectile. Now, in addition to the shadowing function for the target nucleus, there is a shadowing function for the projectile nucleus that is essentially that of Fig. 4 since here low x corresponds to large negative rapidity. Thus the AA/pp ratios are symmetric around $y = 0$.

Conclusions

We have studied the effects of k_T broadening and nuclear shadowing on charm and bottom production over a wide range of energies. We have found that the $Q\bar{Q}$ p_T , the single quark p_T , and the pair ϕ distribution are most sensitive to the effects of k_T broadening while the pair and single quark rapidities are sensitive to shadowing. There is significantly less distortion of the nuclear effects in the pair distributions which are the most difficult to measure. The same results may be obtained through measurements of the single heavy quarks even though the definitions of x and k_T are smeared relative to those of the pair.

References

- [1] P.L. McGaughey *et al.*, Int. J. Mod. Phys. **A10** (1995) 2999.
- [2] N. Kidonakis, E. Laenen, S. Moch, and R. Vogt, hep-ph/0105041.
- [3] M. Glück, J.F. Owens, and E. Reya, Phys. Rev. **D17** (1978) 2324.
- [4] M.L. Mangano, P. Nason, and G. Ridolfi, Nucl. Phys. **B373** (1992) 295.
- [5] M. Derrick *et al.* (ZEUS Collab.), Phys. Lett. **B316** (1993) 515.
- [6] A.D. Martin, W.J. Stirling and R.G. Roberts, Phys. Lett. **306B**, 145 (1993).
- [7] M. Glück, E. Reya, and A. Vogt, Z. Phys. **C53** 127, (1992).
- [8] C. Adloff *et al.* (H1 Collab.), Nucl. Phys. **B497** 3, (1997); J. Breitweg *et al.* (ZEUS Collab.), Eur. Phys. J. **C7** 609, (1999).
- [9] H. Plathow-Besch, ‘PDFLIB: Proton, Pion and Photon Parton Density Functions, Parton Density Functions of the Nucleus, and α_s Calculations’, Users’s Manual - Version 8.04, W5051 PDFLIB, 2000.04.17, CERN-ETT/TT.
- [10] A.D. Martin, R.G. Roberts, and W.J. Stirling, and R.S. Thorne, Eur. Phys. J. **C4** (1998) 463.

- [11] A.D. Martin, R.G. Roberts, and W.J. Stirling, and R.S. Thorne, Phys. Lett. **B443** (1998) 301.
- [12] S.P.K. Tavernier, Rep. Prog. Phys. **50** (1987) 1439. This review contains references to all data prior to 1988, including the ISR measurements.
- [13] R. Ammar *et al.* (LEBC-MPS Collab.), Phys. Rev. Lett. **61** (1988) 2185.
- [14] K. Kodama *et al.* (E653 Collab.), Phys. Lett. **B263** (1991) 573.
- [15] M. Aguilar-Benitez *et al.* (LEBC-EHS Collab.), Z. Phys. **C40** (1988) 321.
- [16] S. Barlag *et al.* (ACCMOR Collab.), Z. Phys. **C39** (1988) 451.
- [17] S. Frixione, M.L. Mangano, P. Nason, and G. Ridolfi, Nucl. Phys. **B431** (1994) 453.
- [18] C. Peterson, D. Schlatter, I. Schmitt, and P. Zerwas, Phys. Rev. **D27** (1983) 105.
- [19] J. Chirn, in proceedings of the ‘International Symposium on the Production and Decay of Heavy Flavors’, Stanford, CA, E. Bloom and A. Fridman editors, (1987) p. 131.
- [20] R.D. Field, *Applications of Perturbative QCD*, Frontiers in Physics Lectures, Vol. 77 (Addison-Wesley, Reading, MA, 1989).
- [21] J.F. Owens, Rev. Mod. Phys. **59** (1987) 465.
- [22] S. Frixione, M.L. Mangano, P. Nason, and G. Ridolfi, in ‘Heavy flavours II’, A.J. Buras and M. Lindner editors, (World Scientific, 1997) p. 609, hep-ph/9702287.
- [23] D.M. Alde *et al.* (E772 Collab.), Phys. Rev. Lett. **66** (1991) 2285.
- [24] J. Badier *et al.* (NA3 Collab.), Z. Phys. **C20** (1983) 101.
- [25] X.-N. Wang, Phys. Rev. Lett. **81** (1998) 2655.
- [26] S. Gavin and M. Gyulassy, Phys. Lett. **B214** (1988) 241; J. Hüfner, Y. Kurihara, and H.J. Pirner, Phys. Lett. **B215** (1988) 218; J.-P. Blaizot and J.-Y. Ollitrault, Phys. Lett. **B217** (1989) 392.
- [27] Z. Lin and R. Vogt, Nucl. Phys. **B544** (1999) 339.
- [28] J.J. Aubert *et al.* (EM Collab.), Nucl. Phys. **B293** 740, (1987); M. Arneodo, Phys. Rep. **240** 301, (1994).
- [29] K.J. Eskola, V.J. Kolhinen and P.V. Ruuskanen, Nucl. Phys. **B535** 351, (1998).
- [30] K.J. Eskola, V.J. Kolhinen and C.A. Salgado, Eur. Phys. J. **C9** (1999) 61.

- [31] K.J. Eskola, V.J. Kolhinen and R. Vogt, hep-ph/0104124, Nucl. Phys. **A**, in press.
- [32] T. Kitagaki *et al.* (E745 Collab.), Phys. Lett. **214** (1988) 281.
- [33] V. Emel'yanov, A. Khodinov, S.R. Klein and R. Vogt, Phys. Rev. **C56**, 2726 (1997).
- [34] V. Emel'yanov, A. Khodinov, S.R. Klein and R. Vogt, Phys. Rev. Lett. **81**, 1801 (1998).
- [35] R. Vogt, Heavy Ion Phys. **9** (1999) 339.
- [36] R. Vogt, Z. Phys. **C71** (1996) 475.
- [37] X.-N. Wang, Phys. Rev. **C61** (2000) 064910.

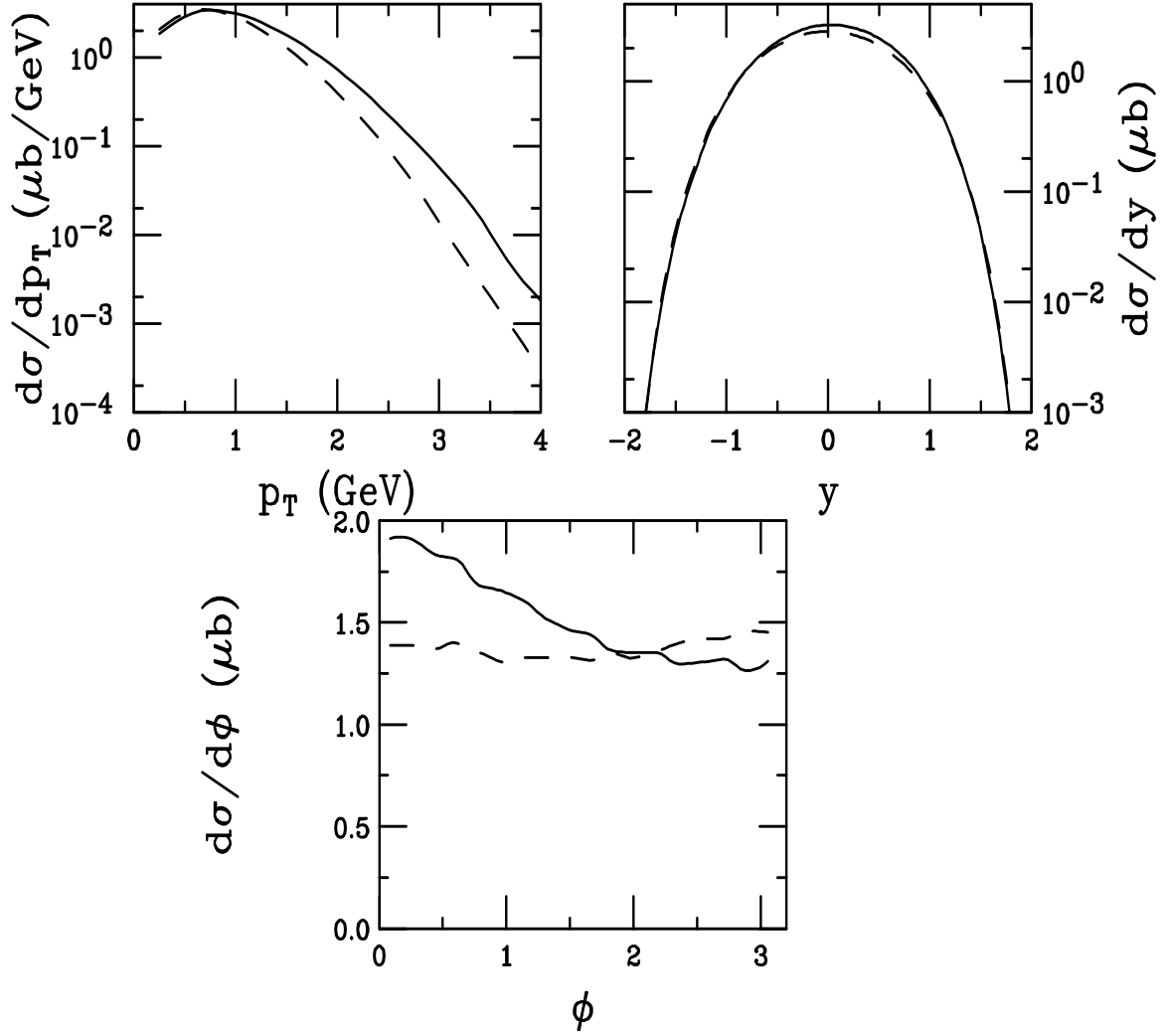


Figure 6: Exclusive NLO $c\bar{c}$ pair production in pp and pA interactions at 158 GeV as a function of p_T , y , and ϕ . The per nucleon cross section is given for pA interactions. The dashed curves are the pp results while the solid curves are the pA results.

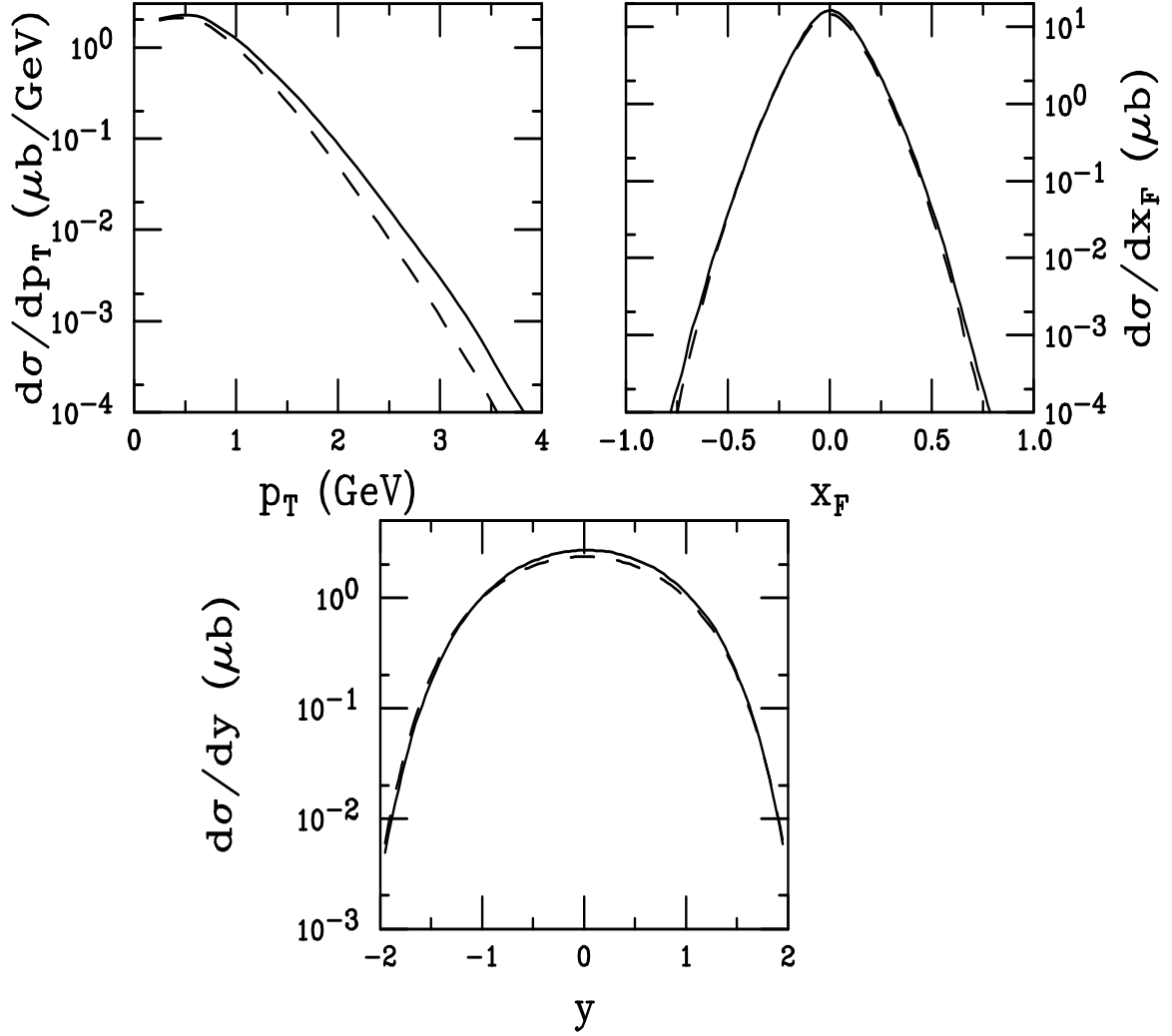


Figure 7: Inclusive NLO c quark production in pp and pA interactions at 158 GeV as a function of p_T , x_F , and y . The p_T distributions are integrated over $x_F > 0$ only. The per nucleon cross section is given for pA interactions. The dashed curves are the pp results while the solid curves are the pA results.

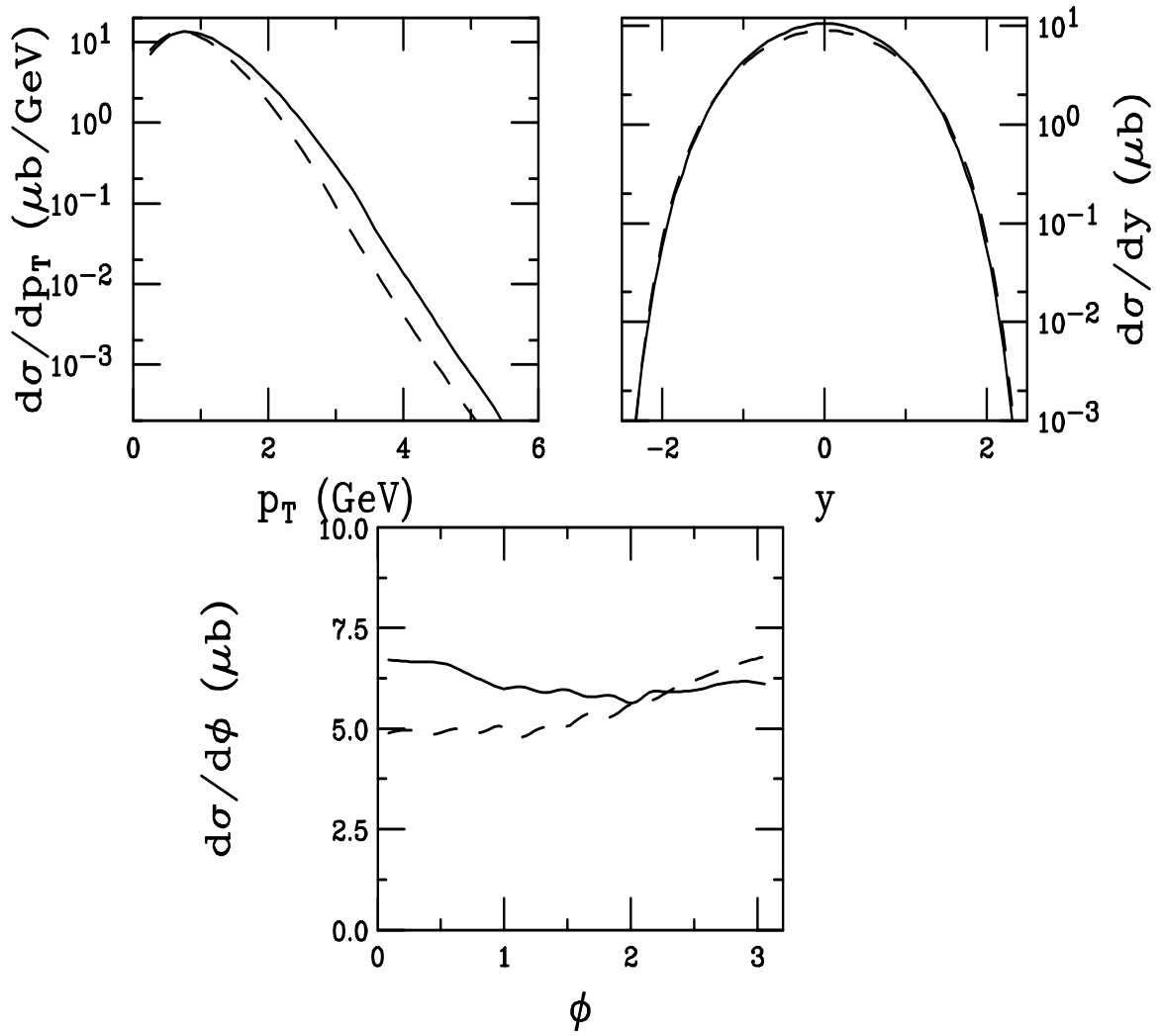


Figure 8: Exclusive NLO $c\bar{c}$ pair production in pp and pA interactions at 450 GeV as a function of p_T , y , and ϕ . The per nucleon cross section is given for pA interactions. The dashed curves are the pp results while the solid curves are the pA results.

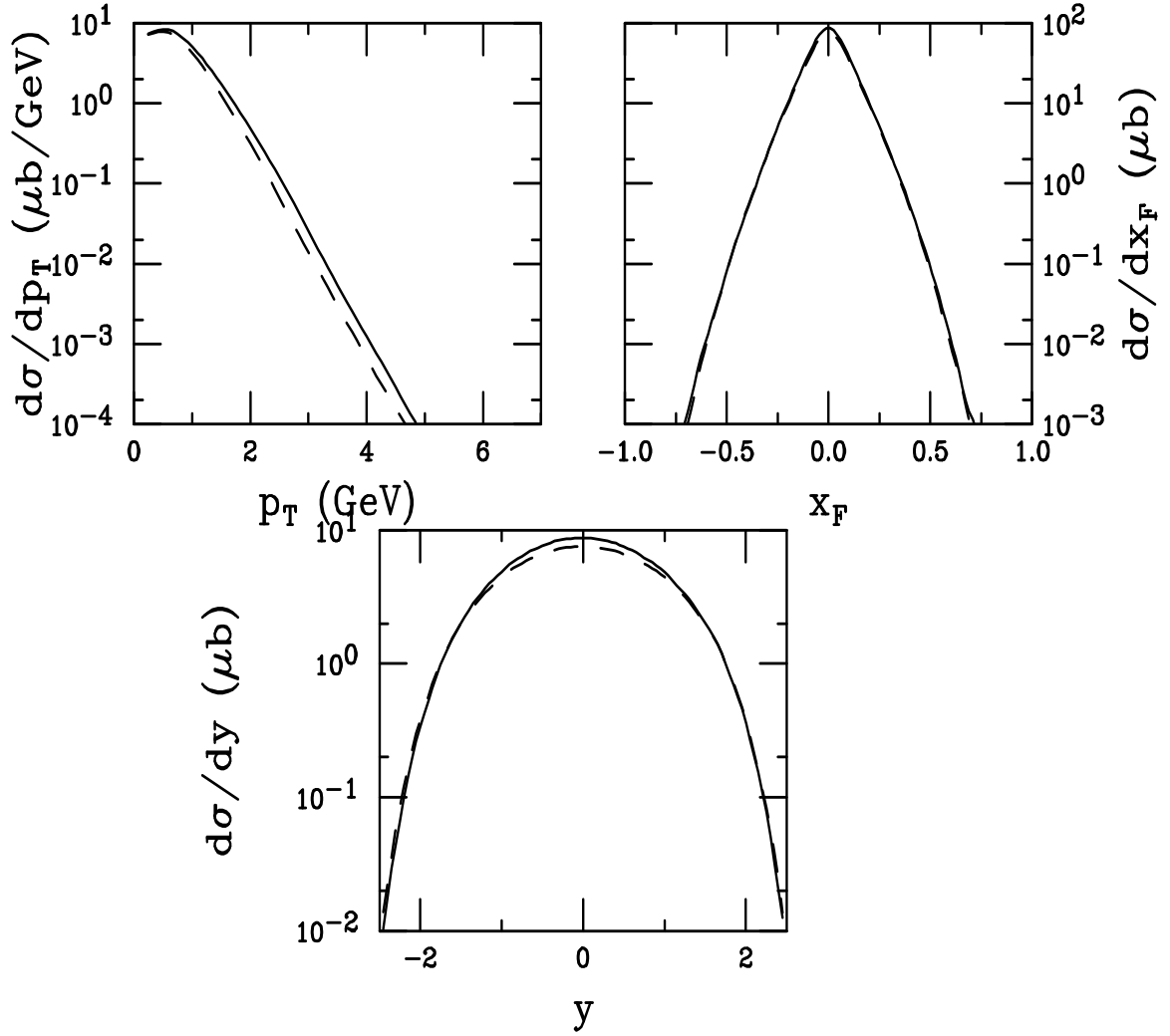


Figure 9: Inclusive NLO c quark production in pp and pA interactions at 450 GeV as a function of p_T , x_F , and y . The p_T distributions are integrated over $x_F > 0$ only. The per nucleon cross section is given for pA interactions. The dashed curves are the pp results while the solid curves are the pA results.

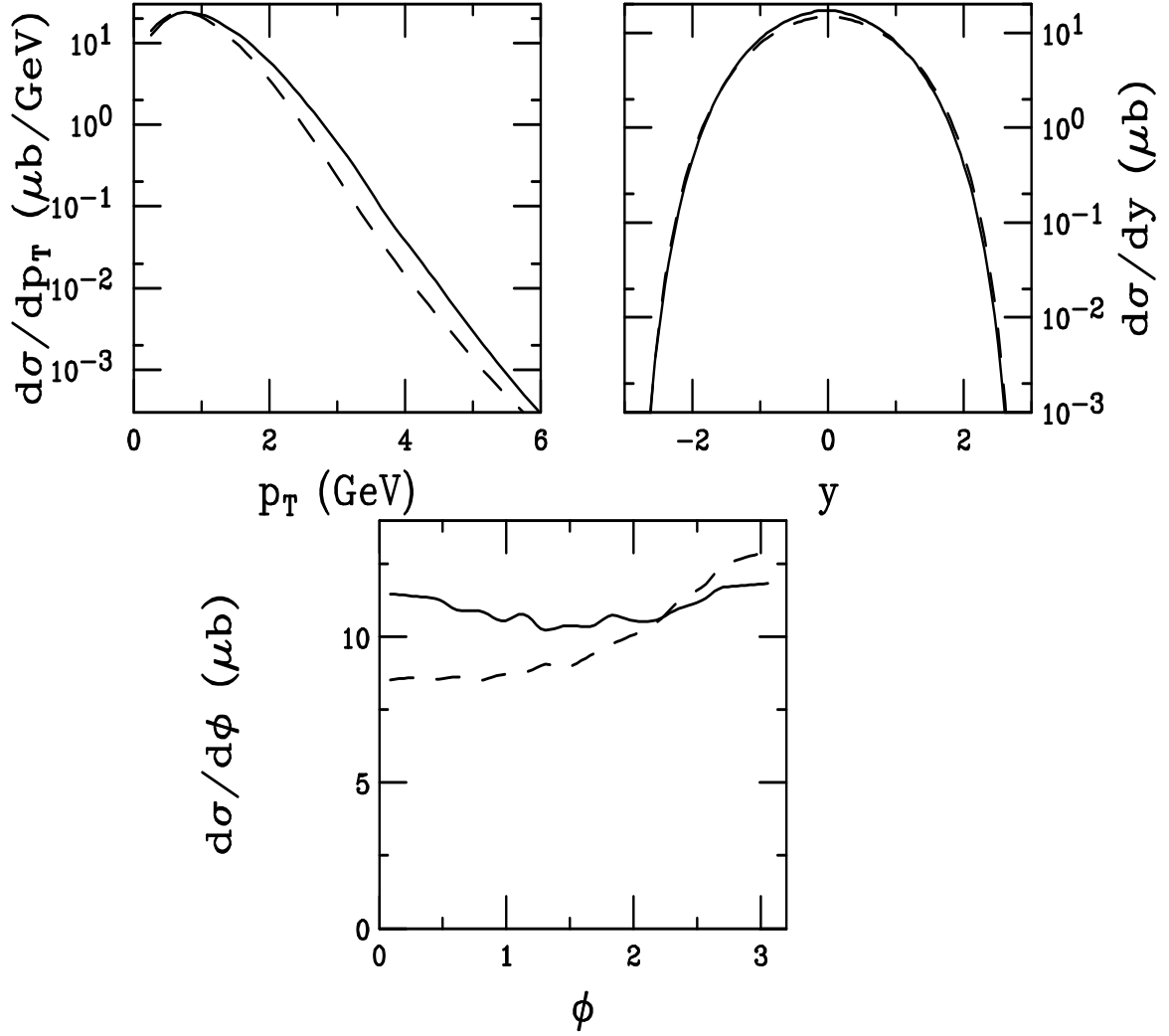


Figure 10: Exclusive NLO $c\bar{c}$ pair production in pp and pA interactions at 800 GeV as a function of p_T , y , and ϕ . The per nucleon cross section is given for pA interactions. The dashed curves are the pp results while the solid curves are the pA results.

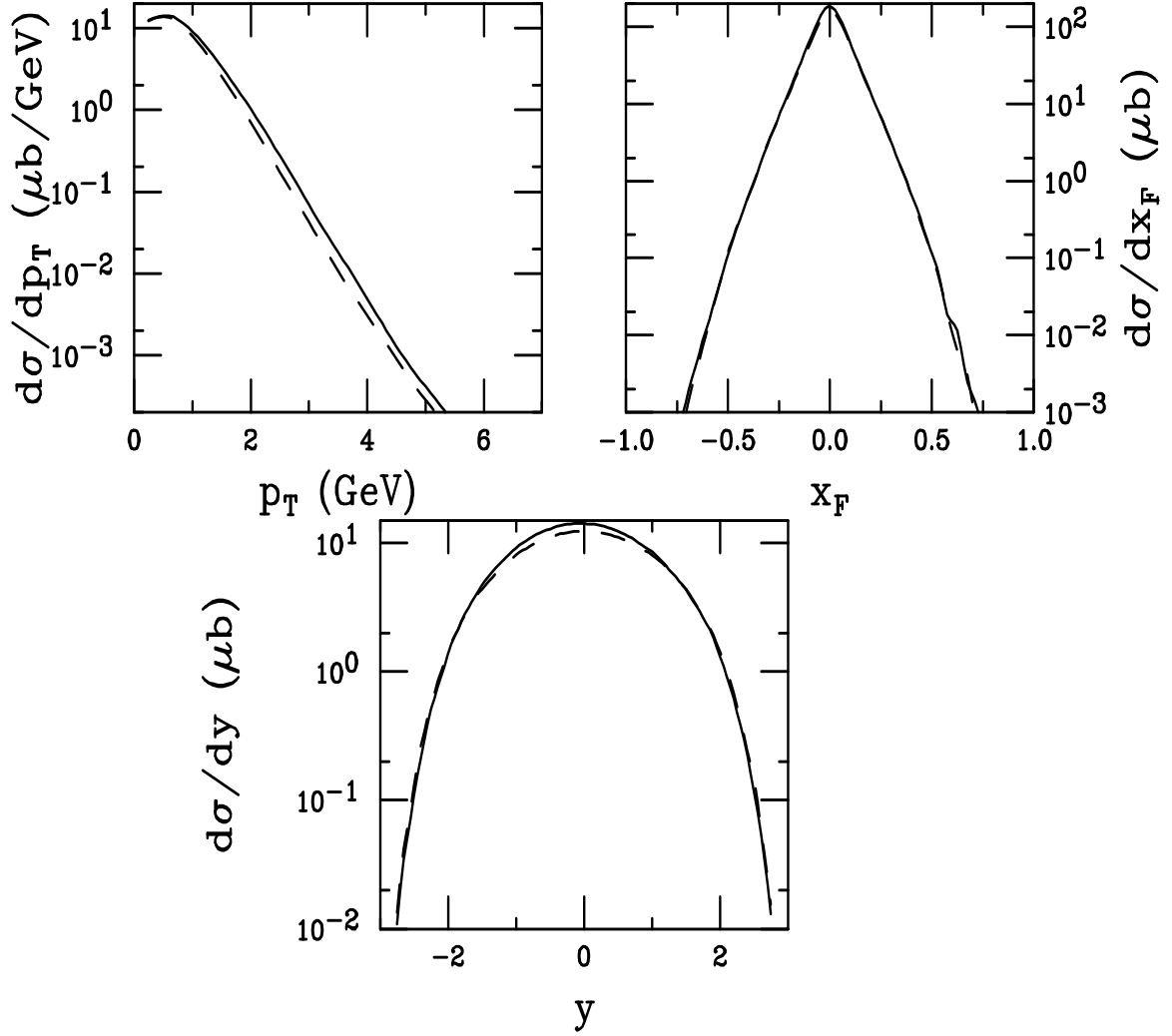


Figure 11: Inclusive NLO c quark production in pp and pA interactions at 800 GeV as a function of p_T , x_F , and y . The p_T distributions are integrated over $x_F > 0$ only. The per nucleon cross section is given for pA interactions. The dashed curves are the pp results while the solid curves are the pA results.

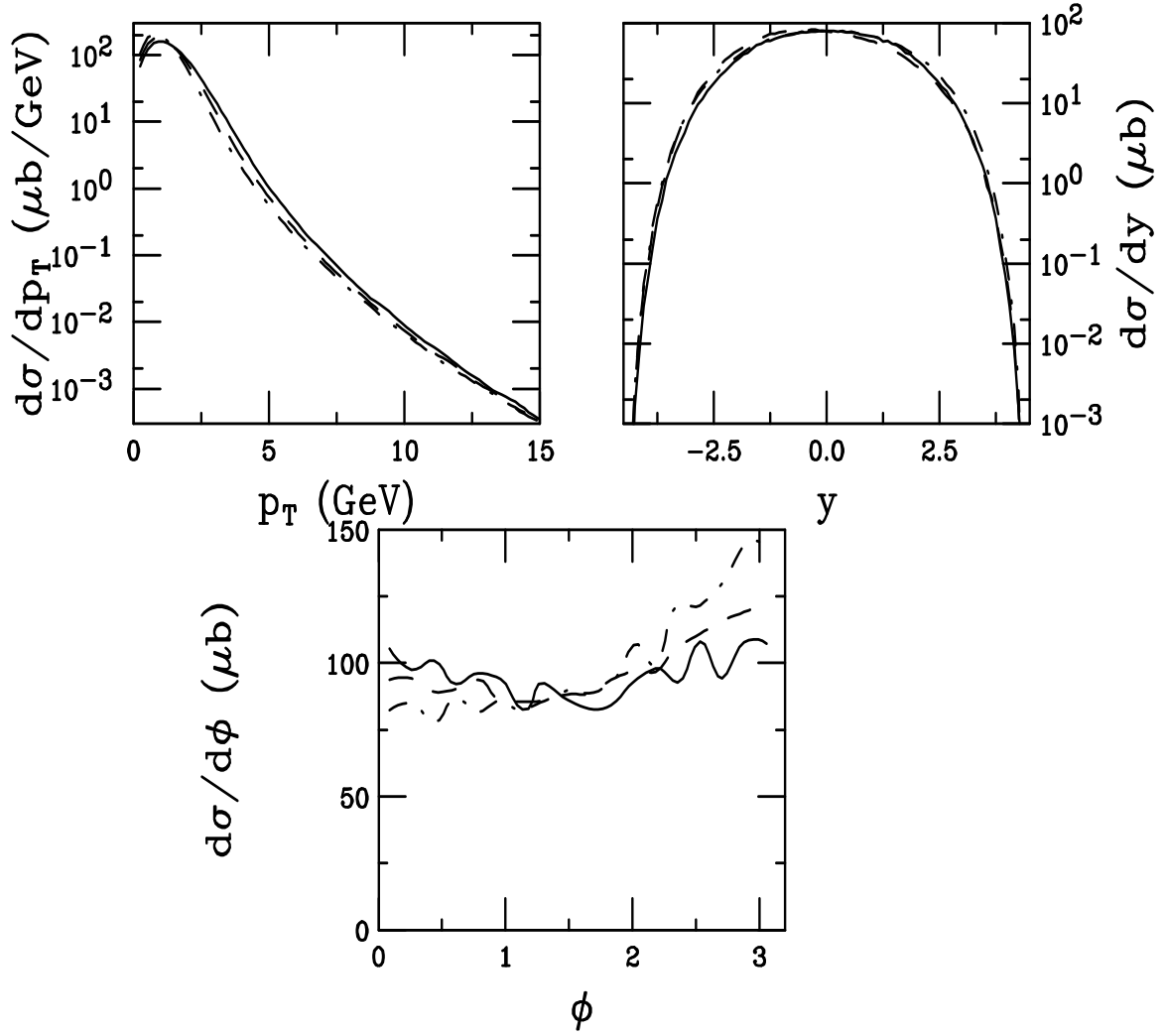


Figure 12: Exclusive NLO $c\bar{c}$ pair production in pp , pA and AA interactions at $\sqrt{s} = 200$ GeV as a function of p_T , y , and ϕ . The per nucleon cross section is given for pA and AA interactions. The dot-dashed curves are the pp results, the dashed curves are the pA results, and the solid curves are the AA results.

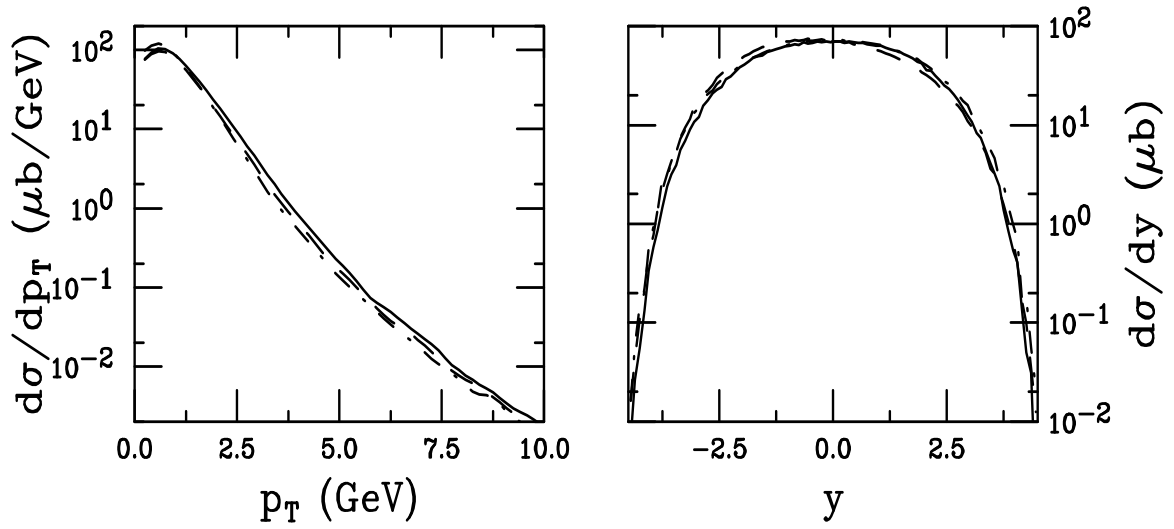


Figure 13: Inclusive NLO c quark production in pp , pA and AA interactions at $\sqrt{s} = 200$ GeV as a function of p_T and y . The p_T distributions are integrated over $x_F > 0$ only. The per nucleon cross section is given for pA and AA interactions. The dot-dashed curves are the pp results, the dashed curves are the pA results, and the solid curves are the AA results.

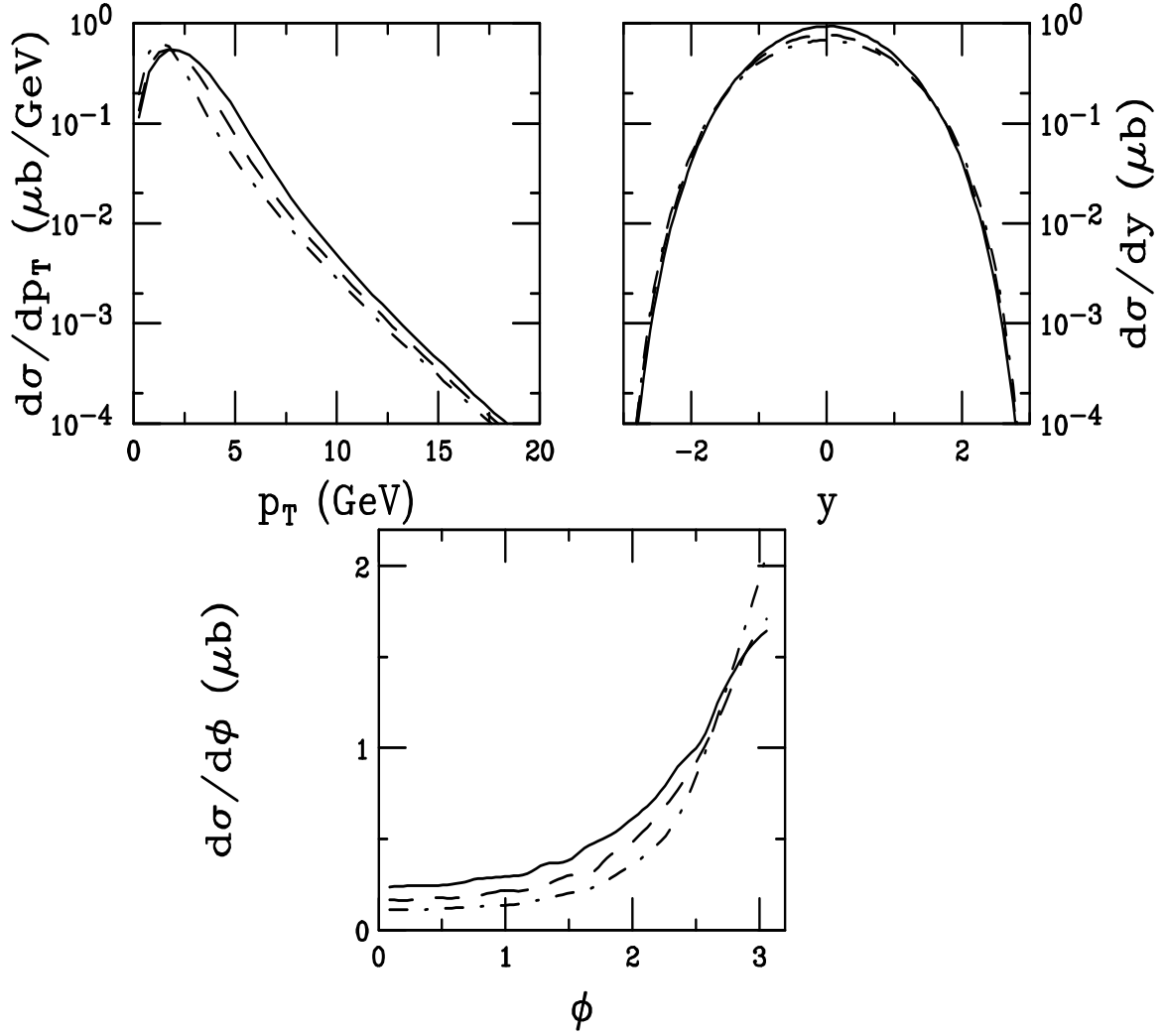


Figure 14: Exclusive NLO $b\bar{b}$ pair production in pp , pA and AA interactions at $\sqrt{s} = 200$ GeV as a function of p_T , y , and ϕ . The per nucleon cross section is given for pA and AA interactions. The dot-dashed curves are the pp results, the dashed curves are the pA results, and the solid curves are the AA results.

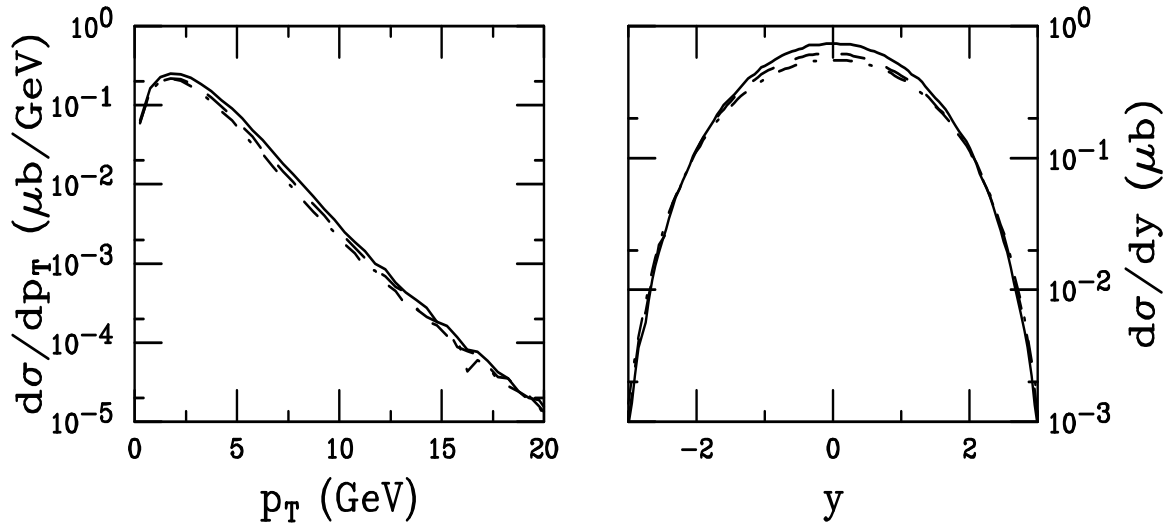


Figure 15: Inclusive NLO b quark production in pp , pA and AA interactions at $\sqrt{s} = 200$ GeV as a function of p_T and y . The p_T distributions are integrated over $x_F > 0$ only. The per nucleon cross section is given for pA and AA interactions. The dot-dashed curves are the pp results, the dashed curves are the pA results, and the solid curves are the AA results.

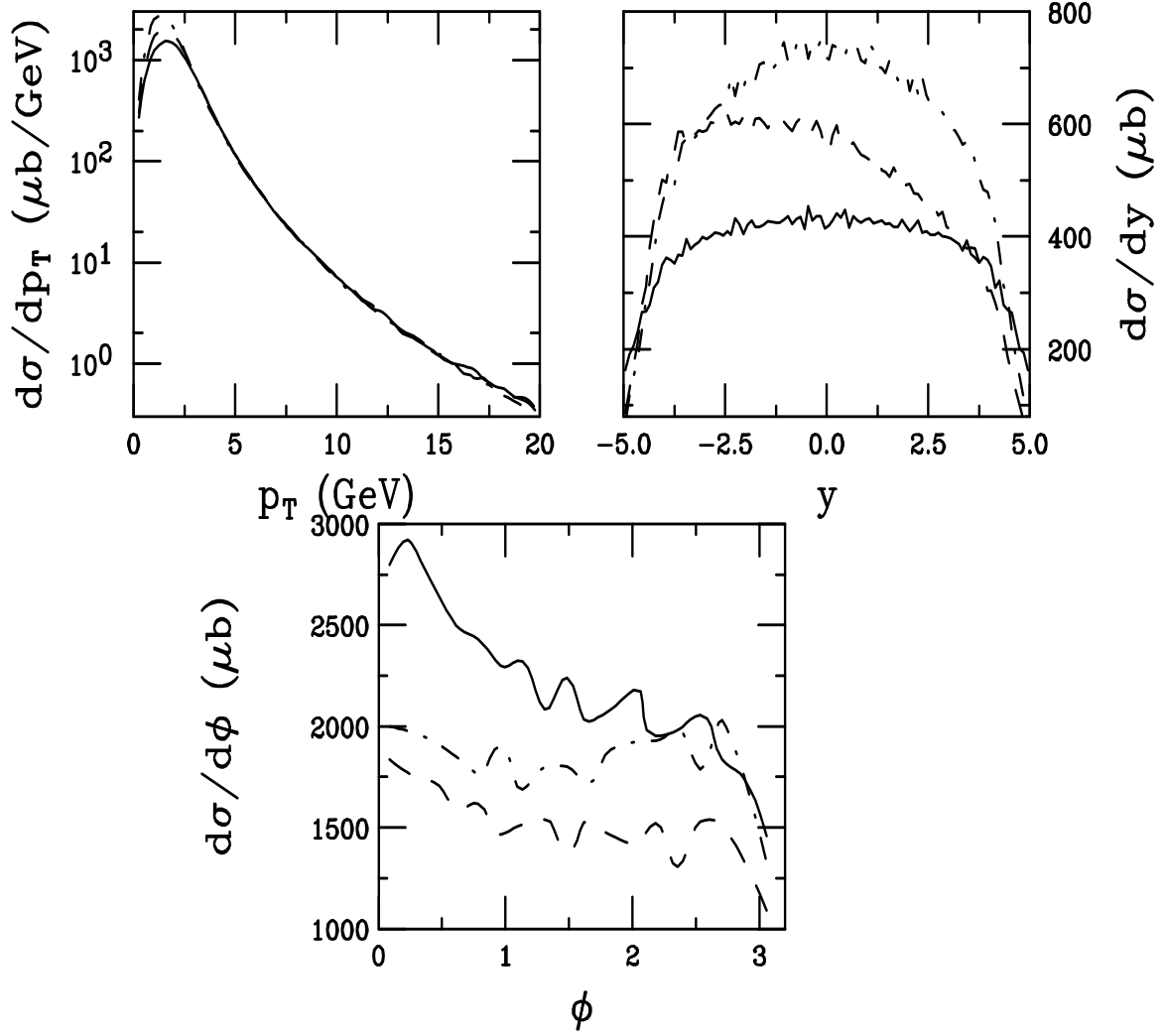


Figure 16: Exclusive NLO $c\bar{c}$ pair production in pp , pA and AA interactions at $\sqrt{s} = 5.5$ TeV as a function of p_T , y , and ϕ . The per nucleon cross section is given for pA and AA interactions. The dot-dashed curves are the pp results, the dashed curves are the pA results, and the solid curves are the AA results.

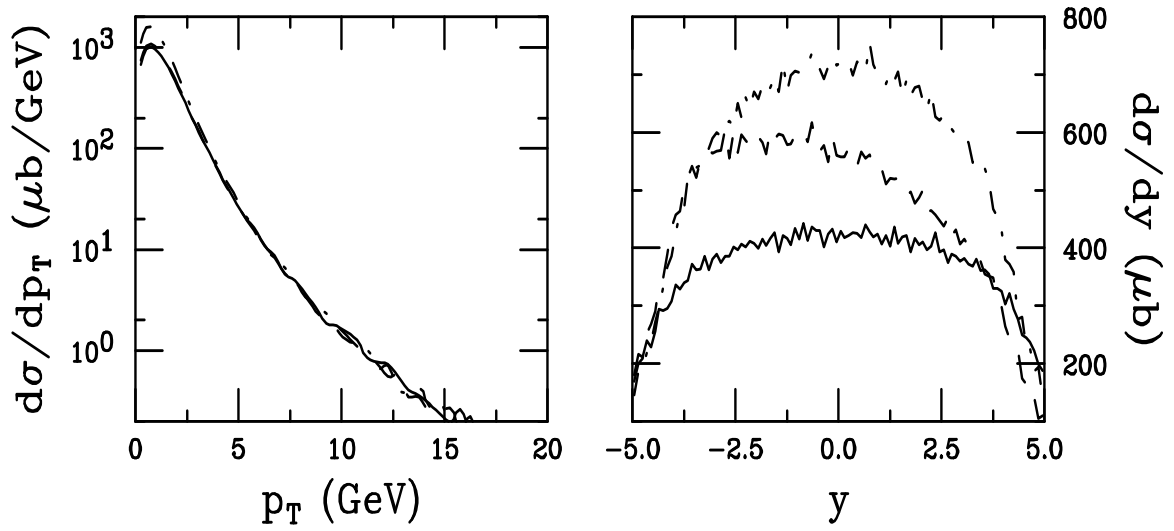


Figure 17: Inclusive NLO c quark production in pp , pA and AA interactions at $\sqrt{s} = 5.5$ TeV as a function of p_T and y . The p_T distributions are integrated over $x_F > 0$ only. The per nucleon cross section is given for pA and AA interactions. The dot-dashed curves are the pp results, the dashed curves are the pA results, and the solid curves are the AA results.

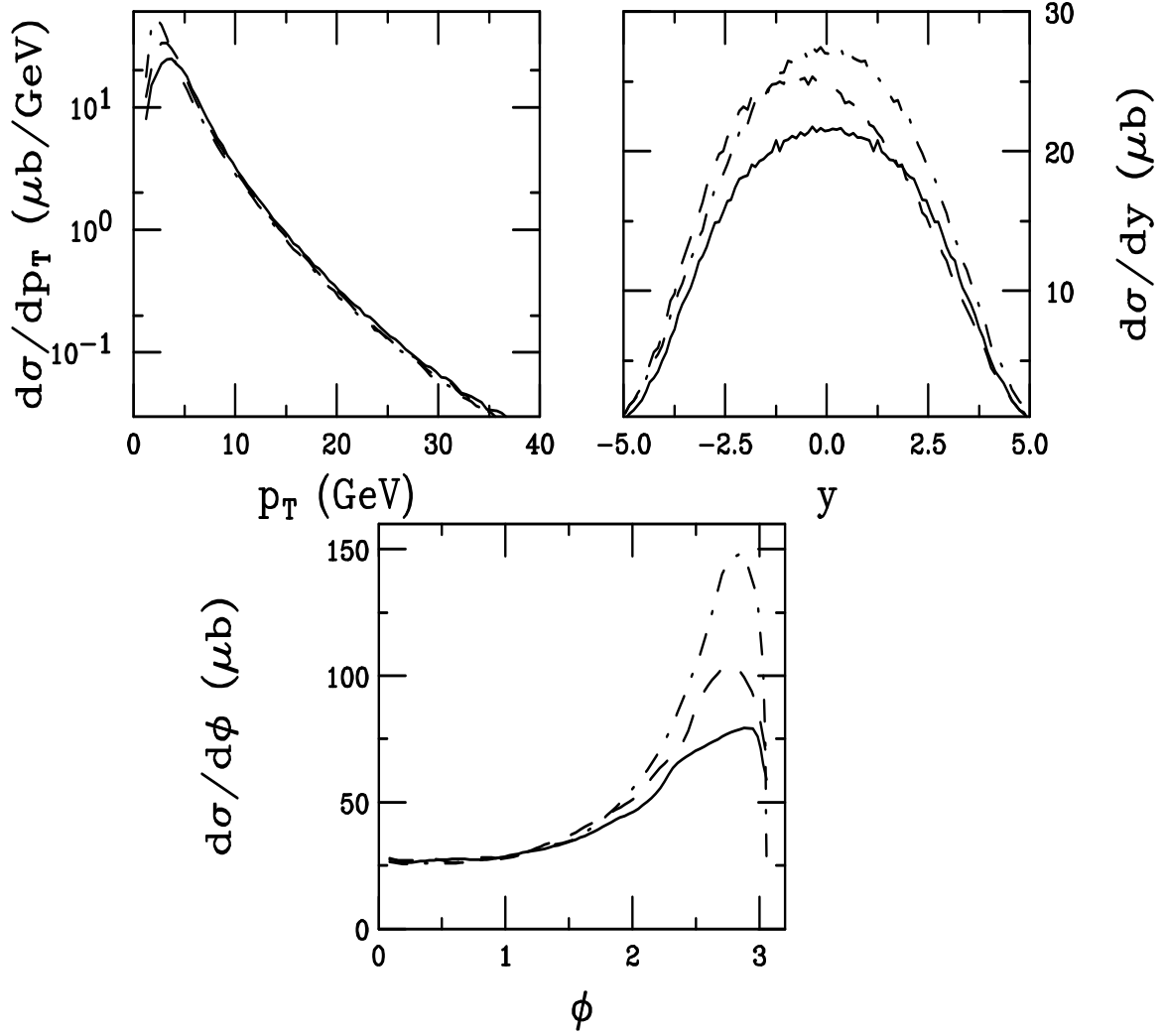


Figure 18: Exclusive NLO $b\bar{b}$ pair production in pp , pA and AA interactions at $\sqrt{s} = 5.5$ TeV as a function of p_T , y , and ϕ . The per nucleon cross section is given for pA and AA interactions. The dot-dashed curves are the pp results, the dashed curves are the pA results, and the solid curves are the AA results.

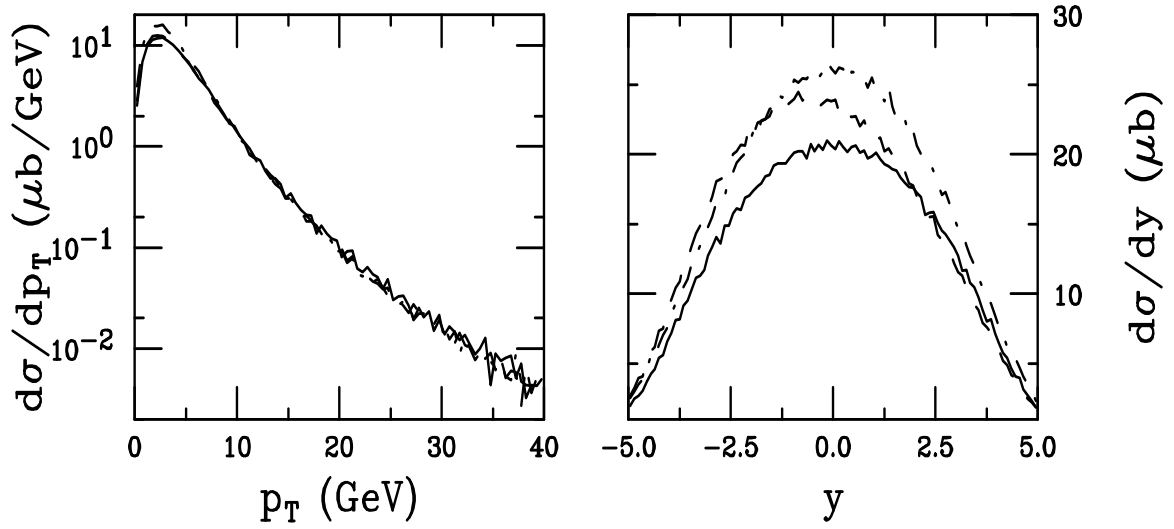


Figure 19: Inclusive NLO b quark production in pp , pA and AA interactions at $\sqrt{s} = 5.5$ TeV as a function of p_T and y . The p_T distributions are integrated over $x_F > 0$ only. The per nucleon cross section is given for pA and AA interactions. The dot-dashed curves are the pp results, the dashed curves are the pA results, and the solid curves are the AA results.

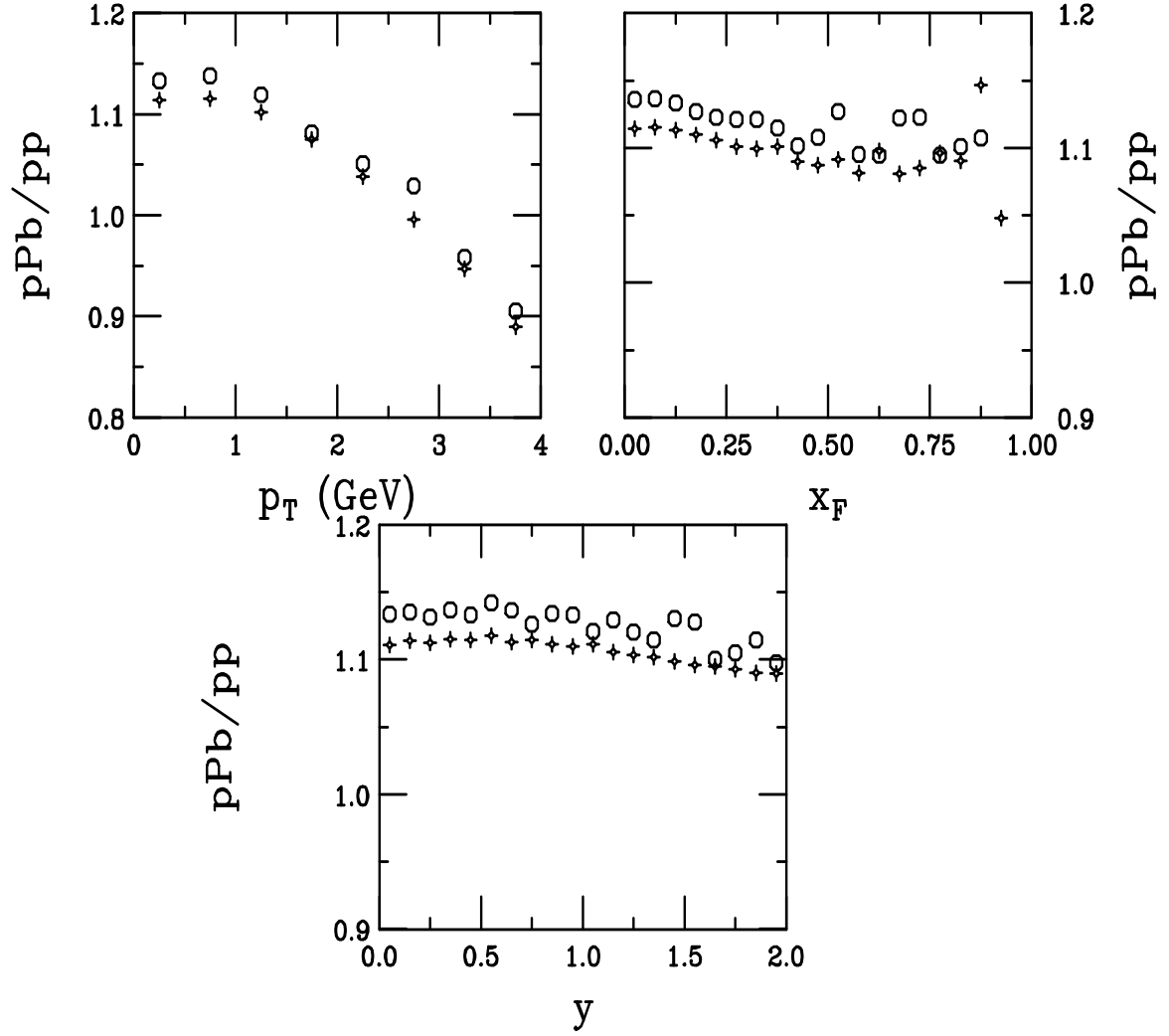


Figure 20: Ratio of c quark production in pA to pp interactions at 158 GeV as a function of p_T , x_F , and y . The crosses are the LO results while the circles are the NLO results.

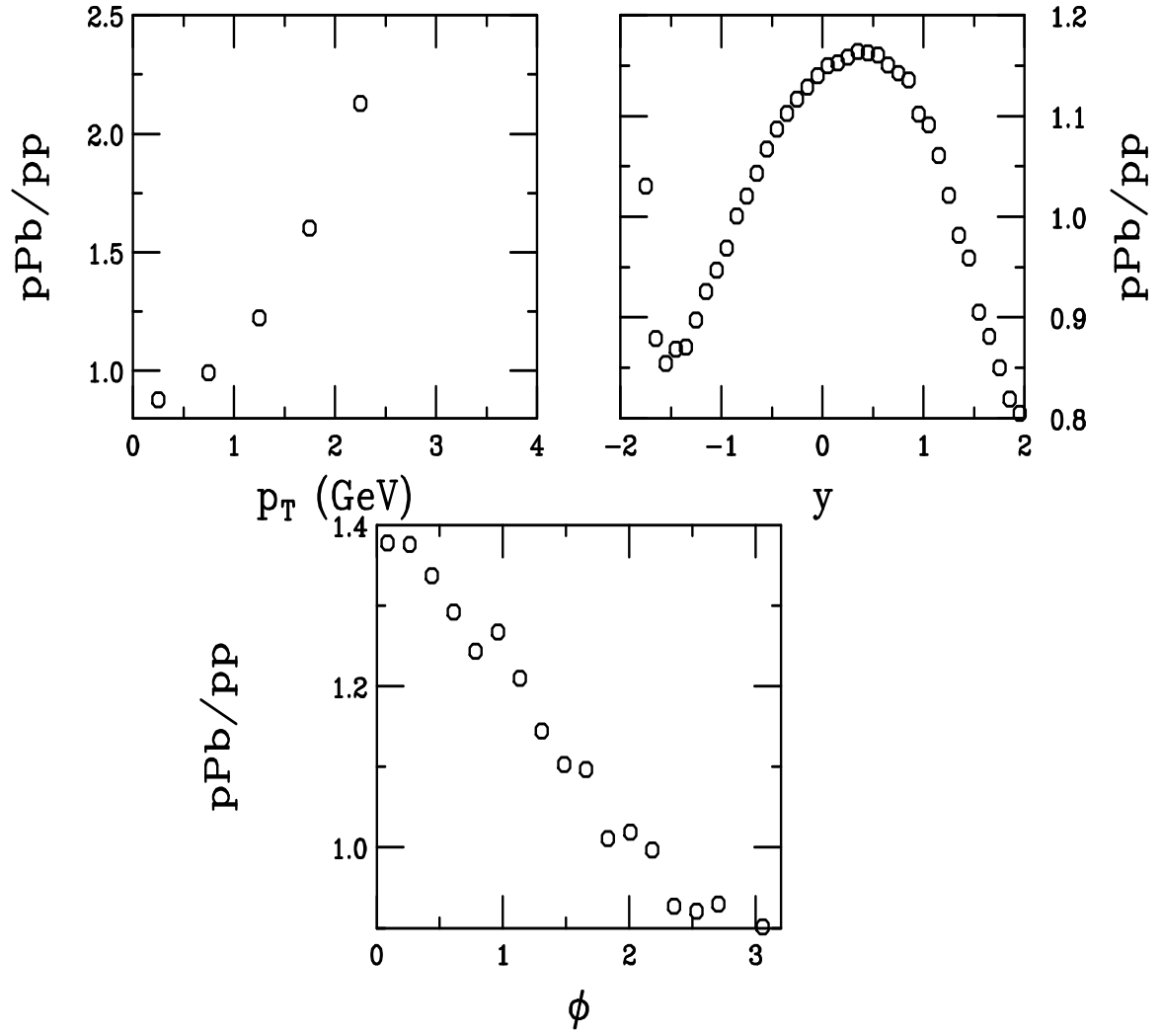


Figure 21: The ratio of pA to pp exclusive NLO $c\bar{c}$ pair production at 158 GeV as a function of p_T , y , and ϕ .

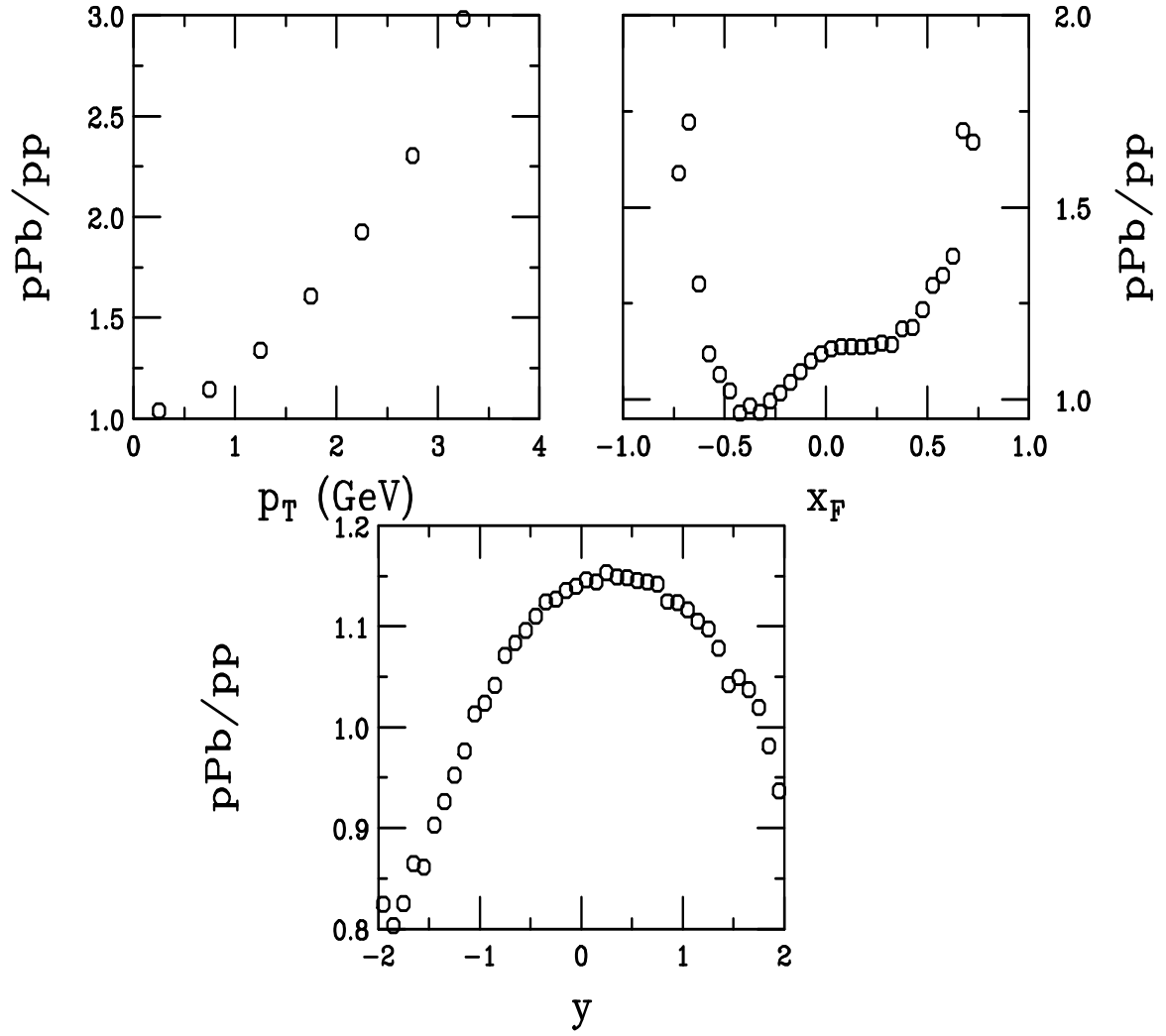


Figure 22: The ratio of pA to pp inclusive NLO c quark production at 158 GeV as a function of p_T , x_F , and y .

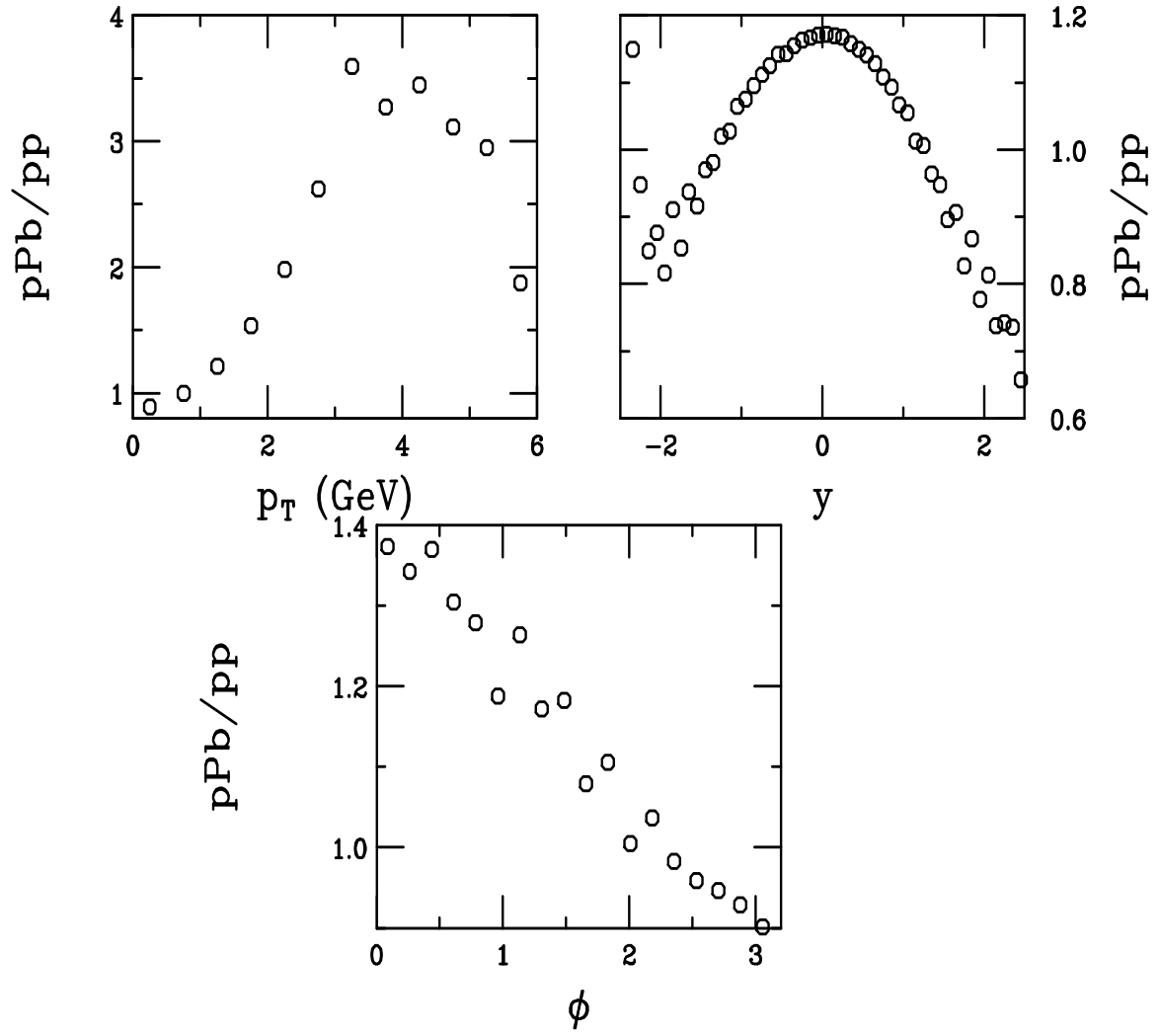


Figure 23: The ratio of pA to pp exclusive NLO $c\bar{c}$ pair production at 450 GeV as a function of p_T , y , and ϕ .

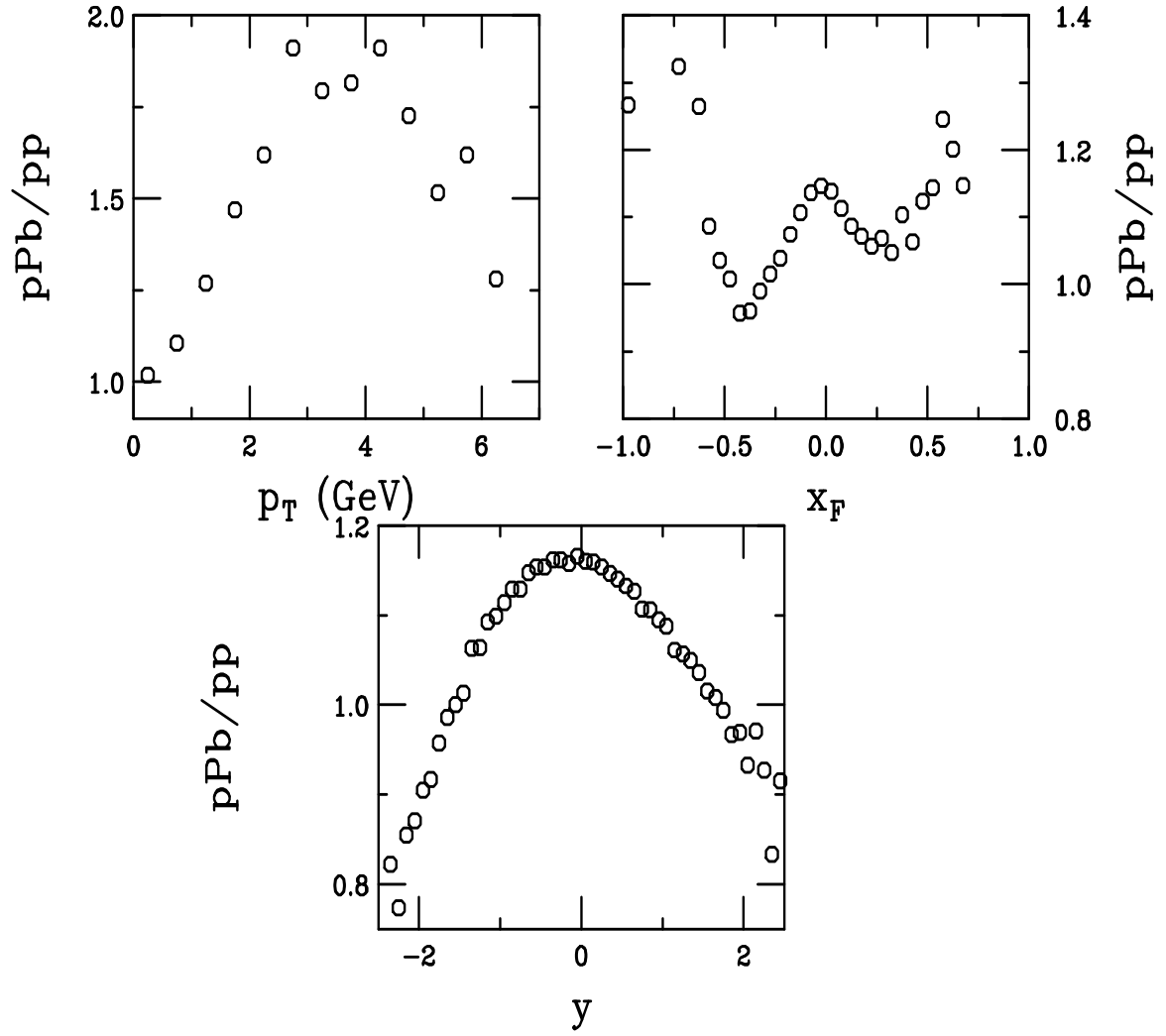


Figure 24: The ratio of pA to pp inclusive NLO c quark production at 450 GeV as a function of p_T , x_F , and y .

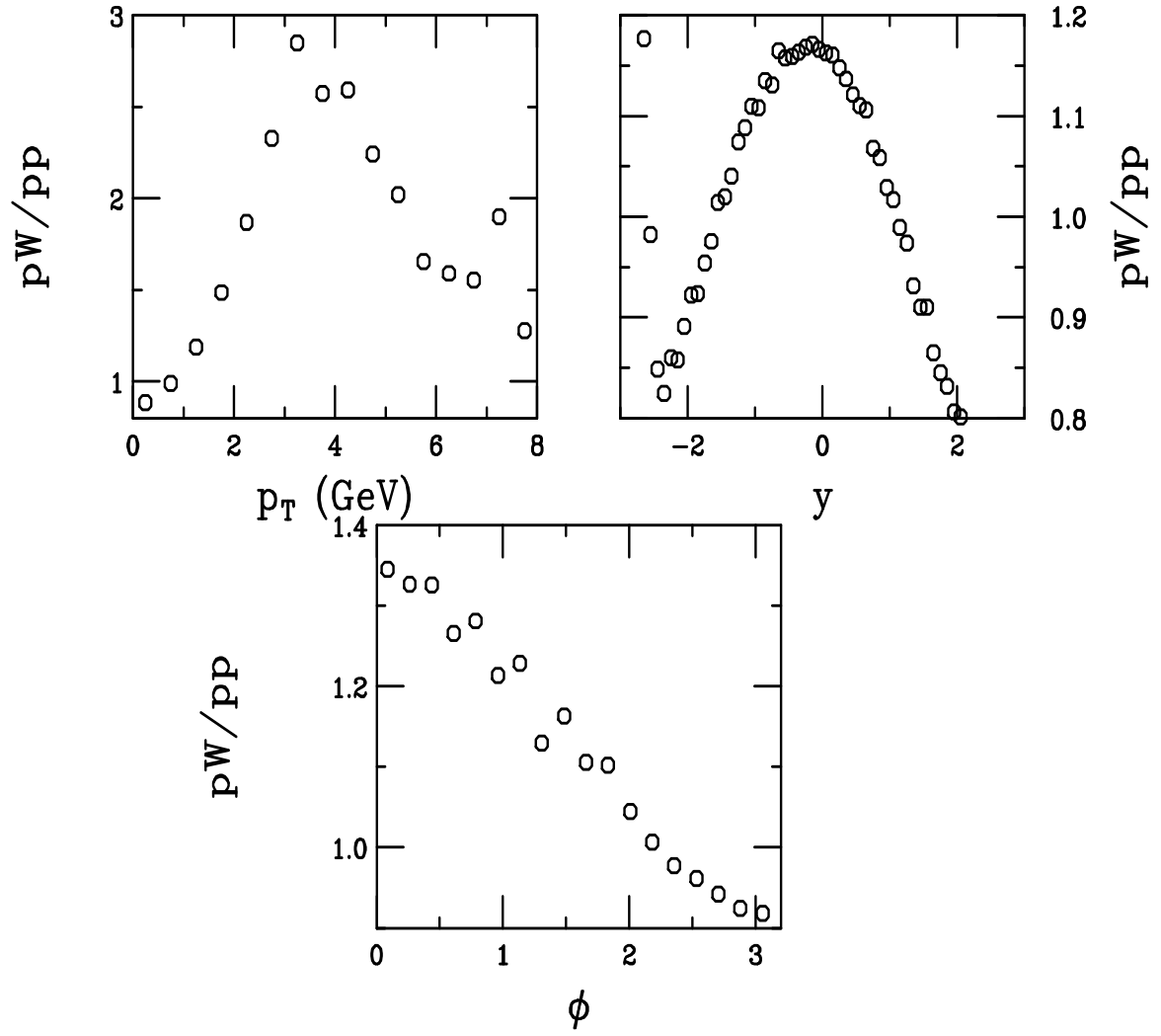


Figure 25: The ratio of pA to pp exclusive NLO $c\bar{c}$ pair production at 800 GeV as a function of p_T , y , and ϕ .

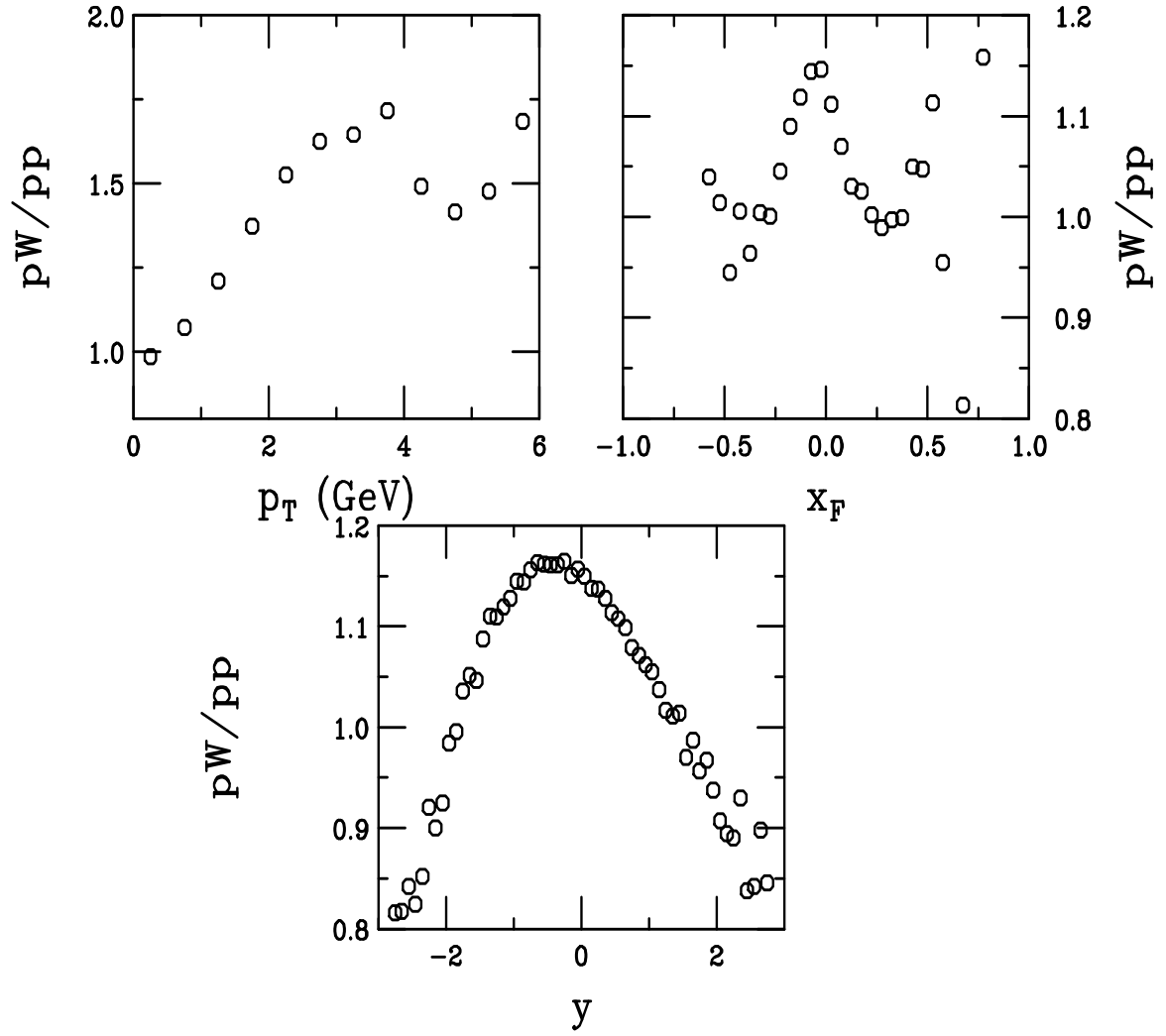


Figure 26: The ratio of pA to pp inclusive NLO c quark production at 800 GeV as a function of p_T , x_F , and y .

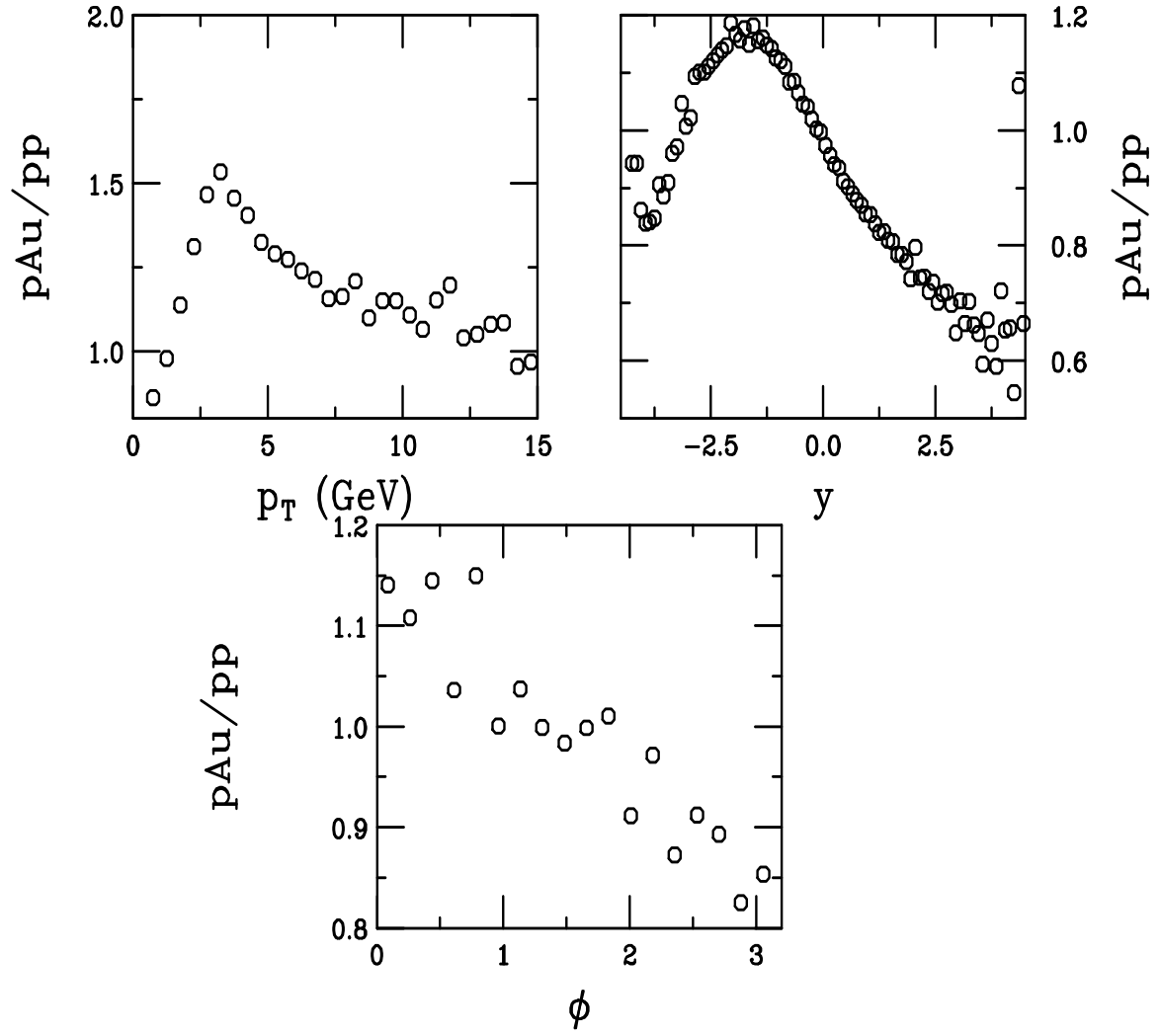


Figure 27: The ratio of pA to pp exclusive NLO $c\bar{c}$ pair production at $\sqrt{s} = 200 \text{ GeV}$ as a function of p_T , y , and ϕ .

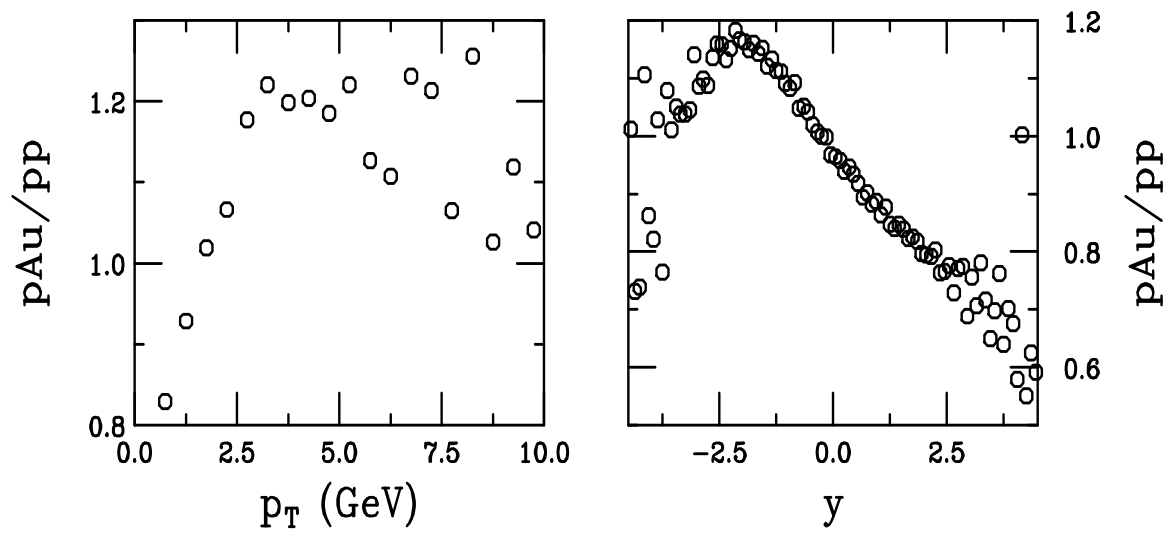


Figure 28: The ratio of pA to pp inclusive NLO c quark production at $\sqrt{s} = 200$ GeV as a function of p_T and y .

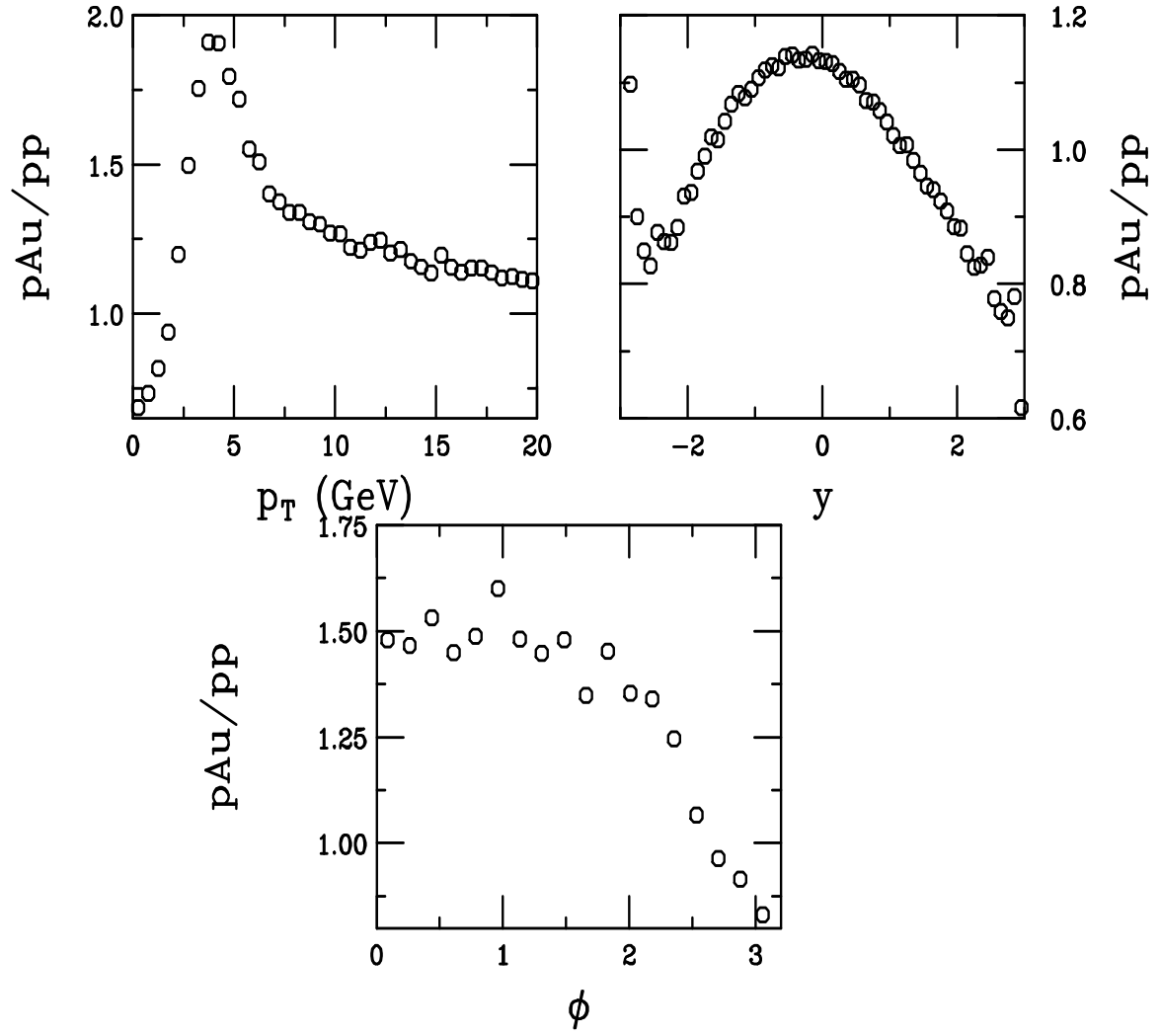


Figure 29: The ratio of pA to pp exclusive NLO $b\bar{b}$ pair production at $\sqrt{s} = 200$ GeV as a function of p_T , y , and ϕ .

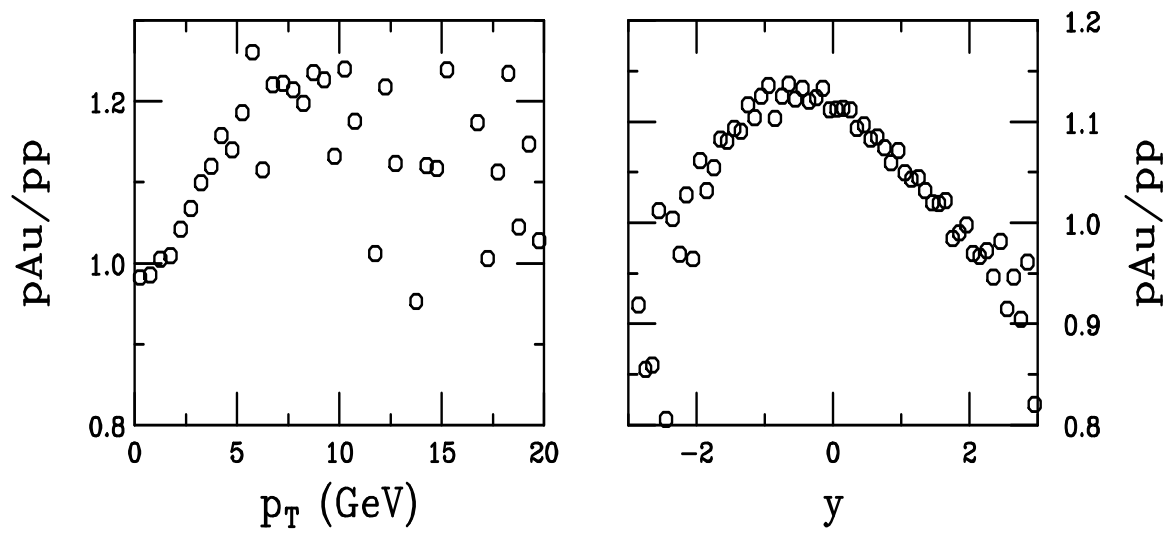


Figure 30: The ratio of pA to pp inclusive NLO b quark production at $\sqrt{s} = 200$ GeV as a function of p_T and y .

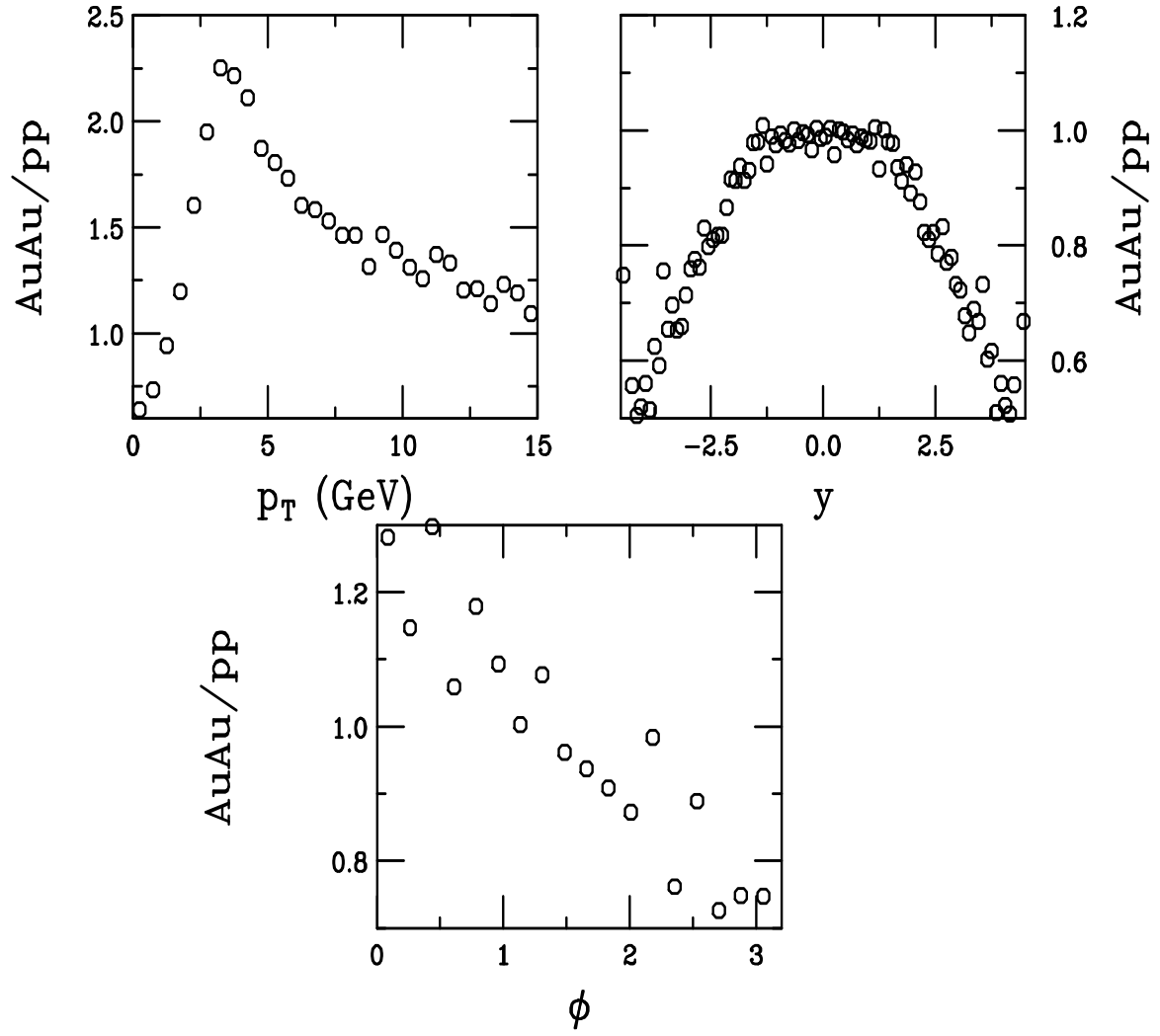


Figure 31: The ratio of AA to pp exclusive NLO $c\bar{c}$ pair production at $\sqrt{s} = 200$ GeV as a function of p_T , y , and ϕ .

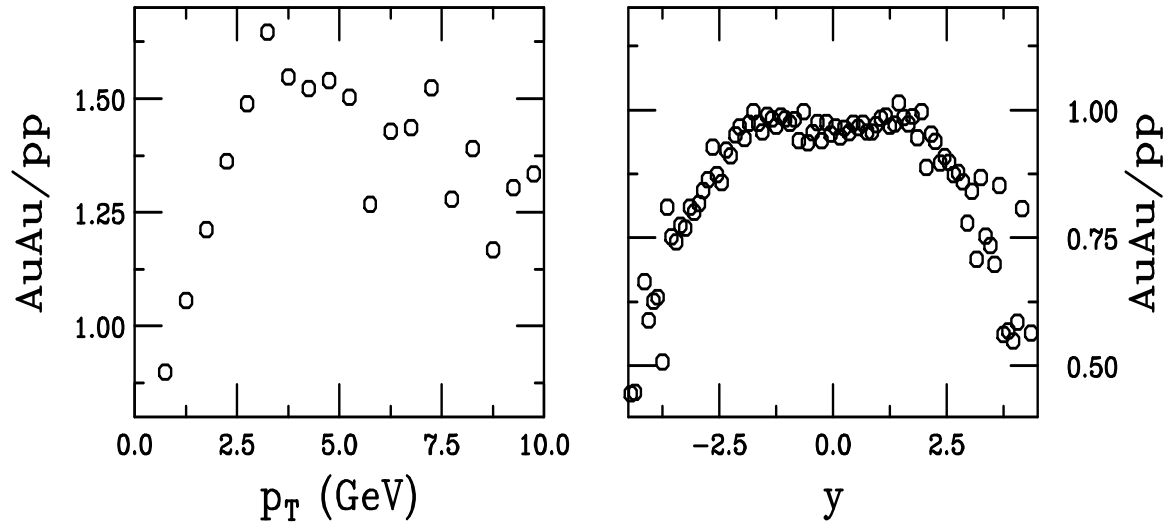


Figure 32: The ratio of AA to pp inclusive NLO c quark production at $\sqrt{s} = 200$ GeV as a function of p_T and y .

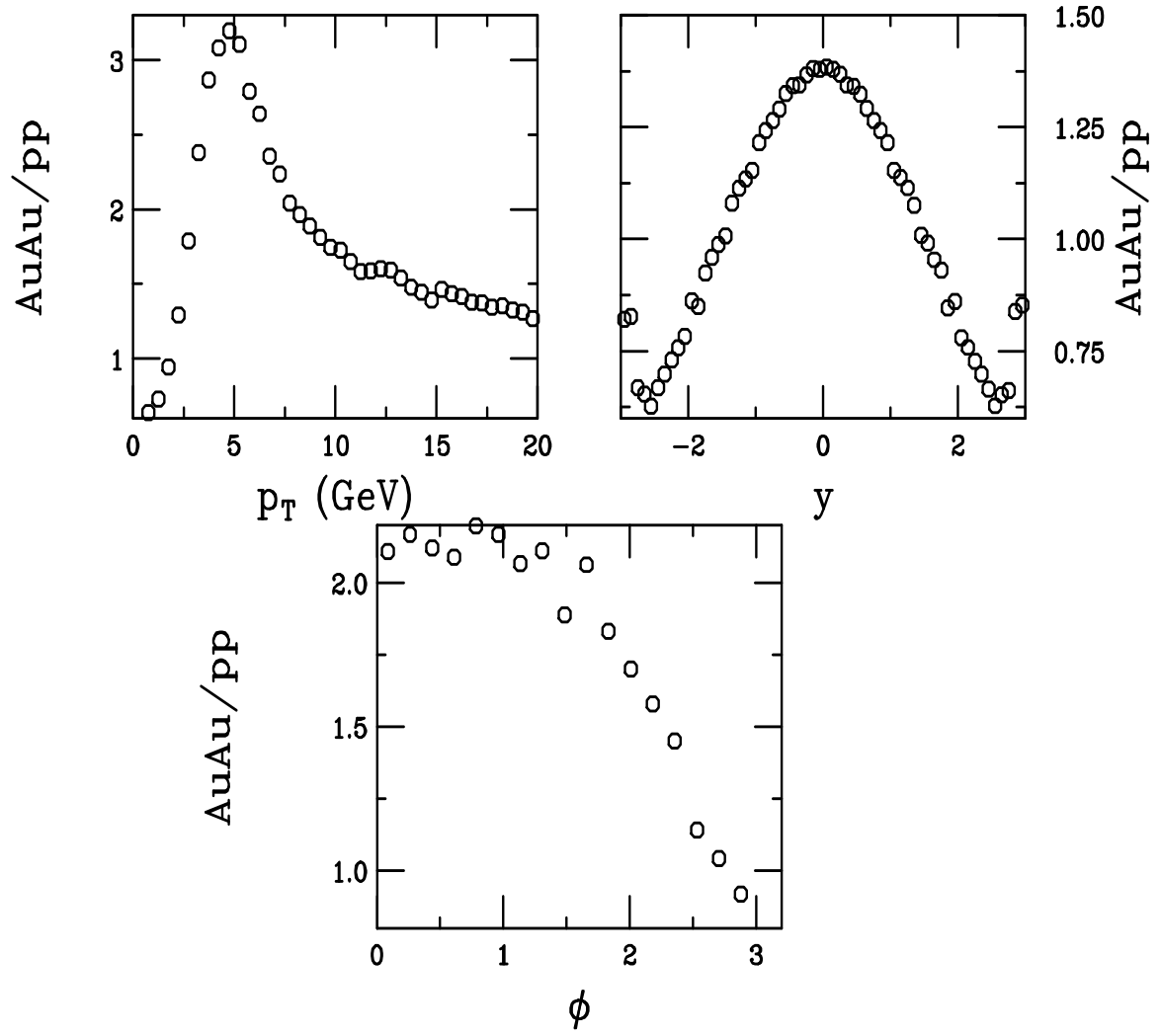


Figure 33: The ratio of AA to pp exclusive NLO $b\bar{b}$ pair production at $\sqrt{s} = 200$ GeV as a function of p_T , y , and ϕ .

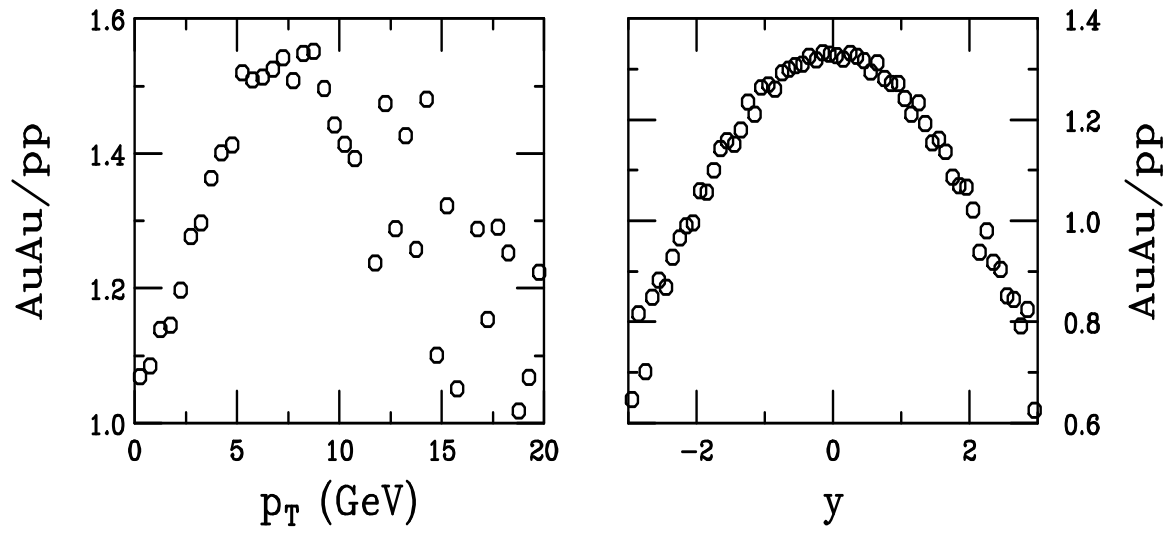


Figure 34: The ratio of AA to pp inclusive NLO b quark production at $\sqrt{s} = 200$ GeV as a function of p_T and y .

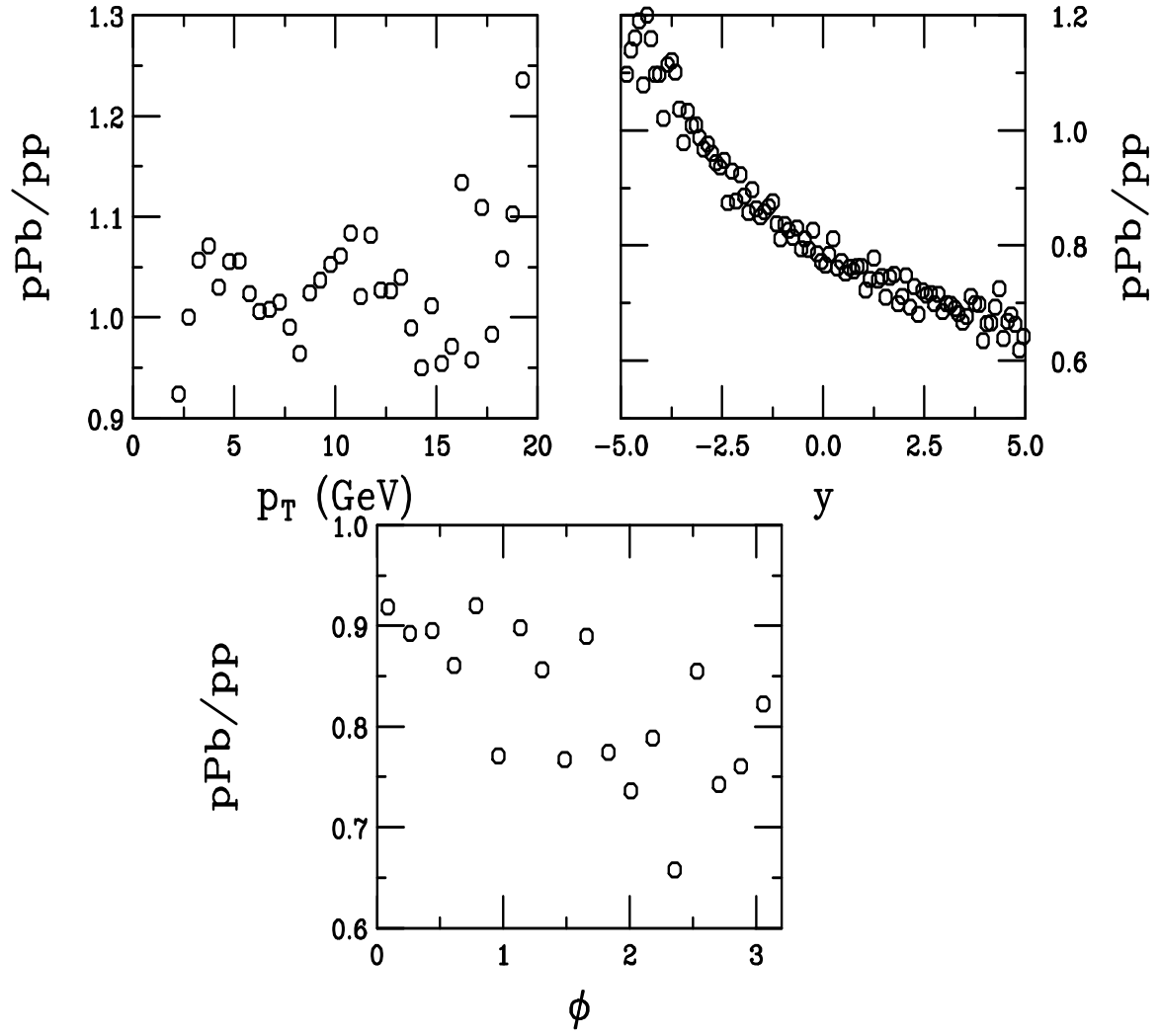


Figure 35: The ratio of pA to pp exclusive NLO $c\bar{c}$ pair production at $\sqrt{s} = 5.5$ TeV as a function of p_T , y , and ϕ .

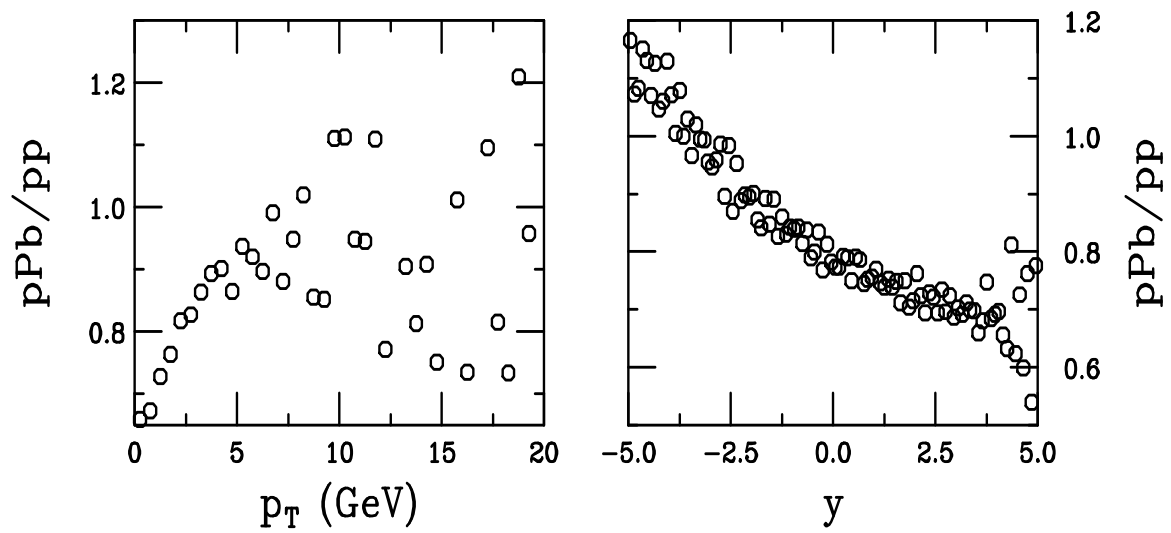


Figure 36: The ratio of pA to pp inclusive NLO c quark production at $\sqrt{s} = 5.5$ TeV as a function of p_T and y .

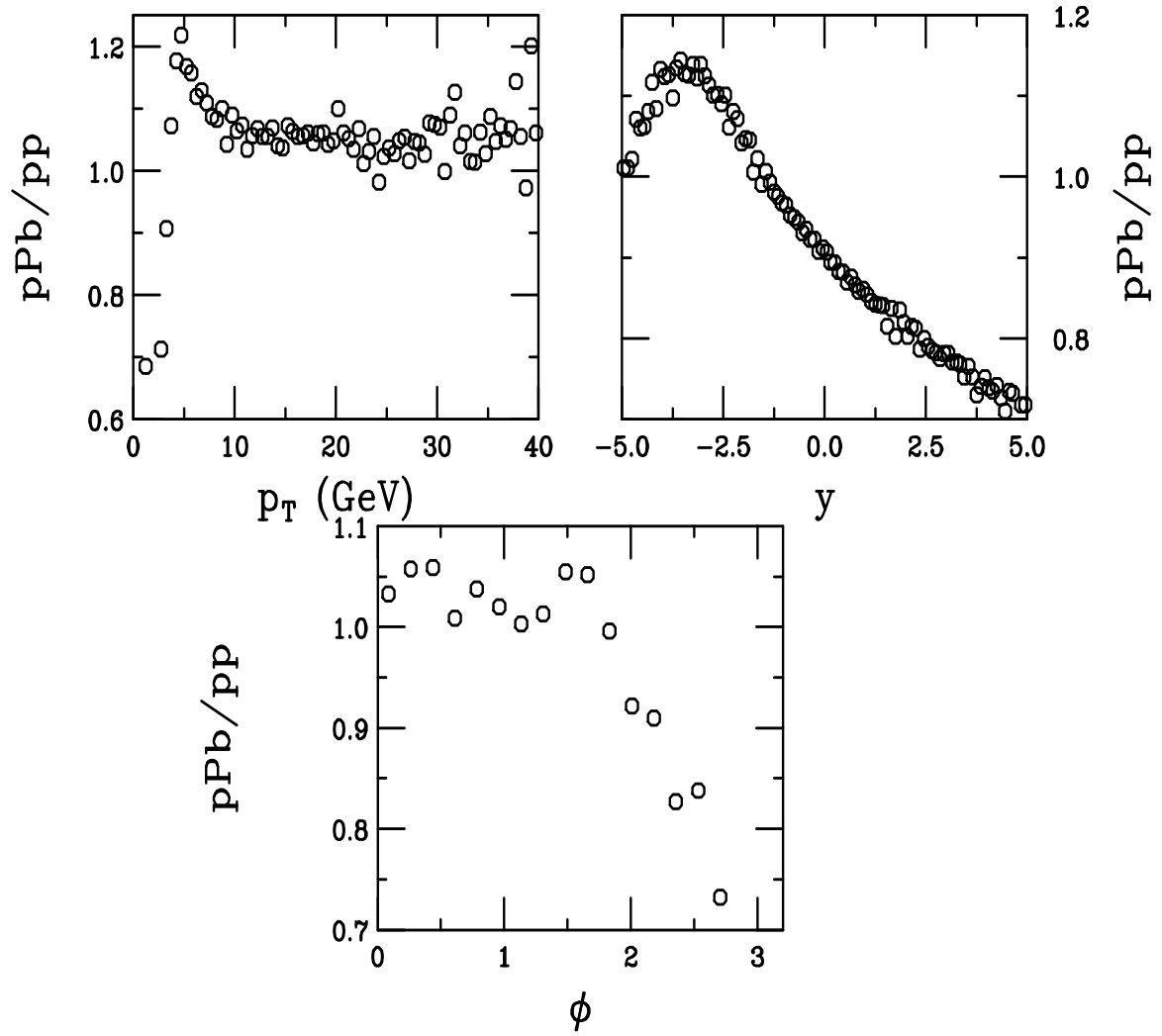


Figure 37: The ratio of pA to pp exclusive NLO $b\bar{b}$ pair production at $\sqrt{s} = 5.5$ TeV as a function of p_T , y , and ϕ .

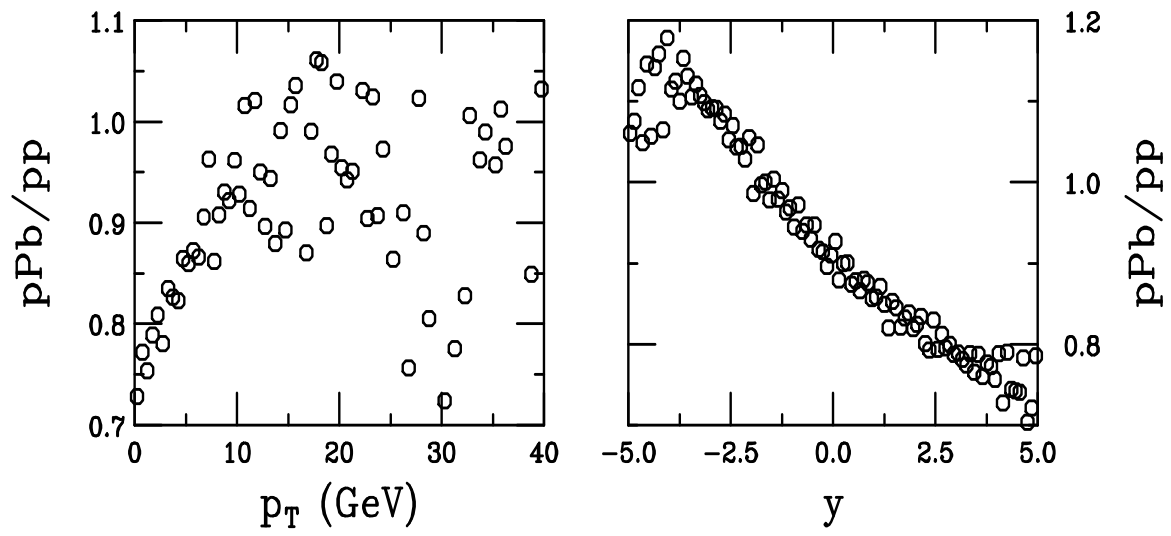


Figure 38: The ratio of pA to pp inclusive NLO b quark production at $\sqrt{s} = 5.5$ TeV as a function of p_T and y .

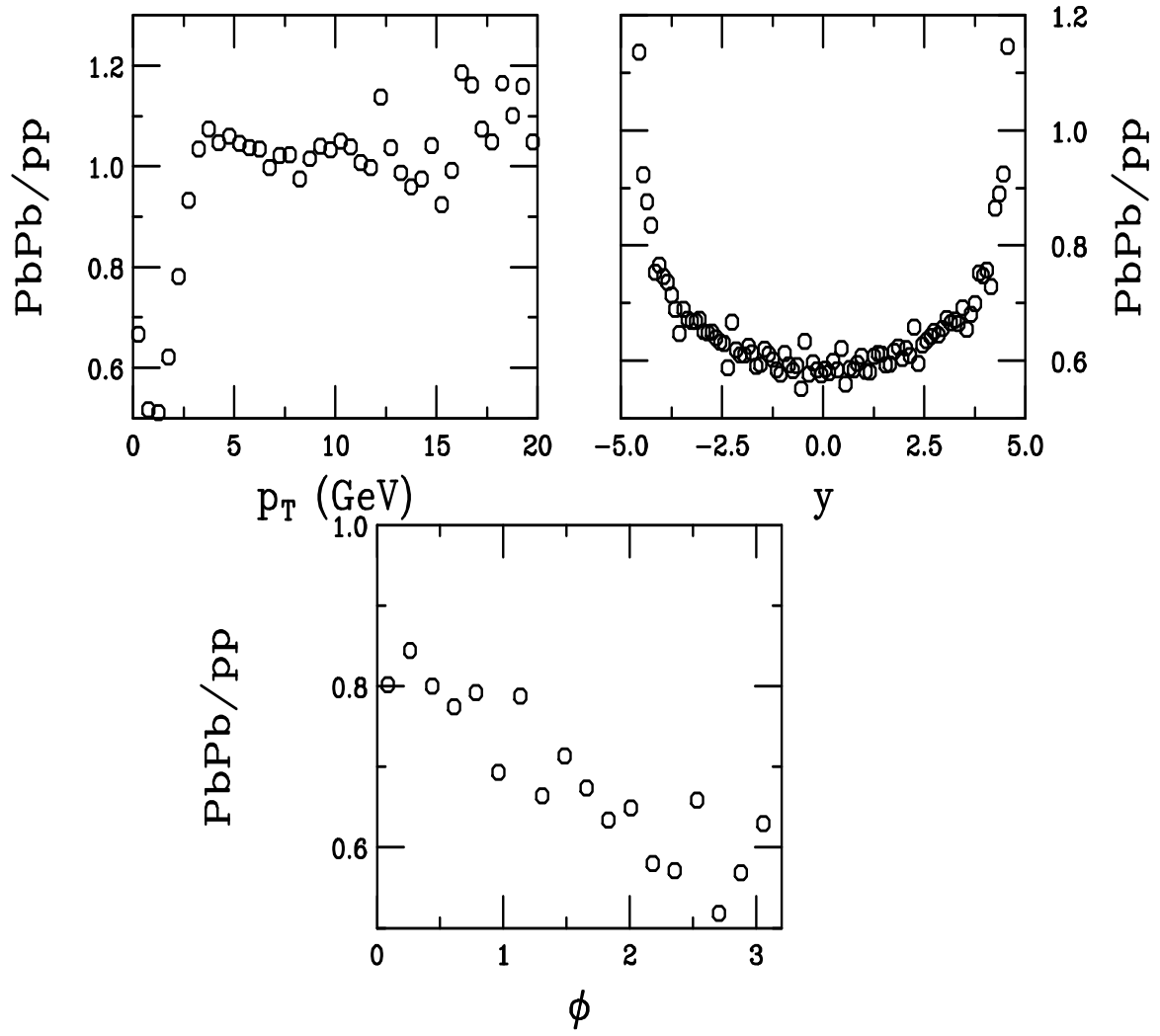


Figure 39: The ratio of AA to pp exclusive NLO $c\bar{c}$ pair production at $\sqrt{s} = 5.5$ TeV as a function of p_T , y , and ϕ .

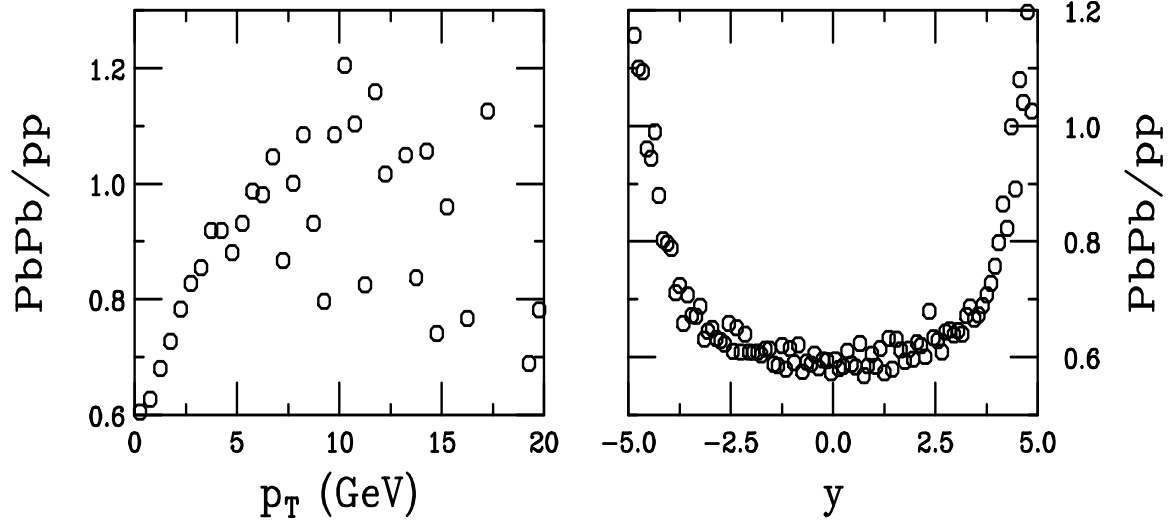


Figure 40: The ratio of AA to pp inclusive NLO c quark production at $\sqrt{s} = 5.5$ TeV as a function of p_T and y .

p_T (GeV)	$d\sigma_{c\bar{c}}/dp_T$ (nb/GeV)		$d\sigma_c/dp_T$ (nb/GeV)	
	pp	pA	pp	pA
0.25	2104.000	1848.000	1970.400	2046.000
0.75	3470.000	3440.000	1669.400	1909.400
1.25	2048.000	2504.000	527.000	705.200
1.75	747.600	1197.000	115.180	185.060
2.25	198.080	421.600	20.100	38.720
2.75	38.140	116.940	3.040	7.006
3.25	5.188	27.220	0.391	1.166
3.75	0.788	3.852	0.044	0.135
4.25	0.107	0.867	0.008	0.017

Table 3: The NLO exclusive $c\bar{c}$ and inclusive single charm p_T distributions for a proton beam of 158 GeV. The exclusive $c\bar{c}$ distributions are integrated over all rapidity while the inclusive single charm p_T distributions are integrated over $x_F > 0$ only. The distributions for pp and pA interactions are both given. The per nucleon cross section is given for pA interactions. Recall that the intrinsic $\langle k_T^2 \rangle$ is 1 GeV² for pp interactions and 1.35 GeV² for pA interactions.

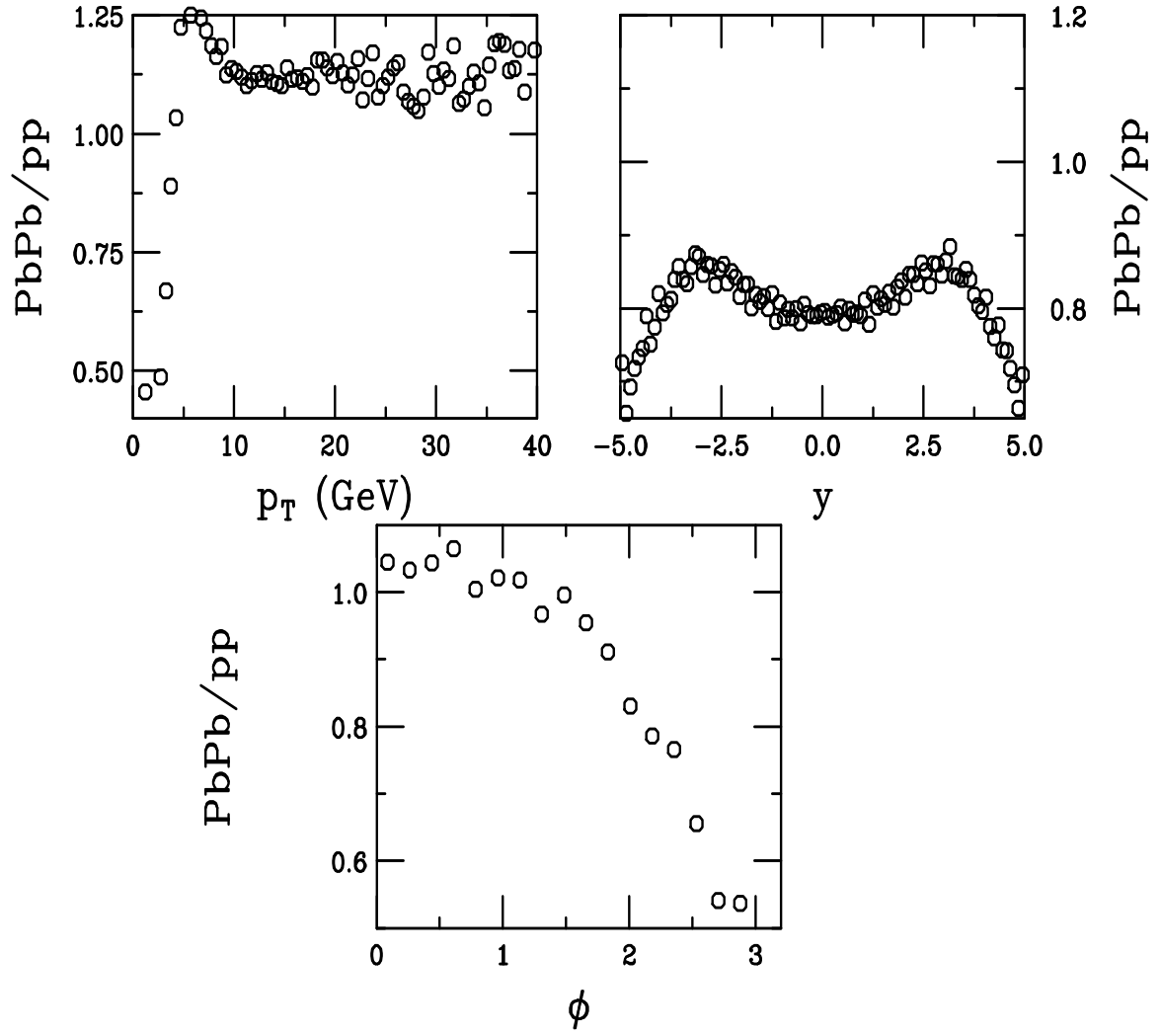


Figure 41: The ratio of AA to pp exclusive NLO $b\bar{b}$ pair production at $\sqrt{s} = 5.5$ TeV as a function of p_T , y , and ϕ .

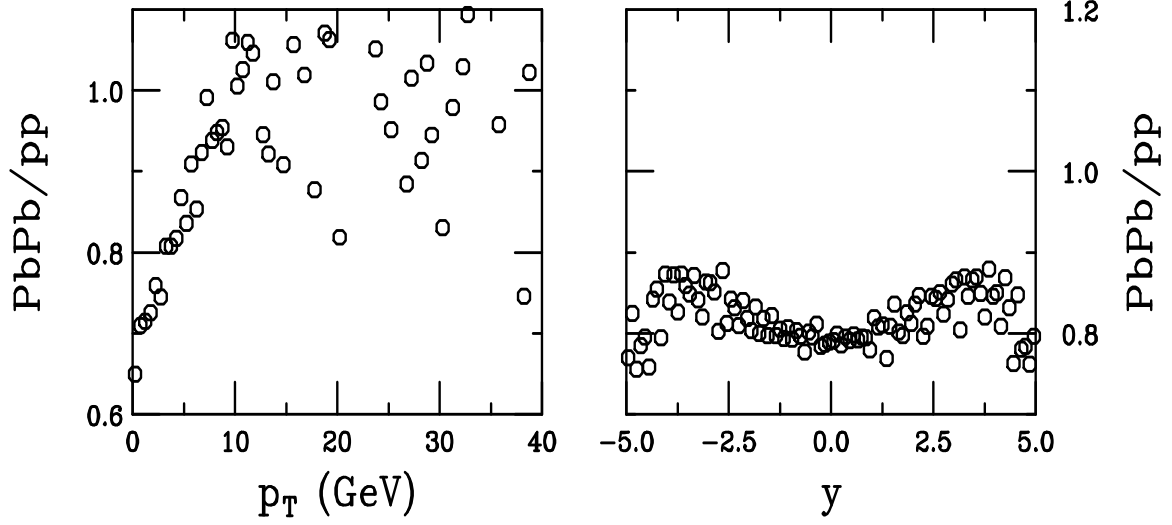


Figure 42: The ratio of AA to pp inclusive NLO b quark production at $\sqrt{s} = 5.5$ TeV as a function of p_T and y .

p_T (GeV)	$d\sigma_{c\bar{c}}/dp_T$ (nb/GeV)		$d\sigma_c/dp_T$ (nb/GeV)	
	pp	pA	pp	pA
0.25	8044.000	7156.000	7214.000	7342.000
0.75	13546.000	13544.000	6704.000	7416.000
1.25	8352.000	10130.000	2456.000	3118.000
1.75	3268.000	5020.000	642.200	943.800
2.25	939.200	1862.600	152.060	246.200
2.75	210.600	552.400	29.800	56.960
3.25	40.220	144.480	6.476	11.616
3.75	8.492	27.780	1.405	2.552
4.25	1.934	6.662	0.313	0.598
4.75	0.476	1.481	0.078	0.135
5.25	0.128	0.378	0.020	0.030
5.75	0.042	0.078	0.004	0.007
6.25	0.011	0.024	0.001	0.001

Table 4: The NLO exclusive $c\bar{c}$ and inclusive single charm p_T distributions for a proton beam of 450 GeV. The exclusive $c\bar{c}$ distributions are integrated over all rapidity while the inclusive single charm p_T distributions are integrated over $x_F > 0$ only. The distributions for pp and pA interactions are both given. The per nucleon cross section is given for pA interactions. Recall that the intrinsic $\langle k_T^2 \rangle$ is 1 GeV² for pp interactions and 1.35 GeV² for pA interactions.

p_T (GeV)	$d\sigma_{c\bar{c}}/dp_T$ (nb/GeV)		$d\sigma_c/dp_T$ (nb/GeV)	
	pp	pA	pp	pA
0.25	14168.000	12530.000	12486.000	12300.000
0.75	24160.000	23880.000	12100.000	12952.000
1.25	15346.000	18216.000	4788.000	5790.000
1.75	6266.000	9312.000	1383.600	1899.800
2.25	1902.400	3558.000	356.200	543.000
2.75	480.600	1119.000	86.240	140.140
3.25	109.220	311.200	21.080	34.680
3.75	27.720	71.280	5.578	9.570
4.25	7.820	20.280	1.661	2.478
4.75	2.456	5.510	0.493	0.698
5.25	0.787	1.591	0.166	0.245
5.75	0.297	0.491	0.048	0.081
6.25	0.111	0.176	0.018	0.021
6.75	0.044	0.068	0.005	0.007
7.25	0.014	0.027	0.002	0.003

Table 5: The NLO exclusive $c\bar{c}$ and inclusive single charm p_T distributions for a proton beam of 800 GeV. The exclusive $c\bar{c}$ distributions are integrated over all rapidity while the inclusive single charm p_T distributions are integrated over $x_F > 0$ only. The distributions for pp and pA interactions are both given. The per nucleon cross section is given for pA interactions. Recall that the intrinsic $\langle k_T^2 \rangle$ is 1 GeV² for pp interactions and 1.35 GeV² for pA interactions.

p_T (GeV)	$d\sigma_{c\bar{c}}/dp_T$ ($\mu\text{b}/\text{GeV}$)			$d\sigma_c/dp_T$ ($\mu\text{b}/\text{GeV}$)		
	pp	pA	AA	pp	pA	AA
0.25	106.640	84.080	68.300	98.400	75.740	77.900
0.75	204.800	176.440	150.640	113.660	94.220	102.140
1.25	162.540	158.960	153.020	60.160	55.860	63.540
1.75	89.340	101.580	106.940	25.480	25.960	30.880
2.25	38.820	50.860	62.220	10.330	11.016	14.720
2.75	15.744	23.080	30.700	4.082	4.806	6.076
3.25	6.390	9.796	14.398	1.612	1.967	2.652
3.75	2.918	4.246	7.614	0.752	0.902	1.164
4.25	1.433	2.014	3.024	0.377	0.454	0.574
4.75	0.765	1.013	1.433	0.185	0.220	0.285
5.25	0.421	0.543	0.761	0.101	0.123	0.152
5.75	0.243	0.310	0.422	0.058	0.066	0.074
6.25	0.145	0.180	0.233	0.034	0.038	0.048
6.75	0.091	0.110	0.143	0.021	0.026	0.030
7.25	0.058	0.067	0.089	0.013	0.015	0.019
7.75	0.038	0.044	0.055	0.008	0.009	0.010
8.25	0.024	0.029	0.035	0.005	0.006	0.007
8.75	0.017	0.019	0.023	0.004	0.004	0.005
9.25	0.011	0.013	0.016	0.002	0.003	0.003
9.75	0.008	0.009	0.011	0.002	0.002	0.002

Table 6: The NLO exclusive $c\bar{c}$ and inclusive single charm p_T distributions for collisions at $\sqrt{s} = 200$ GeV. The exclusive $c\bar{c}$ distributions are integrated over all rapidity while the inclusive single charm p_T distributions are integrated over $x_F > 0$ only. The distributions for pp , pA and AA interactions are all given. The per nucleon cross section is given for pA and AA interactions. Recall that the intrinsic $\langle k_T^2 \rangle$ is 1 GeV² for pp interactions, 1.35 GeV² for pA interactions, and 1.7 GeV² for AA .

p_T (GeV)	$d\sigma_{c\bar{c}}/dp_T$ ($\mu\text{b}/\text{GeV}$)			$d\sigma_c/dp_T$ ($\mu\text{b}/\text{GeV}$)		
	pp	pA	AA	pp	pA	AA
0.25	407.800	301.400	271.800	1123.800	740.400	679.600
0.75	1791.000	1221.600	924.400	1604.400	1078.800	1005.800
1.25	2732.000	1921.200	1395.200	1202.200	875.000	817.400
1.75	2464.000	1932.400	1531.600	755.600	577.000	549.600
2.25	1615.200	1492.800	1262.000	428.800	350.800	335.600
2.75	938.400	939.000	875.600	242.200	200.400	200.400
3.25	540.200	570.800	559.000	143.700	124.140	122.820
3.75	324.200	347.200	348.200	85.380	76.260	78.460
4.25	207.800	214.000	217.600	53.500	48.260	49.200
4.75	133.820	141.280	141.760	36.640	31.680	32.280
5.25	92.220	97.380	96.480	23.160	21.700	21.580
5.75	65.940	67.480	68.420	16.696	15.368	16.480
6.25	47.900	48.180	49.540	11.192	10.042	10.974
6.75	35.580	35.880	35.480	8.354	8.282	8.742
7.25	26.420	26.820	27.000	6.568	5.788	5.694
7.75	20.400	20.200	20.860	4.900	4.650	4.902
8.25	16.306	15.728	15.904	3.378	3.446	3.664
8.75	12.646	12.958	12.840	2.886	2.468	2.688
9.25	9.750	10.112	11.420	2.316	1.973	1.844
9.75	7.740	8.150	7.996	1.631	1.812	1.769
10.25	6.162	6.538	6.474	1.267	1.411	1.527
10.75	5.046	5.468	5.238	1.159	1.099	1.279
11.25	4.216	4.304	4.246	1.024	0.968	0.846
11.75	3.512	3.798	3.504	0.660	0.733	0.765
12.25	2.850	2.928	3.242	0.719	0.554	0.730
12.75	2.474	2.540	2.566	0.406	0.580	0.554
13.25	2.016	2.096	1.990	0.386	0.350	0.405
13.75	1.881	1.862	1.804	0.430	0.349	0.360
14.25	1.601	1.522	1.562	0.283	0.257	0.299
14.75	1.280	1.296	1.334	0.322	0.241	0.238
15.25	1.200	1.146	1.184	0.203	0.271	0.195
15.75	1.011	0.982	1.022	0.176	0.178	0.261
16.25	0.799	0.905	0.947	0.223	0.164	0.171
16.75	0.752	0.720	0.873	0.117	0.166	0.174
17.25	0.647	0.718	0.695	0.102	0.111	0.114
17.75	0.576	0.566	0.604	0.128	0.104	0.171

Table 7: The NLO exclusive $c\bar{c}$ and inclusive single charm p_T distributions for collisions at $\sqrt{s} = 5.5$ TeV. The exclusive $c\bar{c}$ distributions are integrated over all rapidity while the inclusive single charm p_T distributions are integrated over $x_F > 0$ only. The distributions for pp , pA and AA interactions are all given. The per nucleon cross section is given for pA and AA interactions. Recall that the intrinsic $\langle k_T^2 \rangle$ is 1 GeV² for pp interactions, 1.35 GeV² for pA interactions, and 1.7 GeV² for AA .

p_T (GeV)	$d\sigma_{b\bar{b}}/dp_T$ (nb/GeV)			$d\sigma_b/dp_T$ (nb/GeV)		
	pp	pA	AA	pp	pA	AA
0.25	196.260	134.740	115.740	60.320	59.260	64.460
0.75	512.400	375.200	326.800	152.900	150.680	165.800
1.25	632.600	516.800	461.600	199.820	200.800	227.600
1.75	583.400	547.400	549.200	218.200	220.200	249.800
2.25	411.800	493.600	531.400	205.200	213.800	245.600
2.75	271.200	406.000	484.400	176.080	188.020	224.800
3.25	167.880	294.400	399.200	143.840	158.220	186.580
3.75	108.580	207.400	311.200	112.120	125.600	152.840
4.25	72.620	138.440	223.800	83.480	96.660	116.940
4.75	51.360	92.200	164.180	64.340	73.340	90.860
5.25	36.100	62.080	112.040	44.880	53.240	68.200
5.75	26.980	41.860	75.280	32.120	40.500	48.460
6.25	20.000	30.180	52.800	24.240	27.040	36.680
6.75	15.304	21.440	36.080	16.774	20.480	25.580
7.25	11.450	15.744	25.620	11.866	14.502	18.294
7.75	8.794	11.774	17.932	8.878	10.784	13.860
8.25	6.684	8.946	13.118	6.260	7.496	9.694
8.75	5.188	6.792	9.788	4.486	5.542	6.958
9.25	4.046	5.260	7.328	3.276	4.020	4.902
9.75	3.178	4.036	5.552	2.472	2.798	3.564
10.25	2.464	3.124	4.256	1.741	2.158	2.460
10.75	1.970	2.408	3.254	1.340	1.575	1.866
11.25	1.572	1.906	2.488	0.891	1.168	1.434
11.75	1.220	1.512	1.939	0.810	0.820	1.022
12.25	0.969	1.209	1.554	0.567	0.691	0.835
12.75	0.772	0.929	1.229	0.448	0.503	0.577
13.25	0.625	0.759	0.963	0.301	0.432	0.430
13.75	0.511	0.601	0.756	0.276	0.263	0.347
14.25	0.413	0.478	0.596	0.187	0.210	0.277
14.75	0.342	0.388	0.475	0.166	0.185	0.182
15.25	0.266	0.318	0.389	0.123	0.152	0.162
15.75	0.217	0.250	0.311	0.112	0.088	0.118
16.25	0.176	0.201	0.250	0.043	0.079	0.081
16.75	0.142	0.164	0.195	0.060	0.070	0.077
17.25	0.116	0.134	0.160	0.051	0.051	0.059
17.75	0.095	0.108	0.128	0.033	0.037	0.042

Table 8: The NLO exclusive $b\bar{b}$ and inclusive single bottom p_T distributions for collisions at $\sqrt{s} = 200$ GeV. The exclusive $b\bar{b}$ distributions are integrated over all rapidity while the inclusive single bottom p_T distributions are integrated over $x_F > 0$ only. The distributions for pp , pA and AA interactions are all given. The per nucleon cross section is given for pA and AA interactions. Recall that the intrinsic $\langle k_T^2 \rangle$ is 1 GeV² for pp interactions, 2.57 GeV² for pA interactions, and 4.16 GeV² for AA .

p_T (GeV)	$d\sigma_{b\bar{b}}/dp_T$ ($\mu\text{b}/\text{GeV}$)			$d\sigma_b/dp_T$ ($\mu\text{b}/\text{GeV}$)		
	pp	pA	AA	pp	pA	AA
1.25	17.738	12.142	8.068	13.646	10.286	9.754
1.75	45.340	20.480	15.058	15.568	12.280	11.296
2.25	53.480	29.200	18.176	15.502	12.538	11.764
2.75	46.660	33.260	22.700	15.890	12.408	11.838
3.25	36.540	33.120	24.460	13.544	11.308	10.934
3.75	27.760	29.760	24.680	12.574	10.390	10.154
4.25	21.680	25.520	22.420	10.944	9.006	8.946
4.75	16.842	20.520	20.620	8.946	7.738	7.762
5.25	13.938	16.272	17.608	7.910	6.802	6.610
5.75	11.326	13.108	14.156	6.424	5.606	5.840
6.25	9.462	10.594	11.854	5.540	4.798	4.730
6.75	7.872	8.888	9.796	4.524	4.096	4.176
7.25	6.600	7.318	8.036	3.656	3.520	3.624
7.75	5.664	6.156	6.720	3.128	2.696	2.936
8.25	4.798	5.192	5.582	2.616	2.374	2.480
8.75	4.112	4.520	4.868	2.154	2.004	2.056
9.25	3.614	3.768	4.062	1.829	1.686	1.701
9.75	3.096	3.372	3.520	1.502	1.444	1.596
10.25	2.672	2.844	3.022	1.279	1.187	1.286
10.75	2.334	2.504	2.612	1.061	1.078	1.088
11.25	2.094	2.166	2.308	0.904	0.827	0.958
11.75	1.821	1.923	2.026	0.741	0.756	0.775
12.25	1.586	1.693	1.787	0.645	0.613	0.726
12.75	1.430	1.509	1.594	0.608	0.545	0.575
13.25	1.239	1.308	1.400	0.520	0.491	0.479
13.75	1.107	1.184	1.229	0.478	0.420	0.483
14.25	0.985	1.025	1.091	0.387	0.383	0.425
14.75	0.903	0.935	0.994	0.344	0.307	0.313
15.25	0.775	0.831	0.883	0.302	0.307	0.345
15.75	0.698	0.741	0.778	0.261	0.270	0.276
16.25	0.645	0.680	0.720	0.202	0.232	0.237
16.75	0.572	0.605	0.635	0.207	0.180	0.211
17.25	0.518	0.550	0.581	0.183	0.182	0.205
17.75	0.464	0.485	0.510	0.156	0.166	0.137

Table 9: The NLO exclusive $b\bar{b}$ and inclusive single bottom p_T distributions for collisions at $\sqrt{s} = 5.5$ TeV. The exclusive $b\bar{b}$ distributions are integrated over all rapidity while the inclusive single bottom p_T distributions are integrated over $x_F > 0$ only. The distributions for pp , pA and AA interactions are all given. The per nucleon cross section is given for pA and AA interactions. Recall that the intrinsic $\langle k_T^2 \rangle$ is 1 GeV² for pp interactions, 2.57 GeV² for pA interactions, and 4.16 GeV² for AA .

y	$d\sigma_{c\bar{c}}/dy$ (μb)		$d\sigma_c/dy$ (μb)	
	pp	pA	pp	pA
-1.85	0.000	0.000	0.017	0.014
-1.65	0.009	0.008	0.084	0.072
-1.45	0.069	0.060	0.247	0.223
-1.25	0.243	0.218	0.530	0.505
-1.05	0.601	0.569	0.888	0.900
-0.85	1.131	1.132	1.295	1.349
-0.65	1.707	1.781	1.699	1.841
-0.45	2.237	2.431	2.009	2.230
-0.25	2.642	2.951	2.254	2.541
-0.05	2.834	3.231	2.346	2.674
0.05	2.828	3.252	2.340	2.682
0.25	2.644	3.063	2.248	2.593
0.45	2.238	2.602	2.011	2.309
0.65	1.710	1.968	1.692	1.936
0.85	1.129	1.282	1.300	1.462
1.05	0.600	0.655	0.885	0.988
1.25	0.243	0.248	0.532	0.584
1.45	0.069	0.066	0.250	0.261
1.65	0.009	0.008	0.083	0.086
1.85	0.000	0.000	0.017	0.017

Table 10: The NLO exclusive $c\bar{c}$ and inclusive single charm y distributions for a proton beam of 158 GeV. The distributions for pp and pA interactions are both given. The per nucleon cross section is given for pA interactions. Recall that the intrinsic $\langle k_T^2 \rangle$ is 1 GeV² for pp interactions and 1.35 GeV² for pA interactions.

y	$d\sigma_{c\bar{c}}/dy$ (μb)		$d\sigma_c/dy$ (μb)	
	pp	pA	pp	pA
-2.25	0.004	0.004	0.085	0.066
-2.05	0.043	0.038	0.301	0.262
-1.85	0.210	0.192	0.708	0.648
-1.65	0.604	0.566	1.365	1.346
-1.45	1.367	1.326	2.214	2.243
-1.25	2.389	2.437	3.158	3.360
-1.05	3.719	3.960	4.162	4.572
-0.85	5.147	5.639	5.200	5.870
-0.65	6.516	7.329	6.102	7.002
-0.45	7.712	8.813	6.783	7.824
-0.25	8.536	9.930	7.319	8.505
-0.05	8.998	10.530	7.506	8.750
0.05	8.998	10.540	7.529	8.736
0.25	8.534	9.964	7.284	8.406
0.45	7.702	8.851	6.807	7.761
0.65	6.507	7.344	6.071	6.840
0.85	5.152	5.632	5.193	5.743
1.05	3.722	3.925	4.178	4.543
1.25	2.387	2.402	3.149	3.327
1.45	1.367	1.295	2.176	2.254
1.65	0.605	0.548	1.394	1.405
1.85	0.211	0.183	0.710	0.686
2.05	0.043	0.035	0.292	0.272
2.25	0.004	0.003	0.083	0.077

Table 11: The NLO exclusive $c\bar{c}$ and inclusive single charm y distributions for a proton beam of 450 GeV. The distributions for pp and pA interactions are both given. The per nucleon cross section is given for pA interactions. Recall that the intrinsic $\langle k_T^2 \rangle$ is 1 GeV² for pp interactions and 1.35 GeV² for pA interactions.

y	$d\sigma_{c\bar{c}}/dy$ (μb)		$d\sigma_c/dy$ (μb)	
	pp	pA	pp	pA
-2.45	0.015	0.013	0.187	0.154
-2.25	0.106	0.091	0.555	0.510
-2.05	0.390	0.347	1.199	1.109
-1.85	1.019	0.941	2.164	2.155
-1.65	2.093	2.042	3.320	3.490
-1.45	3.506	3.576	4.685	5.096
-1.25	5.345	5.741	6.120	6.789
-1.05	7.181	7.967	7.684	8.666
-0.85	9.321	10.580	9.081	10.390
-0.65	11.060	12.880	10.340	12.030
-0.45	12.860	14.910	11.290	13.110
-0.25	14.050	16.420	11.980	13.950
-0.05	14.610	17.040	12.300	14.230
0.05	14.640	17.020	12.270	14.110
0.25	14.030	16.100	11.970	13.610
0.45	12.860	14.420	11.330	12.620
0.65	11.060	12.230	10.320	11.340
0.85	9.324	9.872	9.030	9.675
1.05	7.191	7.314	7.720	8.143
1.25	5.347	5.209	6.141	6.242
1.45	3.510	3.196	4.672	4.737
1.65	2.103	1.819	3.297	3.255
1.85	1.014	0.844	2.189	2.118
2.05	0.391	0.313	1.209	1.097
2.25	0.107	0.078	0.550	0.490
2.45	0.015	0.011	0.193	0.161

Table 12: The NLO exclusive $c\bar{c}$ and inclusive single charm y distributions for a proton beam of 800 GeV. The distributions for pp and pA interactions are both given. The per nucleon cross section is given for pA interactions. Recall that the intrinsic $\langle k_T^2 \rangle$ is 1 GeV² for pp interactions and 1.35 GeV² for pA interactions.

y	$d\sigma_{c\bar{c}}/dy$ (μb)			$d\sigma_c/dy$ (μb)		
	pp	pA	AA	pp	pA	AA
-4.25	0.003	0.003	0.002	0.148	0.109	0.056
-3.95	0.125	0.105	0.070	0.939	0.772	0.588
-3.65	1.022	0.925	0.604	2.988	3.223	2.422
-3.35	3.398	3.263	2.367	7.240	7.515	5.610
-3.05	8.264	8.325	5.900	13.420	15.310	10.730
-2.75	15.050	16.570	11.480	20.550	22.350	17.740
-2.45	23.850	26.750	19.320	28.580	33.120	24.520
-2.15	33.690	38.640	29.170	36.600	43.300	34.830
-1.85	43.780	50.660	41.070	45.650	52.460	44.450
-1.55	54.080	63.880	52.950	53.330	61.470	51.050
-1.25	63.830	73.310	60.100	60.650	67.530	58.730
-0.95	69.960	78.450	69.490	65.320	70.720	63.590
-0.65	75.700	82.120	75.790	68.690	72.230	68.490
-0.35	79.700	82.990	79.100	71.950	72.470	70.220
-0.05	80.720	80.510	79.630	72.860	70.470	69.430
0.05	80.840	78.680	79.990	72.730	70.150	70.350
0.35	79.520	74.340	79.610	72.890	68.970	69.670
0.65	75.930	67.520	75.420	69.340	61.990	67.540
0.95	70.440	60.230	69.290	65.230	57.870	63.320
1.25	64.000	52.670	59.680	61.030	51.720	59.100
1.55	54.240	43.760	53.000	53.110	44.530	52.360
1.85	43.610	33.690	40.990	46.350	37.890	43.830
2.15	33.430	24.880	29.270	37.400	29.630	35.640
2.45	23.680	17.420	19.480	27.760	21.260	25.230
2.75	15.050	10.820	11.600	20.230	15.600	17.760
3.05	8.150	5.742	5.894	12.770	9.649	10.740
3.35	3.403	2.252	2.345	7.394	5.295	5.571
3.65	1.006	0.674	0.606	2.844	2.169	2.426
3.95	0.125	0.090	0.070	0.980	0.662	0.537
4.25	0.003	0.002	0.002	0.180	0.099	0.050

Table 13: The NLO exclusive $c\bar{c}$ and inclusive single charm y distributions for collisions at $\sqrt{s} = 200$ GeV. The distributions for pp , pA and AA interactions are all given. The per nucleon cross section is given for pA and AA interactions. Recall that the intrinsic $\langle k_T^2 \rangle$ is 1 GeV² for pp interactions, 1.35 GeV² for pA interactions, and 1.7 GeV² for AA .

y	$d\sigma_{c\bar{c}}/dy$ (μb)			$d\sigma_c/dy$ (μb)		
	pp	pA	AA	pp	pA	AA
-4.85	117.0	128.4	190.7	186.8	200.4	216.2
-4.55	234.1	278.6	265.9	237.5	268.7	228.0
-4.25	369.4	428.5	308.5	331.2	346.9	291.3
-3.95	485.5	495.9	362.1	426.5	457.1	336.4
-3.65	532.9	586.9	367.1	522.0	522.1	343.8
-3.35	561.1	580.0	377.3	542.4	553.1	364.0
-3.05	594.1	586.8	399.1	590.5	564.2	380.4
-2.75	627.1	602.2	407.0	614.5	606.1	386.3
-2.45	650.1	616.5	409.4	650.6	565.6	396.7
-2.15	683.6	600.0	422.8	642.2	577.1	411.1
-1.85	685.5	587.8	428.7	681.9	582.8	415.0
-1.55	710.3	603.6	421.4	694.6	588.5	426.7
-1.25	705.9	618.8	424.9	672.0	578.2	416.3
-0.95	711.8	595.5	435.7	703.2	589.7	414.9
-0.65	735.9	611.1	435.5	736.7	617.2	435.9
-0.35	743.6	590.1	428.8	692.5	577.4	402.3
-0.05	720.6	556.8	414.6	716.7	560.5	410.3
0.05	715.6	548.0	419.2	721.1	557.8	429.4
0.35	741.4	564.0	433.3	699.3	552.3	427.0
0.65	744.0	567.4	436.3	706.2	555.3	440.3
0.95	708.6	541.4	430.2	701.5	530.4	424.2
1.25	702.3	546.4	426.7	704.2	520.6	403.4
1.55	713.9	506.9	423.0	664.2	497.5	419.4
1.85	689.1	482.1	429.9	678.2	477.1	416.1
2.15	687.6	476.7	418.2	639.9	462.9	396.7
2.45	651.9	470.5	409.3	620.5	447.6	393.0
2.75	625.8	437.6	407.2	606.6	422.2	390.0
3.05	589.7	412.5	397.3	591.6	415.5	382.4
3.35	564.0	384.7	374.7	555.1	388.1	380.9
3.65	532.9	379.3	362.5	516.0	350.9	355.4
3.95	479.2	304.0	358.4	430.2	297.4	325.7
4.25	371.3	257.4	321.1	357.9	226.2	294.6
4.55	230.3	153.8	263.9	226.4	164.3	244.7
4.85	112.1	69.4	192.8	193.4	104.4	198.5

Table 14: The NLO exclusive $c\bar{c}$ and inclusive single charm y distributions for collisions at $\sqrt{s} = 5.5$ TeV. The distributions for pp , pA and AA interactions are all given. The per nucleon cross section is given for pA and AA interactions. Recall that the intrinsic $\langle k_T^2 \rangle$ is 1 GeV² for pp interactions, 1.35 GeV² for pA interactions, and 1.7 GeV² for AA .

y	$d\sigma_{b\bar{b}}/dy$ (nb)			$d\sigma_b/dy$ (nb)		
	pp	pA	AA	pp	pA	AA
-2.65	0.8	0.7	0.5	14.1	12.1	12.0
-2.45	4.8	4.2	3.2	33.0	26.6	28.7
-2.25	16.6	14.3	12.1	61.1	59.2	59.1
-2.05	41.1	38.3	32.2	103.7	100.0	103.2
-1.85	82.8	80.2	70.4	150.0	154.8	158.6
-1.65	138.2	140.8	132.5	203.4	220.3	232.5
-1.45	213.3	222.4	214.9	262.8	287.3	302.5
-1.25	289.1	313.4	321.9	323.3	361.1	399.4
-1.05	382.7	417.3	441.6	383.9	432.0	485.2
-0.85	463.7	518.7	576.3	443.2	489.1	558.3
-0.65	543.8	609.8	702.0	482.7	548.9	627.4
-0.45	606.8	692.5	814.8	520.3	589.4	681.2
-0.25	651.4	739.2	890.1	547.5	615.2	722.1
-0.05	674.7	764.2	930.9	555.3	617.2	738.3
0.05	674.1	762.7	933.5	553.5	615.6	734.7
0.25	650.8	726.9	890.2	545.0	606.1	725.8
0.45	607.3	671.0	814.3	520.1	570.5	684.9
0.65	543.3	582.9	701.9	481.7	522.5	632.2
0.85	463.9	491.0	576.4	440.1	466.3	559.4
1.05	383.1	391.0	442.2	387.5	406.7	481.3
1.25	289.0	291.1	322.1	323.5	338.0	399.0
1.45	213.3	205.7	215.1	264.0	269.3	304.8
1.65	138.7	130.4	132.3	205.7	210.2	233.8
1.85	82.9	75.3	70.2	148.6	147.1	159.0
2.05	41.2	36.4	32.1	102.1	99.0	104.3
2.25	16.6	13.7	12.1	59.9	58.3	58.7
2.45	4.8	4.0	3.2	31.3	30.7	28.2
2.65	0.8	0.6	0.5	13.5	12.8	11.4

Table 15: The NLO exclusive $b\bar{b}$ and inclusive single bottom y distributions for collisions at $\sqrt{s} = 200$ GeV. The distributions for pp , pA and AA interactions are all given. The per nucleon cross section is given for pA and AA interactions. Recall that the intrinsic $\langle k_T^2 \rangle$ is 1 GeV² for pp interactions, 2.57 GeV² for pA interactions, and 4.16 GeV² for AA .

y	$d\sigma_{b\bar{b}}/dy$ (μb)			$d\sigma_b/dy$ (μb)		
	pp	pA	AA	pp	pA	AA
-4.85	1.811	1.831	1.189	3.012	3.239	2.484
-4.55	2.940	3.117	2.157	4.652	5.331	3.699
-4.25	5.035	5.625	3.782	6.328	7.331	5.407
-3.95	7.070	7.946	5.609	8.606	9.596	7.215
-3.65	9.872	11.200	8.283	10.500	12.110	9.164
-3.35	12.260	13.800	10.220	12.780	14.330	11.140
-3.05	14.330	16.330	12.480	14.770	16.100	12.750
-2.75	17.350	19.110	14.890	16.950	18.230	13.600
-2.45	19.100	21.030	16.430	18.730	20.040	15.780
-2.15	21.350	22.880	17.990	20.070	20.650	16.870
-1.85	22.890	23.940	19.050	21.300	22.290	17.730
-1.55	24.010	23.790	19.440	23.250	22.740	18.530
-1.25	25.320	24.830	20.760	24.040	23.790	19.360
-0.95	26.500	25.570	20.850	25.360	23.960	20.110
-0.65	26.660	25.160	21.330	25.380	24.050	19.720
-0.35	27.460	25.330	21.770	25.480	23.380	20.670
-0.05	27.050	24.680	21.470	26.170	23.810	20.650
0.05	27.010	24.500	21.500	25.790	23.920	20.390
0.35	27.330	24.130	21.680	25.320	22.810	20.150
0.65	26.660	23.340	21.300	25.380	21.990	20.100
0.95	26.460	22.770	20.900	25.480	21.810	19.870
1.25	25.310	21.310	20.760	23.830	20.230	19.310
1.55	24.080	19.630	19.390	22.540	19.050	18.840
1.85	22.830	19.060	18.930	21.370	17.920	17.640
2.15	21.320	17.380	18.040	20.000	16.690	16.930
2.45	19.100	15.280	16.470	18.770	15.570	15.870
2.75	17.360	13.580	14.940	17.320	13.780	14.260
3.05	14.410	11.260	12.460	14.670	11.580	12.710
3.35	12.140	9.320	10.240	12.740	10.040	10.770
3.65	9.831	7.393	8.249	10.430	7.929	8.860
3.95	7.049	5.294	5.607	8.431	6.380	7.131
4.25	5.017	3.721	3.810	6.190	4.889	5.378
4.55	2.925	2.147	2.171	4.660	3.450	3.950
4.85	1.797	1.290	1.193	3.080	2.222	2.346

Table 16: The NLO exclusive $b\bar{b}$ and inclusive single bottom y distributions for collisions at $\sqrt{s} = 5.5$ TeV. The distributions for pp , pA and AA interactions are all given. The per nucleon cross section is given for pA and AA interactions. Recall that the intrinsic $\langle k_T^2 \rangle$ is 1 GeV² for pp interactions, 2.57 GeV² for pA interactions, and 4.16 GeV² for AA .